DRYING OF LONGAN: ITS DRYING KINETICS AND PERFORMANCE OF LONGAN DRYERS

By
Niroot Lamlert

A Thesis Submitted in Partial Fulfillment of the Requirements for the Degree
DOCTOR OF PHILOSOPHY
Department of PHYSICS
Graduate School
SILPAKORN UNIVERSITY
2010

DRYING OF LONGAN: ITS DRYING KINETICS AND PERFORMANCE OF LONGAN DRYERS

By
Niroot Lamlert

A Thesis Submitted in Partial Fulfillment of the Requirements for the Degree
DOCTOR OF PHILOSOPHY
Department of PHYSICS
Graduate School
SILPAKORN UNIVERSITY
2010

การอบแห้งลำไย: ไคเนติกส์ของการอบแห้ง และสมรรถนะของเครื่องอบแห้งลำไย

โดย
นายนิรุธ ล้ำเลิศ

วิทยานิพนธ์นี้เป็นส่วนหนึ่งของการศึกษาตามหลักสูตรปริญญาปรัชญาดุษฎีบัณฑิต
สาขาวิชาฟิสิกส์
ภาควิชาฟิสิกส์
บัณฑิตวิทยาลัย มหาวิทยาลัยศิลปากร
ปีการศึกษา 2553

The Graduate School, Silpakorn University has approved and accredited the Thesis title of "Drying of longan: its drying kinetics and performance of longan dryers" submitted by MR.Niroot Lamlert as a partial fulfillment of the requirements for the degree of Doctor of Philosophy in Physics

…….....

(Assistant Professor Panjai Tantatsanawong ,Ph.D.)
Dean of Graduate School

...../...../.....

The Thesis Advisor

Associate Professor Serm Janjai, Ph.D.

The Thesis Examination Committee

..... Chairman

(Professor Virulh Sa-yakanit, Ph.D.)

...../...../.....

..... Member

(Associate Professor Sirichai Thepa, D.Sc.)

...../...../.....

..... Member

(Associate Professor Serm Janjai, Ph.D.)

...../...../.....

50306802 : MAJOR : PHYSICS
KEY WORDS : LONGAN/ DRYING KINETICS/ DIFFUSIVITY/ FINITE ELEMENT MODELING/ LONGAN DRYER
NIROOT LAMLERT : DRYING OF LONGAN: ITS DRYING KINETICS AND PERFORMANCE OF LONGAN DRYERS. THESIS ADVISOR : ASSOC.PROF.SERM JANJAI, Ph.D. 106 pp.

In this work, drying kinetics of longan drying and performance evaluation of longan dryers has been carried out. For the drying kinetics, thin layer drying of peeled longan was conducted under controlled condition of temperature and relative humidity. Drying air temperature has great influence on the drying rate of peeled longan. The moisture content of peeled longan were function of air temperature and relative humidity. Page model was found to be the best model to predict the moisture content of peeled longan during drying. Moisture diffusivities of different parts of longan fruit have also determined. It was found that the diffusivity of the flesh of longan fruit increased with temperature but the diffusivities of shell, seed coat, seed and seed stalk were temperature independent.

A two dimension finite element model has been developed to simulate moisture diffusion in longan fruit using the diffusivities of different parts of longan fruit obtained from this work. Shrinkage of the flesh of longan during drying was also taken into account. This finite element model satisfactorily predicted the moisture diffusion in longan fruit.

The performance of a side loading type solar tunnel dryer for drying peeled longan has been evaluated. Five full-scale experimental runs were conducted and 100 kg of peeled longan was dried in each experimental run. The drying time in this tunnel dryer was 16 h for drying peeled longan from an initial moisture content of 84% (wb) to a final moisture content of 12% (wb). A system of partial differential equations describing heat and moisture transfer during drying of peeled longan in this solar tunnel dryer was also developed. The simulated results agreed well with the experimental data.

Finally, the performance of a batch type longan dryer using biomass burner with air flow reversal was investigated. The dryer consists of biomass burner and a drying bin with an arrangement for periodic air flow reversal. Three sets for drying runs of whole longan for loading capacity of 2000 kg, 1500 kg and 1000 kg were carried out. The drying time of whole longan in the longan dryer was 60 h, 54 h and 48 h, for 2000 kg, 1500 kg and 1000 kg, respectively. The quality of dried product was also good in comparison to high quality product in markets. Additionally, a set of partial differential equations was also developed to simulate the performance of this dryer. It was found that the simulated results agreed well with the experimental data. This model can be used to provide the design data and it is also essential for optimal design of the dryer.

Department of Physics Graduate School, Silpakorn University Academic Year 2010
Student's signature .....
Thesis Advisor's signature .....

50306802 : สาขาวิชาฟิสิกส์
คำสำคัญ : ลำไย/ ไคเนติกส์ของการอบแห้ง/ ค่าสัมประสิทธิ์การแพร่/ แบบจำลองไฟไนต์เอลิเมนต์/ เครื่องอบแห้งลำไย

นิรุธ ล้ำเลิศ : การอบแห้งลำไย : ไคเนติกส์ของการอบแห้ง และสมรรถนะของเครื่องอบแห้งลำไย. อาจารย์ที่ปรึกษาวิทยานิพนธ์ : รศ.ดร.เสริม จันทร์ฉาย. 106 หน้า.

ในงานวิจัยนี้ผู้วิจัยทำการศึกษาไคเนติกส์ของการอบแห้ง และสมรรถนะของเครื่องอบแห้งลำไย ในการศึกษาไคเนติกส์ของการอบแห้งผู้วิจัยจะทำการทดลองอบแห้งเนื้อลำไยแบบชั้นบางโดยควบคุมอุณหภูมิและความชื้นสัมพัทธ์ของอากาศ จากการทดลองพบว่าอุณหภูมิของอากาศมีอิทธิพลอย่างมากต่ออัตราการแห้งลำไย โดยความชื้นของลำไยจะเป็นฟังก์ชันของอุณหภูมิและความชื้นสัมพัทธ์ของอากาศ และพบว่าแบบจำลองของ Page สามารถที่จะทำนายการลดลงของความชื้นของการอบแห้งลำไยได้ดีที่สุด ในลำดับต่อไปผู้วิจัยได้ทำการหาค่าสัมประสิทธิ์การแพร่ของความชื้นของส่วนต่างๆของผลลำไย ผลการศึกษาพบว่า ค่าสัมประสิทธิ์การแพร่ของเนื้อลำไยจะเพิ่มขึ้นตามอุณหภูมิ ส่วนค่าสัมประสิทธิ์การแพร่ของเมล็ด เปลือกหุ้มเมล็ด เปลือก และขั้ว ของลำไยจะไม่ขึ้นกับอุณหภูมิ จากนั้นผู้วิจัยได้ทำการพัฒนาแบบจำลองไฟไนต์เอลิเมนต์ 2 มิติของการแพร่ความชื้นในผลลำไยโดยใช้สัมประสิทธิ์การแพร่ของส่วนต่างๆของลำไยข้างต้น แบบจำลองดังกล่าวจะพิจารณาการหดตัวของเนื้อลำไยด้วย ผลการศึกษาพบว่าแบบจำลองดังกล่าวสามารถทำนายการแพร่ของความชื้นในผลลำไยได้ดี

หลังจากนั้นผู้วิจัยได้ทำการศึกษาสมรรถนะของเครื่องอบแห้งพลังงานแสงอาทิตย์แบบอุโมงค์ลมในการอบแห้งเนื้อลำไย โดยทำการอบแห้ง 5 ครั้งๆละ 100 กิโลกรัม ผลการทดลองพบว่าความชื้นของลำไยลดลงจากความชื้นเริ่มต้น 84% (wb) จนถึงความชื้นสุดท้าย 12% (wb) โดยใช้เวลา 16 ชั่วโมง นอกจากนี้ผู้วิจัยได้ทำการสร้างแบบจำลองทางคณิตศาสตร์สำหรับอธิบายการถ่ายเทมวลและความร้อนในเครื่องอบแห้ง ผลการศึกษาพบว่า ผลการคำนวณจากแบบจำลองสอดคล้องกับผลการวัด

สุดท้ายผู้วิจัยได้ทำการศึกษาสมรรถนะเครื่องอบแห้งลำไยแบบสลับอากาศร้อนโดยใช้เครื่องเผาไหม้ชีวะมวลเป็นแหล่งให้ความร้อน โดยทำการทดลองอบแห้งลำไยทั้งผลจำนวน 3 ครั้ง โดยครั้งที่ 1 ใช้ลำไย 2000 กิโลกรัม ครั้งที่ 2 ใช้ลำไย 1500 กิโลกรัม และ ครั้งที่ 3 ใช้ลำไย 1000 กิโลกรัม ผลการทดลองพบว่า เวลาที่ใช้ในการอบแห้งลำไย 2000 กิโลกรัม 1500 กิโลกรัม และ 1000 กิโลกรัม มีค่าเท่ากับ 60 ชั่วโมง 54 ชั่วโมง และ 48 ชั่วโมงตามลำดับ ลำไยอบแห้งที่ได้จากเครื่องอบแห้งดังกล่าวมีคุณภาพที่ดี นอกจากนี้ผู้วิจัยได้พัฒนาแบบจำลองทางคณิตศาสตร์สำหรับทำนายสมรรถนะเครื่องอบแห้งลำไยดังกล่าว ผลที่ได้พบว่าแบบจำลองสามารถทำนายสมรรถนะของเครื่องอบแห้งลำไยได้สอดคล้องกับผลการทดลอง โดยที่แบบจำลองทางคณิตศาสตร์ที่พัฒนาขึ้นสามารถนำไปใช้ในการออกแบบเครื่องอบแห้งลำไยที่เหมาะสมกับสภาวะการใช้งานต่างๆ ต่อไป

Acknowledgments

A thesis entitled “Drying of longan: its drying kinetics and performance of longan dryers” is submitted in partial fulfillment of the requirements for the degree of Doctor of Philosophy (Physics), Graduate School, Silpakorn University.

This research is a part of the research project SFB 564 (“Research for Sustainable Land Use and Rural Development in Mountainous Regions of Southeast Asia”), funded by Deutsche Forchungsgemeinschaft (DFG), Germany, and co-funded by the National Research Council of Thailand and the Ministry of Science, Technology and Environment, Vietnam. I gratefully acknowledge this financial support. Prof. Dr. Joachim Mueller is gratefully acknowledged for his support to this research work.

I would like to express my sincere thanks to Assoc. Prof. Dr. Serm Janjai, my supervisor for his helpful guidance and support throughout this study. My sincerely gratitude is also given to Prof. B.K. Bala for the scientific support and valuable advice.

I am grateful to Assoc. Prof. Chumnong Thamrongmas, Head of Department of Physics, for the administrative support during the study. Prof. Dr. Virulh Sa-yakanit and Assoc. Prof. Dr. Sirichai Thepa are gratefully acknowledged for examining this thesis.

I would like to thank Mr. Chalermchai Ngamdee, Mr. Sarawut Naebnean, Mr. Yuttasak Boonrod, Mr. Pipop Leethochawalit and all researchers in Solar Energy Research Laboratory of Silpakorn University for their helps and friendship during the study.

Finally, I would like to specially express my gratitude and deepest appreciation to my parents and relatives for their love and support throughout my life.

Table of Contents

Page

Abstract English…… c

Abstract Thai …… d

Acknowledgments……...……. f

List of Tables…… j

List of Figures…….. k

Chapter

1 Introduction……. 1

Rationale of this work …….. 1

Objectives…….. 1

Organization of the thesis…….. 2

2 Thin Layer Drying of Peeled Longan…….. 3

Introduction…… 3

Materials and methods…… 3

Materials…… 3

Drying apparatus and experimental procedure……. 4

Mathematical modeling……. 6

Colour Measurement …… 8

Results and discussion……. 8

Drying behaviour of peeled longan……. 8

Mathematical modeling of thin layer drying…… 10

Colour change…….. 19

Conclusions…… 21

3 Moisture Diffusivity Determination of Different Parts of Longan Fruit……. 22

Introduction……...…. 22

Materials and methods…… 23

Theoretical consideration…… 24

Determination of diffusivities……. 25

Results and discussion……. 25

Conclusions…… 28

4 Finite Element Simulation of Drying of Longan Fruit…… 29

Introduction……. 29

Materials and method……. 30

Finite element modeling of longan drying…… 31

Thermo-physical properties of longan…….. 35

Moisture diffusivity of longan……...…… 35

Chapter Page

Shrinkage of Longan…… 37

Equilibrium moisture content……..……... 38

Surface Mass Transfer Coefficient……...……...…… 38

Results and discussion……..……..……...……..……. 38

Conclusions……..…… 43

5 Solar Drying of Peeled Longan Using a Side Loading Type Solar Tunnel Dryer: Experimental and Simulated Performance…… 44

Introduction……. 44

Experimental study……. 45

Mathematical modeling……... 48

Energy balances in the collector…… 48

Energy and mass balances in the drying unit……. 51

Results and discussion……. 53

Experimental results……... 53

Simulated results……. 57

Conclusions……..…… 59

6 Experimental and Simulated Performances of a Batch Type Longan dryer with Air Flow Reversal Using Biomass Burner as a Heat Source……. 60

Introduction…….. 60

Materials and methods……. 61

Experimental study……. 61

Uncertainty analysis…… 64

Water activity measurement of dried longan…….. 65

Colour measurement of dried longan…….. 65

Economic evaluation…… 66

Mathematical modeling……...…….. 67

Results and discussions…….. 70

Experimental results……. 70

Results of equilibrium moisture content…… 75

Simulated results……..… 76

Qualities of dried whole longan…… 78

Economic result…… 79

Conclusions ……...… 80

7 Conclusions……..…… 81

References…… 82

Page

Appendixes……...… 94

Appendix 1…….……. 95

Appendix 2……... 96

Appendix 3 ……. 101

Autobiography…… 106

List of Tables

Tables		Page
1	Selected thin layer drying models……..	7
2	Parameter values, coefficient of determination (R^2) and root mean square error (RMSE) values for different models ……	12
3	Equation of drying parameters……	13
4	Colour variations of peeled longan dried at different temperatures……	20
5	Diffusivities of different components of longan fruit……..	27
6	Diffusivities of different components of longan fruit……..	36
7	Critical water activity to inhibit microorganisms……	65
8	The analysis of Variance (ANOVA) for temperature distributions in different positions inside the dryer ……	75
9	The analysis of Variance (ANOVA) for moisture content distributions in different positions inside the dryer ……	75
10	Colour variations of fresh and dried whole longan……..	79
11	Computation of payback period……..	80

List of Figures

Figures		Page
1	Peeled longan on a tray for thin layer drying experiment……	4
2	Schematic diagram of the laboratory drying……	5
3	Details of the drying compartment……..	5
4	Thin layer drying of peeled longan at different temperatures (50, 60 and 70 ºC)……	9
5	Thin layer drying of peeled longan at different relative humidities (10, 20 and 25%)…..	10
6	Predicted and observed moisture content of peeled longan using Page model …….	14
7	Predicted and observed moisture content of peeled longan using Two-term model……..	15
8	Predicted and observed moisture content of peeled longan using modified Henderson and Pabis model…….	16
9	Plot of residual between observed moisture content (M_{obs}) and predicted moisture content (M_{pre}) of peeled longan from Page model for different temperatures and relative humidities……	17
10	Plot of residual between observed moisture content (M_{obs}) and predicted moisture content (M_{pre}) of peeled longan from Two-term model for different temperatures and relative humidities……	17
11	Plot of residual between observed moisture content (M_{obs}) and predicted moisture content (M_{pre}) of peeled longan from modified Henderson and Pabis model for different temperatures and relative humidities……	18
12	Comparison of predicted moisture content from Page model and observed moisture content of peeled longan at different temperatures and relative humidities ……	18
13	Comparison of predicted moisture content from Two-term model and observed moisture content of peeled longan at different temperatures and relative humidities……	19
14	Comparison of predicted moisture content from modified Henderson and Pabis model and observed moisture content of peeled longan at different temperatures and relative humidities……	19
15	Influence of drying temperature on lightness L*, hue angle (h) and chroma (C*) of peeled longan……..	20
16	Anatomy of Longan fruit ……	23
17	Influences of the drying air temperatures on drying curves for different components of longan fruit……..……	26
18	Comparison of predicted values and experimental data of flesh of longan fruit for temperature of 50°C, 60°C, 70°C, and 80°C……..……	27
19	Variation of the moisture diffusivity of flesh of longan fruit as a function of the reciprocal of absolute drying air temperature……..	28

Figures Page

20 Schematic diagram of the laboratory dryer……. 31

21 Finite element grid for half of a single fruit of longan ……... 34

22 Comparison of the predicted moisture contents on a wet basis of longan fruit with the experimental data obtained from Phupaichitkun et al. (2005)…… 39

23 Comparison of the predicted moisture contents on a wet basis of longan fruit with the experimental data from this study…….…… 40

24 Variations of the moisture contents on a wet basis with time in the different components of the longan fruit…… 41

25 Moisture within the longan fruit after 1, 5, 10 and 15 hours after drying at the drying air temperature of 70 °C and relative humidity of 14%. Values in the contour represent the moisture contents in %, wb. ……. 42

26 Schematic diagram of the side loading type solar tunnel dryer…… 46

27 Positions of the thermocouples (T) and hygrometers (rh) and product sample for moisture determination (M)……. 47

28 Heat transfer in the solar collector…… 48

29 Energy balances in the drying unit…… 51

30 Variations of the solar radiation during a typical experimental run……. 54

31 The variations of the temperatures (T) at different positions inside the collector…… 54

32 The variations of the temperatures at different positions inside the drying unit……..… 55

33 Variations of relative humidities (rh) at three different positions inside the drying unit during a typical experimental run…… 56

34 Variations of mass flow rate inside the dryer during a typical experimental run……. 56

35 Variations of the moisture contents (M) in the different locations of the drying unit for a typical experimental run during drying of peeled longan. The positions of the measurement of moisture contents are shown in Fig. 5.2 …….. 57

36 Comparison of the simulated and observed collector outlet temperature during drying of peeled longan for a typical full scale experimental run…… 58

37 Comparison of the simulated and observed moisture content during drying of peeled longan for a typical full scale experimental run……. 58

38 Pictorial view of the longan dryer…….. 62

39 The structure and dimension of the longan dryer…….. 62

Figures Page

40 Positions of the thermocouples (T), hygrometers (rh) and product samples for weights (M). x, y and z are the axis of reference…….…… 63

41 Element of the bed……... 67

42 Show the hot air chamber and sample boxes…… 69

43 Variations of inlet temperature and outlet temperature of the dryer and ambient temperature during a typical experimental run of a loading capacity of 1000 kg ….…….. 71

44 Variations of the temperatures at bottom, middle and top positions of the dryer a) front section, b) middle section and c) behind section…… 71-72

45 Temperatures at different positions inside the drying bed for periodic air reversal of a loading capacity of 1000 kg……. 73

46 Variations of ambient, inlet and outlet relative humidity during a typical experimental runs of a loading capacity of 1000 kg …….. 73

47 Moisture content changes at different positions (middle, sides and corners) inside the drying bed …….. 74

48 Moisture content of longan inside dryer during typical drying runs…… 75

49 Measured sorption isotherms (points) for whole longan at the temperature levels of 40°C, 50°C and 60°C …… 76

50 Comparison of the simulated and observed moisture content during drying of whole longan 1000 kg, 1500 kg and 2000 kg …….…….. 77

51 Comparison of the simulated and observed drying air temperature (T_f) during drying for 1000 kg of whole longan …….. 77

52 Comparison of the simulated and observed relative humidity during drying for 1000 kg of whole longan …….……. 78

53 The simulated result of product temperature (T_p) during drying for 1000 kg of whole longan …….. 78

A1 Roof-integrated solar drying system…….. 96

A2 Heat transfer in the collector…….. 97

A3 Solar radiation on the south and north facing solar collector……. 98

A4 Variations of the ambient temperature and temperature of the outlet air from the south-facing collector for the drying test of longan……..…….. 99

A5 Variations of the ambient temperature and temperature of the outlet air from the north-facing collector for the drying test of longan ……..…….. 99

Figures Page
A6 Average temperature rise above the ambient inside at the outlet of the collector…… 100
A7 Comparison of experimental and simulated moisture contents…… 100

Chapter 1
Introduction

1.1 Rationale of this work

Lonagan (*Dimocarpus Longan* Lour.) is a small fruits (Ca. 1.5 – 2 cm diameter) spherical shape and light brown in colour. Longan is one of the important fruit of northern Thailand with an annual export value of 109 million US dollars and its production volume was 495,000 tons in 2007 (Office of Agriculture Economics, Thailand, 2007). It is a seasonal fruit with a harvesting season about 3 months (July – September). It is consumed both as fresh and dried products. Dried longan is mainly exported to China with an annual volume of 193,000 tons.

There are two types of dried longan, namely dried whole longan fruit and dried peeled longan. For the first type, longan is dried as a whole fruit without peeling. For the second type, longan fruit is peeled and de-stoned and only the longan flesh is dried. The whole longan fruit is usually dried by using a batch type static bed dryer. More than 20,000 dryers are now in operation for production of dried whole longan fruit in Thailand and these dryers are static bed dryers. The dryers use liquefied petroleum gas (LPG) as fuel. Normally, non-uniform drying is obtained. To ensure uniformly died product, drying operators usually turn the fruit layer upside down and inside out thoroughly in 12 hours interval and this causes damage and cracks of a significant fraction of dried longan during drying. Additionally, the turning of the bed is labour intensive operation.

Most of the peeled longan is dried in a large open flat bed using hot stoves burning fuel wood and charcoals. This procedure usually results in poor quality dried product due to dirt and dust from the burning stoves. Some peeled longan is also dried under the sun on mats. During sun drying, peeled longan fruits on mats are exposed to the open environment and are contaminated by dust and insects, resulting in poor quality dried fruits with less value addition.

In this work, we proposed alternative methods to dry peeled longan with a side loading solar tunnel dryer and to dry whole longan fruits with a batch type dryer with air flow reversal using biomass burner as a heat source. The work includes both modeling and experiments. As the variation of moisture content of longan depends on several drying parameters, the drying kinetics of longan drying was also investigated in this study. Additionally, the diffusivities of different parts of longan was determined and used in the finite element simulation of the drying of longan fruit.

1.2 Objectives

1) To study the thin layer drying of peeled longan
2) To determine the diffusivity of different parts of longan fruits
3) To carry out the finite element simulation of drying of longan fruit
4) To investigate the performance of a side loading tunnel dryer for drying peeled longan

5) To evaluate the performance of a batch type longan dryer with air flow reversal using biomass burner as a heat source

1.3 Organization of the thesis

This thesis composes of 7 chapters. Chapter 1 gives the rationale of the work and its objectives. The thin layer drying of peeled longan is presented in chapter 2. Chapter 3 presents the diffusivities of different parts of longan. Chapter 4 comprises the work on finite element simulation of longan drying. The performance of side loading tunnel dryer for drying peeled longan is presented in chapter 5, whereas the performance of a longan dryer with air flow reversal for drying whole longan fruit is presented in chapter 6. Finally, chapter 7 presents the conclusion of the work. As chapters 2-6 have been published in international journals, the content of these chapters were written in the same way as that of the published papers.

Chapter 2

Thin Layer Drying of Peeled Longan*

2.1 Introduction

The drying kinetics of food materials such as peeled longan are required to predict the drying behaviour, and for optimization of the drying parameters. Many studies have been conducted on drying kinetics of fruits and vegetables (Murata et al., 1996; Sokhansanj et al., 1997; Kiranoudis et al., 1997; Pal and Chakraverty, 1997; Hashimoto and Kameoka, 1998; Chen et al., 2000; Yaldiz and Ertekin, 2001a&b; Hossain and Bala, 2002; Togrul and Pehlivan, 2002&2003; Krokido et al., 2003; Midilli and Kucuk, 2003; Akpinar et al., 2003a&b; Jain and Pathare, 2004; Erenturk et al., 2004; Ertekin and Yaldiz, 2004; Baini and Langrish, 2006; Menges and Ertekin, 2006; Goyal et al., 2006; Janjai et al., 2007; Kashaninejad et al., 2007; Xanthopoulos et al., 2007). Limited studies have been reported on drying of longan fruit (Achariyaviriya, 2001; Achariyaviriya, et al., 2001). Achariyaviriya et al. (2001) reported quality tests of dried peeled longan and found that the maximum permissible air drying temperature for production of the desired golden brown colour of the peeled longan is 65 °C.

Recently Varith et al. (2007) reported drying of peeled longan using combined microwave-hot air and also reported drying kinetics using Sherwood's exponential equation, quality indices and specific energy consumption. More recently a study on finite element simulation of longan fruit with different diffusivities for different components of the longan has been conducted to explain the complex drying phenomena of longan fruit which results from nonhomogeneity and interfaces between different components of the longan fruit (Janjai et al., 2008). However, no detailed studies are found in literature on drying kinetics of peeled longan. The objectives of this study are: (a) to study the effect of temperature and relative humidity on drying characteristics of peeled longan and (b) to develop a suitable thin-layer drying model to provide design data and also for simulation and optimal design of dryers for drying peeled longan.

2.2 Materials and methods

2.2.1 Materials

The mature longan fruit is a small (ca. 1.5 – 2.0 cm diameter) conical, heart shaped or spherical in shape and light brown in colour. It has a thin, leathery, and indehiscent shell surrounding a succulent, edible white flesh. The flesh contains a relatively dark brown seed.

---

* This chapter has been published in Journal of Food Science and Technology Research vol. 17 no. 4. (2011)

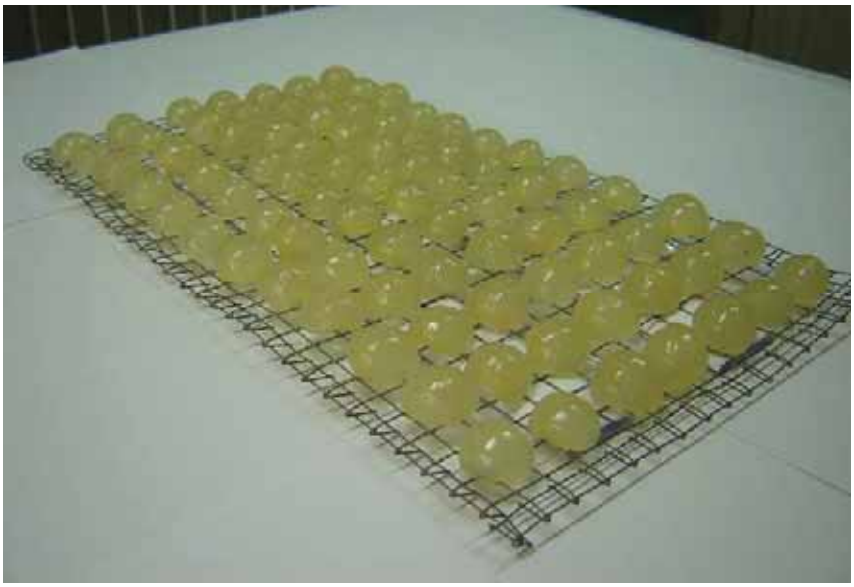

Fig. 1 Peeled longan on a tray for thin layer drying experiment

The longan fruits used in this investigation had an initial moisture content about 445-484 % (db). They was stored at 5 ºC and then left at room temperature before starting the experiments. The longan fruits were peeled and de-stoned. Each peeled longan has a spherical shape (ca. 2.0 cm diameter). For each experiment, the peeled longan was placed on the drying tray as shown in Fig. 1. The tray has the width of 17 cm and the length of 38 cm. The space between each peeled longan is about 0.5 cm. The tray with peeled longans was placed inside the drying compartment of a laboratory dryer. The length of tray is parallel to the air flow direction. The drying compartment has the width of 30 cm, the length of 50 cm and the height of 4 cm.

2.2.2 Drying apparatus and experimental procedure

The laboratory dryer developed at the Institute of Agricultural Engineering, Hohenheim University, Germany was used to conduct thin layer drying experiments of peeled longan. The dryer can be regulated to desired drying conditions with high accuracy. The schematic diagram of this dryer is shown in Fig. 2 and Fig. 3 (El Fadil, 1998).

The dryer is composed of an air flow control assembly (section 1), humidity assembly (section 2), primary heating assembly and drying compartment (section 3). Each section is electronically controlled by a proportional controller. The air flow control assembly in section 1 consists of a blower, a flow controller and an orifice manometer for monitoring air flow (FSM Electronik GmbH, model DPS, Germany). It regulates the amount of fresh air entering the humidity assembly in section 2 at the accuracy of ± 0.05 m/s. The humidity assembly is composed of a ceramic packed-bed, a water heater and a compression-type water cooler. The ceramic packed-bed has a square cross-section (50 cm x 50

cm) and the depth of 20 cm. Water from the water heater or water cooler at a given temperature is sprayed to the top of the ceramic packed-bed to humidify this packed-bed.

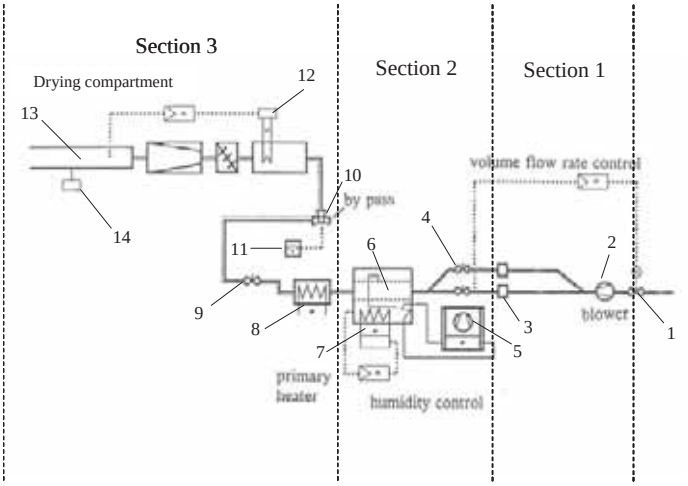

Fig. 2 Schematic diagram of the laboratory drying showing section 1 with the entrance gate valve and orifice manometer (1), blower (2), fixed reducer and proportional integral (PI) controller(3); section 2 with the control valve (4), compression type a water cooler (5), ceramic packed-bed (humidifier) (6), water heater (7); section 3 with the primary air heater (8), control valve (9), 3-way valve (10), monoflap (11), secondary air heater (12), drying compartment (13), load cell and PI controller (14).

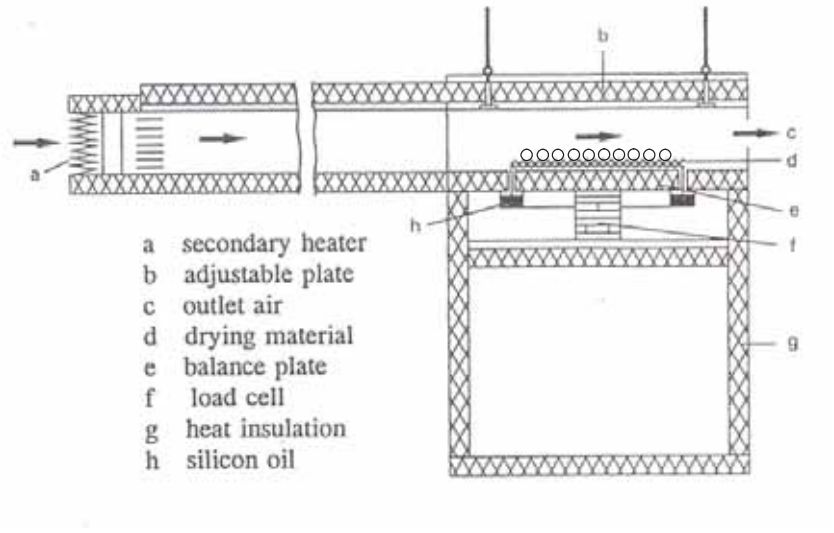

Fig. 3 Details of the drying compartment

Fresh air from section 1 is forced from the bottom to the top of the humid packed-bed. The air absorbs moisture while it passes through the packed-bed. At the top of the packed-bed, this air leaves in a humidified condition a given temperature. Then this saturated air is heated in the primary heating

assembly in section 3 at a desired temperature. This air is finally channeled to the drying compartment. At the drying compartment, the air is further exposed to secondary heating elements to obtain uniform temperature distribution at the accuracy of ± 0.5 °C. Weighing of samples inside the drying compartment is done automatically through a load cell every 30 minutes. During weighing, the drying air was temporarily diverted through a by-pass to avoid the distribution of the air flow to the weighing system. Air temperatures are measured by using Pt 100 temperature sensors (Rössel, model 109483, Germany). The drying air temperature can be varied in the range of 30 to 100 °C. The air speed could be kept constant during drying experiments at a desired level ranging from 0.1 to 1.2 m/s with the accuracy of ± 0.05 m/s. The desired dew point temperature of the drying air is adjustable by controlling the temperature of water sprayed to the ceramic packed-bed. With the air temperature and the dew point temperature, the relative humidity of the air can be determined. This relative humidity is also checked with a hygrometer (Greisinger electronic GmbH, Germany). All data recording and system control are carried through a program in a personal computer.

For each drying experiment, the tray loaded with peeled longans was placed in the drying compartment. The homogeneity of air temperature and air flow was checked by using thermocouples and a hot wire anemometer. Both temperature and air flow in the compartment were uniform. In all experiments, the air speed of 0.5 m/s was used.

Before starting an experiment, the dryer was allowed to run for half an hour to obtain steady temperature. Thin layer drying of peeled longan was conducted at a temperature of 50, 60 and 70°C and the relative humidity of drying air from 10-25%. The weighing system was set up to weigh peeled longan in the dryer every 30 minutes. Each weighing takes about 30 seconds. As the total drying time of each experiment is about 21 hours, the effect of weighing time on the drying behavior of peeled longan is negligible. In total, nine sets of experiments were conducted for drying of peeled longan.

2.3 Mathematical modeling

There are three approaches to the modeling of thin layer drying of agricultural products (Bala, 1998). These approaches are (a) theoretical approach, (b) semi-theoretical approach and (c) empirical approach. Theoretical equation gives better understanding of the transport processes but empirical equation gives better fit to the experimental data without any understanding of the transport processes involved. The semi-theoretical equation gives some understanding of the transport processes.

Thin layer drying models selected for fitting experimental data of peeled longan are expressed in the form of moisture content ratio of samples during drying and it is expressed as:

$$MR = \frac{M - M_e}{M_0 - M_e} \quad (1)$$

where: MR is the dimensionless moisture content ratio; and M, M_0 and M_e are the moisture content at any given time, the initial moisture content and equilibrium moisture content, respectively.

In this work, the final moisture content which has achieved equilibrium i.e. it has become constant for considerable period of time under constant conditions of temperature and relative humidity, was assumed as the equilibrium moisture content of the products.

To select a suitable model for describing the drying process of peeled longan, eight different thin layer drying models were selected to fit the thin layer experimental data of peeled longan. The selected thin layer drying models are presented in Table 1. The models were fitted to the experimental data by direct least square. The coefficient of determination R^2 was one of the main criteria for selecting the best equation. In addition to the coefficient of determination, the goodness of fit was determined by various statistical parameters such as root mean square error RMSE. For the best fit, R^2 value should be higher and RMSE values should be lower. The root mean square error (RMSE) and coefficient of determination (R^2) are defined as:

$$RMSE = \left[\frac{\sum_{i=1}^{n} \left(M_{pre,i} - M_{obs,i} \right)^2}{n} \right]^{0.5} \tag{2}$$

$$R^2 = 1 - \frac{(\text{Residual sum of squares})}{(\text{Corrected total sum of squares})} \tag{3}$$

where $M_{obs,i}$ and $M_{pre,i}$ are the experimental and predicted dimensionless moisture ratios, respectively and n is the number of observations.

Table 1. Selected thin layer drying models

	Model equation	Name of the model
1	$MR = \exp(-kt)$	Newton (Mujumdar, 1987)
2	$MR = \exp(-k_1 t^n)$	Page (Diamante and Munro, 1993)
3	$MR = \exp(-(kt)^n)$	Modified Page (White et al., 1991)
4	$MR = a\exp(-kt)$	Henderson and Pabis (Zhang and Litchfield, 1991)
5	$MR = a\exp(-kt) + c$	Logarithmic (Yagcioglu et al., 1999)
6	$MR = 1 + a_1 t + b_1 t^2$	Wang and Singh (Wang and Singh, 1978)
7	$MR = a\exp(-kt) + b\exp(-gt)$	Two-term (Henderson, 1978)
8	$MR = a\exp(-kt) + b\exp(-gt) + c\exp(-pt)$	Modified Henderson and Pabis (Karathanos, 1999)

2.4 Colour Measurement

The colour of dried longan samples were measured by a chromometer (CR-400, Minolta Co. Ltd., Japan) in CIE (Commission Internationale l'Eclairage) Lab chromaticity coordinates. L^*, a^* and b^* represent black to white (0 to100), green to red (-ve* to +ve) and from blue to yellow (-ve* to +ve) colours, respectively. Out of five available colour systems, the L*a*b* (Krokida et al., 1998; Lozano and Ibarz, 1997; Maskan, 2001) and L*C*h (Zhang et al., 2003) systems were selected because these are the most used systems for evaluation of the colour of dried food materials. The instrument was standardized each time with a white ceramic plate. Three readings were taken at each place on the surface of samples and then the mean values of L*, a* and b* were averaged. The different colour parameters were calculated using the following equations (Lopez Camelo and Gomez, 2004).

Hue angle (h) indicating colour combination is defined as:

$$h = \begin{cases} \tan^{-1}(b^*/a^*) & (\text{when } a^* > 0) \\ 180° + \tan^{-1}(b^*/a^*) & (\text{when } a^* < 0) \end{cases} \quad (4)$$

and chroma (C*) indicating colour saturation is defined as:

$$C^* = (a^{*2}+b^{*2})^{1/2} \quad (5)$$

2.5 Results and discussion

2.5.1 Drying behaviour of peeled longan

The changes in moisture contents with time for different drying air temperatures are shown in Fig. 4. The final moisture content of samples dried under different conditions ranges from 12.8 % - 15.5% (db). The drying rate is higher for higher air temperature and as a result the time taken to reach the final moisture content is less as shown in Fig. 4. The drying air temperature has also an important effect on drying of peeled longan. The variations of moisture contents with time for different levels of relative humidity in the range of 10% to 25% are shown in Fig. 5 and it is observed from Fig. 5 that there is no effect of relative humidity on drying rate of peeled longan in the range of relative humidity from 10% to 25%.

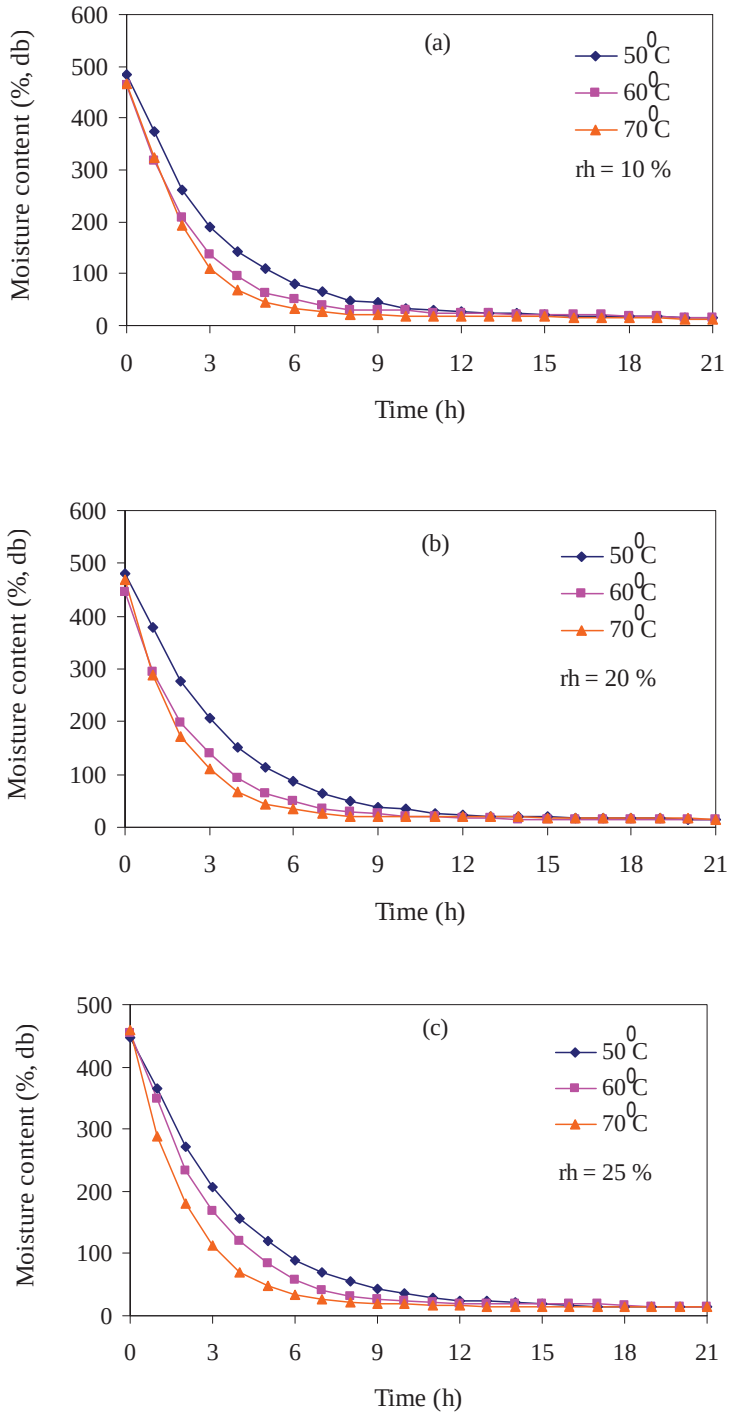

Fig. 4 Thin layer drying of peeled longan at different temperatures (50, 60 and70 ºC)

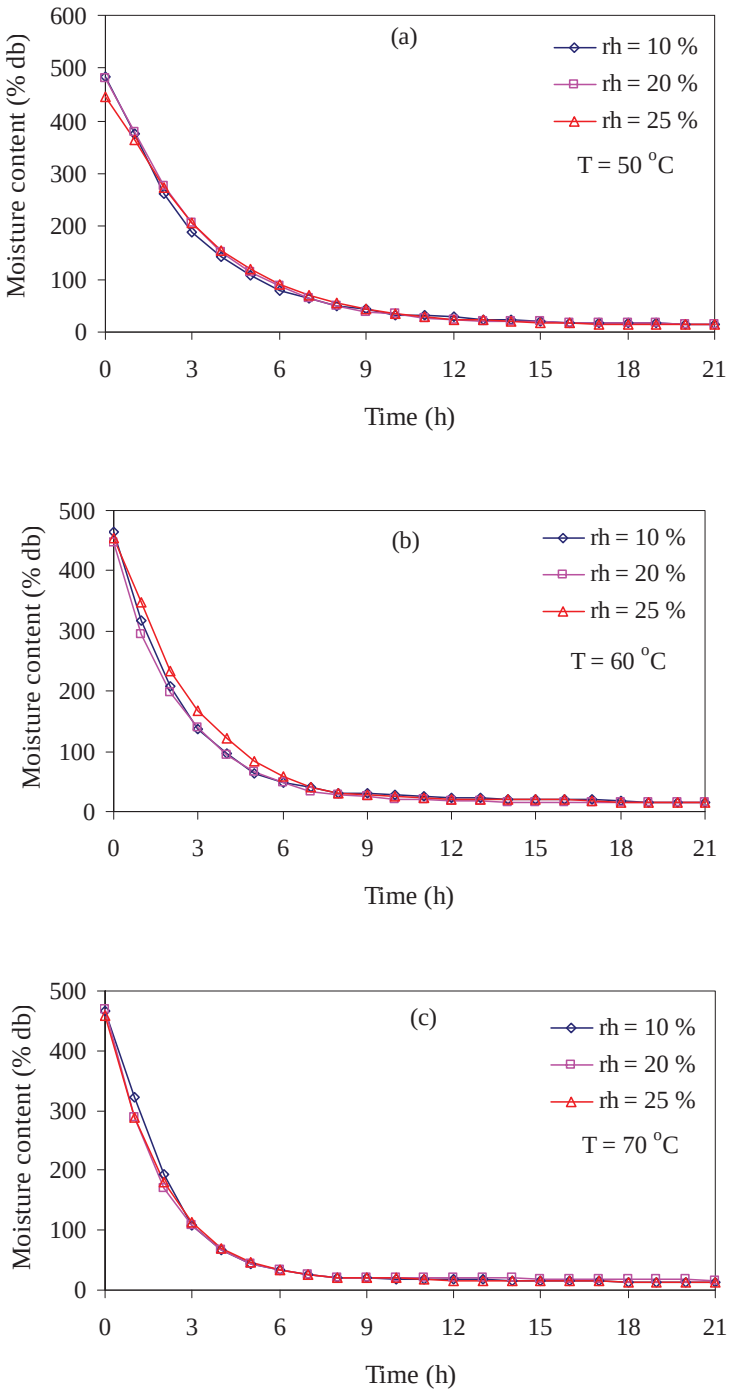

Fig. 5 Thin layer drying of peeled longan at different relative humidities (10, 20 and 25%)

2.5.2 Mathematical modeling of thin layer drying

Eight thin layer drying models were fitted to the experimental data of moisture ratios of peeled longan dried at different temperatures and relative humidities and the fitted thin layer models are shown in Table 2. The parameter values, R^2 and RMSE are also shown in Table 2. Page model was the

best followed by Two-term and modified Henderson and Pabis model. In all these three cases, the value of R^2 was greater than 0.997, indicating a good fit and root mean square errors were also almost same. The values of R^2 and root mean square error (RMSE) for the Page model are 0.9997 and the average RMSE was 4.8%. Empirical expressions were developed for the drying parameters of Page model, Two-term model and modified Henderson and Pabis model and the drying were found to be a function of drying air temperature and relative humidity and high coefficient of determination and these are shown in the Table 3.

Figures 6 to 8 show the comparisons of the predicted and experimental data of thin layer drying of longan for Page model, Two-term model and modified Henderson and Pabis model, respectively. The agreement between the prediction and measured values of these models are excellent and are almost same. Residual plots are used to asses the selected model. Figures 9 to 11 shows the residuals versus the observed moisture contents of these three models. The randomness of the plots of the residuals versus the observed moisture contents shows that there is no systematic pattern. This shows the suitability of the derived models. Figures 12 to 14 show the comparisons of the predicted and experimental data for three different temperatures 50-70°C for Page model, Two-term model and modified Henderson and Pabis model respectively and all values are around the straight lines. This means that these three models are quite capable to predict drying behavior of peeled longan within the temperature ranges of 50-70°C. Although the Page model is the best, either of one of these three models may be considered to describe the thin-layer drying behaviour of peeled longan.

These models are quite general because they express moisture ratio of peeled longan as functions of empirical parameters and time and the parameters are written as functions of drying conditions, namely air temperature and relative humidity. Additionally, peeled longan consists of only the flesh which has relatively homogeneous texture. Therefore, it is expected that these three models are applicable to most peeled longan available in markets.

Table 2. Parameter values, coefficient of determination (R^2) and root mean square error (RMSE) values for different models

Models	T(°C)	rh (%)	k (h^{-1})	k_1 (h^{-n})	a (-)	a_1 (h^{-1})	b (-)	b_1 (h^{-2})	c (-)	n (-)	g (h^{-1})	p (h^{-1})	R^2	RMSE (%)
Newton	50	10	0.3208										0.9994	4.79
	60	10	0.4220										0.9993	5.46
	70	10	0.4787										0.9976	11.66
	50	20	0.3046										0.9989	6.27
	60	20	0.4253										0.9999	1.83
	70	20	0.5300										0.9998	3.55
	50	25	0.2800										0.9993	7.40
	60	25	0.3541										0.9984	8.04
	70	25	0.5012										0.9998	2.73
Page	50	10		0.3021						1.0445			0.9995	5.04
	60	10		0.4117						1.0232			0.9993	6.20
	70	10		0.3990						1.1970			0.9994	6.54
	50	20		0.2613						1.1093			0.9999	2.89
	60	20		0.4292						0.9909			0.9999	7.76
	70	20		0.5180						1.0262			0.9998	6.91
	50	25		0.2295						1.1339			0.9998	3.47
	60	25		0.3016						1.1290			0.9996	1.13
	70	25		0.4859						1.0336			0.9999	3.11
Modified Page	50	10	1.3320							0.2408			0.9994	52.12
	60	10	2.1529							0.1960			0.9993	12.45
	70	10	0.3619							1.3226			0.9975	11.76
	50	20	0.8337							0.3654			0.9989	42.16
	60	20	1.0769							0.3649			0.9999	25.24
	70	20	0.2806							1.8886			0.9998	14.23
	50	25	0.3011							0.9299			0.9983	23.24
	60	25	0.5352							0.6615			0.9984	12.46
	70	25	1.1348							0.4417			0.9998	13.49
Henderson and Pabis	50	10	0.3255		1.0153								0.9995	4.39
	60	10	0.4248		1.0069								0.9993	5.37
	70	10	0.4897		1.0260								0.9979	10.94
	50	20	0.3121		1.0263								0.9992	5.35
	60	20	0.4243		0.9976								0.9999	1.80
	70	20	0.5319		1.0039								0.9998	3.50
	50	25	0.2889		1.0345								0.9988	6.15
	60	25	0.3629		1.0270								0.9987	7.19
	70	25	0.5033		1.0045								0.9999	2.64
Logarithmic	50	10	0.3266		1.0148				0.0010				0.9995	4.38
	60	10	0.4353		1.0027				0.0072				0.9996	5.75
	70	10	0.4917		1.0251				0.0014				0.9979	10.91
	50	20	0.3053		1.0299				-0.0068				0.9993	4.88
	60	20	0.4249		0.9974				0.0004				0.9999	11.79
	70	20	0.5378		1.0016				0.0034				0.9998	2.96
	50	25	0.2795		1.0399				-0.0104				0.9991	6.40
	60	25	0.3606		1.0281				-0.0019				0.9987	7.15
	70	25	0.5045		1.0039				0.0008				0.9999	2.61
Wang and Singh	50	10				-0.1561		0.0006					0.9073	55.91
	60	10				-0.1656		0.0061					0.8029	87.46
	70	10				-0.1706		0.0064					0.7540	65.24
	50	20				-0.1552		0.0055					0.9294	23.45
	60	20				-0.1667		0.0061					0.8112	42.15
	70	20				-0.1724		0.0065					0.6874	38.75
	50	25				-0.1511		0.0053					0.9476	26.45
	60	25				-0.1615		0.0058					0.8860	25.89
	70	25				-0.1714		0.0064					0.7279	43.12
Two-term	50	10	0.3255		0.5076		0.5077				0.3255		0.9995	4.39
	60	10	0.4247		11.696		-10.6880				0.4247		0.9993	5.37
	70	10	0.3792		-26.809		27.8314				0.3826		0.9981	10.27
	50	20	0.2406		5.5089		-4.491				0.2278		0.9996	4.02
	60	20	0.4243		-10.468		11.4662				0.4243		0.9999	2.80
	70	20	0.6217		6.5284		-5.5269				0.6409		0.9998	3.35
	50	25	0.3136		1.1338		-0.1337				2.0307		0.9999	3.36
	60	25	0.3629		0.4003		0.6267				0.3629		0.9987	7.19
	70	25	0.4370		15.1284		-14.1255				0.4328		0.9999	2.43
Modified Henderson and Pabis	50	10	0.3254		0.3347		-0.0007		0.6813		0.1987	0.3253	0.9995	4.38
	60	10	0.4379		0.5072		0.0107		0.4925		0.0258	0.4379	0.9996	4.29
	70	10	0.4897		0.2941		0.3342		0.3977		0.4897	0.4896	0.9998	10.95
	50	20	0.3121		0.3578		0.3481		0.3204		0.3121	0.3121	0.9992	5.34
	60	20	0.4195		0.4959		0.4821		0.0208		0.4189	0.9571	0.9999	1.75
	70	20	0.5318		0.4397		0.4397		0.1246		0.5318	0.5322	0.9998	3.50
	50	25	0.2889		0.3795		0.3287		0.3263		0.2889	0.2889	0.9988	6.15
	60	25	0.3629		0.3425		0.3425		0.3421		0.3629	0.3629	0.9987	7.19
	70	25	0.4563		1.0658		0.7483		-0.8110		0.4567	0.4073	0.9999	2.43

Table 3. Equation of drying parameters

Model	Equation of drying parameter
Page model	k_1 = -0.213788 + 0.0101640T – 0.001372rh n = 1.108816 – 0.0005210T – 0.000061rh
Two-term model	a = 0.374339 – 0.2050430T + 0.6726070rh b = 0.639033 + 0.2050570T + 0.7285800rh g = 1.105957 – 0.0187900T + 0.0330210rh k = -0.174335 + 0.0093050T + 0.0044600rh
Modified Henderson and Pabis	a = 1.880409 – 0.0275530T – 0.1166950rh + 0.0021640Trh b = -0.890136 + 0.0128490T + 0.0207950rh + 0.0000680Trh c = -0.092083 + 0.0166290T + 0.1046900rh – 0.0023770Trh g = -0.964289 + 0.0186920T + 0.0342940rh – 0.0004030Trh p = -0.126497 + 0.0100560T + 0.0044100rh – 0.0000910Trh k = -0.045631 + 0.0083000T – 0.0056230rh + 0.0000490Trh

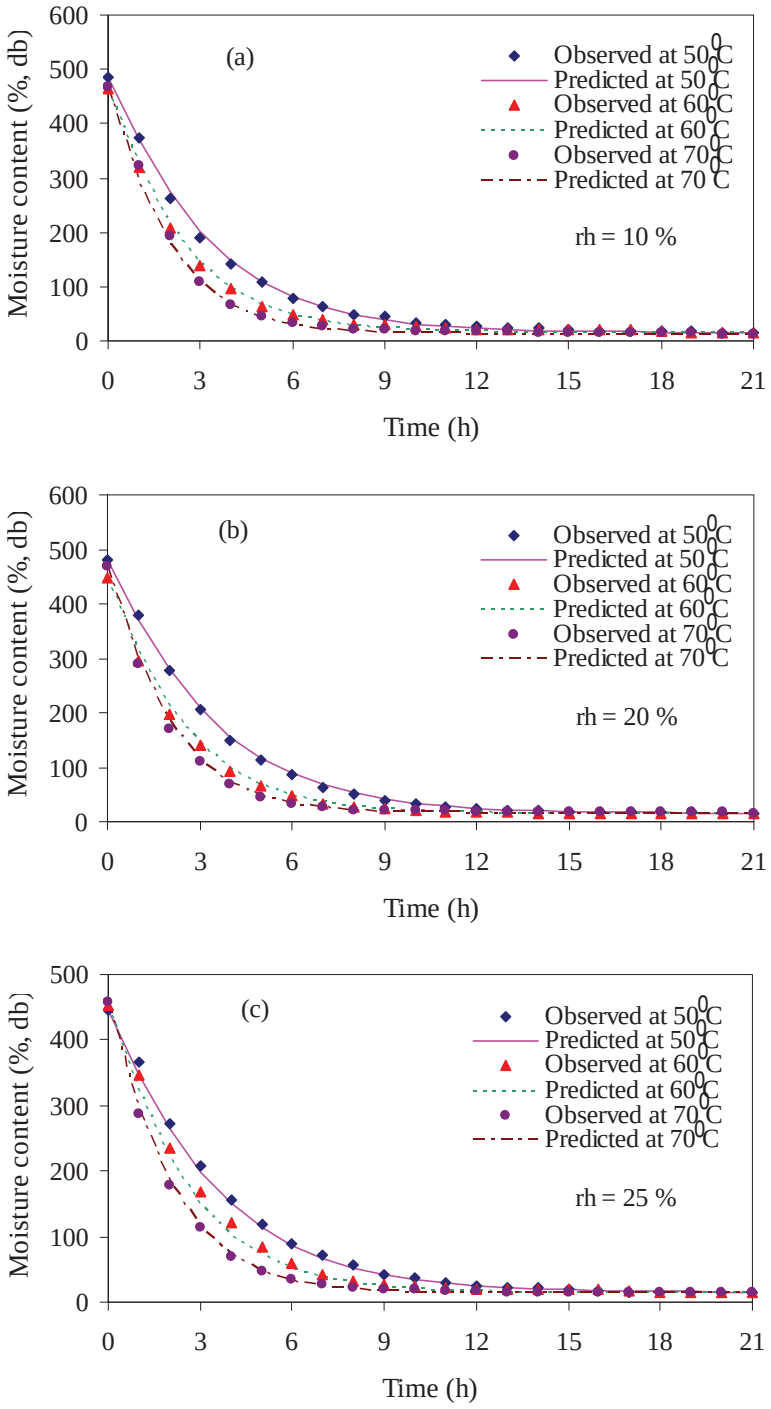

Fig. 6 Predicted and observed moisture content of peeled longan using Page model for a) T = 50, 60 and 70ºC and rh = 10%, b) T = 50, 60 and 70 ºC and rh = 20% and c) T = 50, 60 and 70ºC and rh = 25%

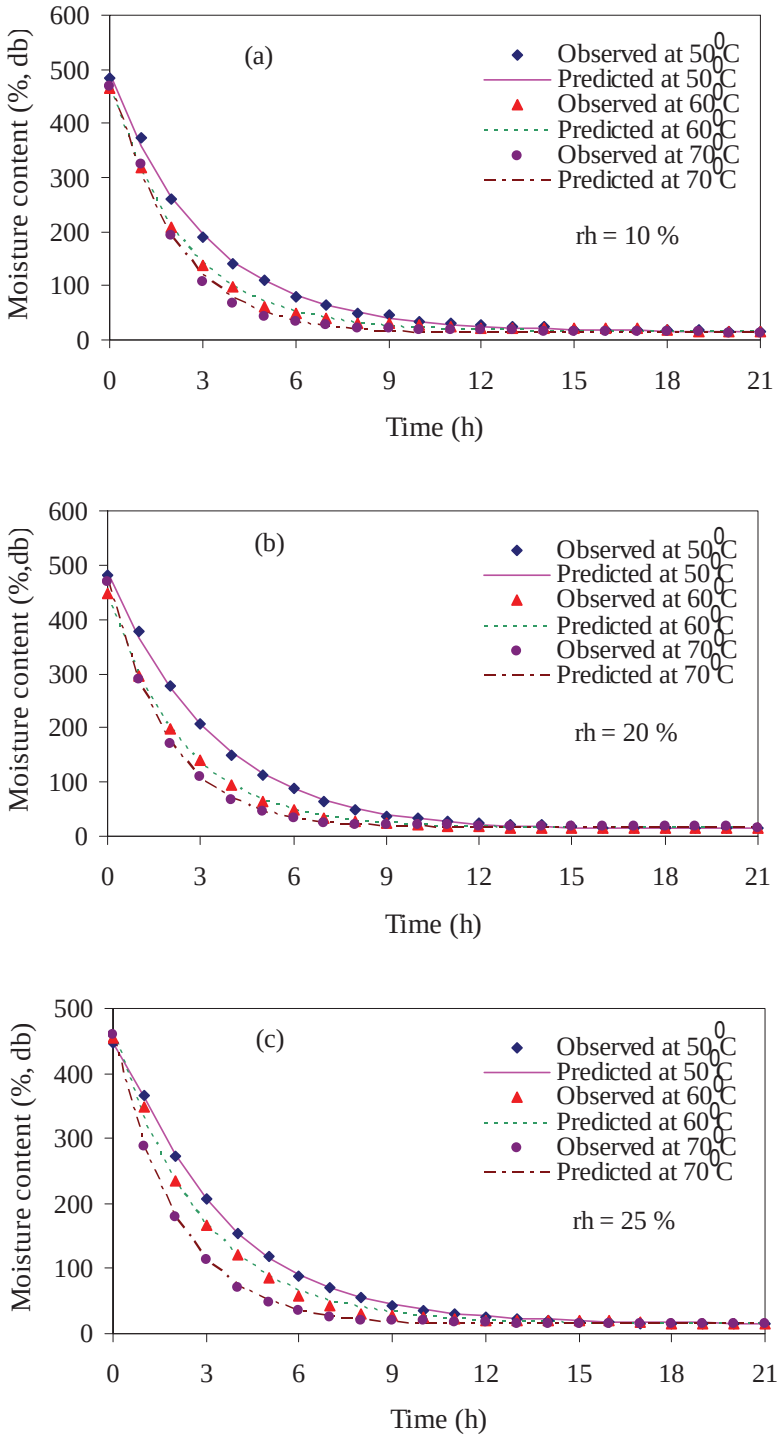

Fig. 7 Predicted and observed moisture content of peeled longan using Two-term model for a) T = 50, 60 and 70ºC and rh = 10%, b) T = 50, 60 and 70 ºC and rh = 20% and c) T = 50, 60 and 70ºC and rh = 25%

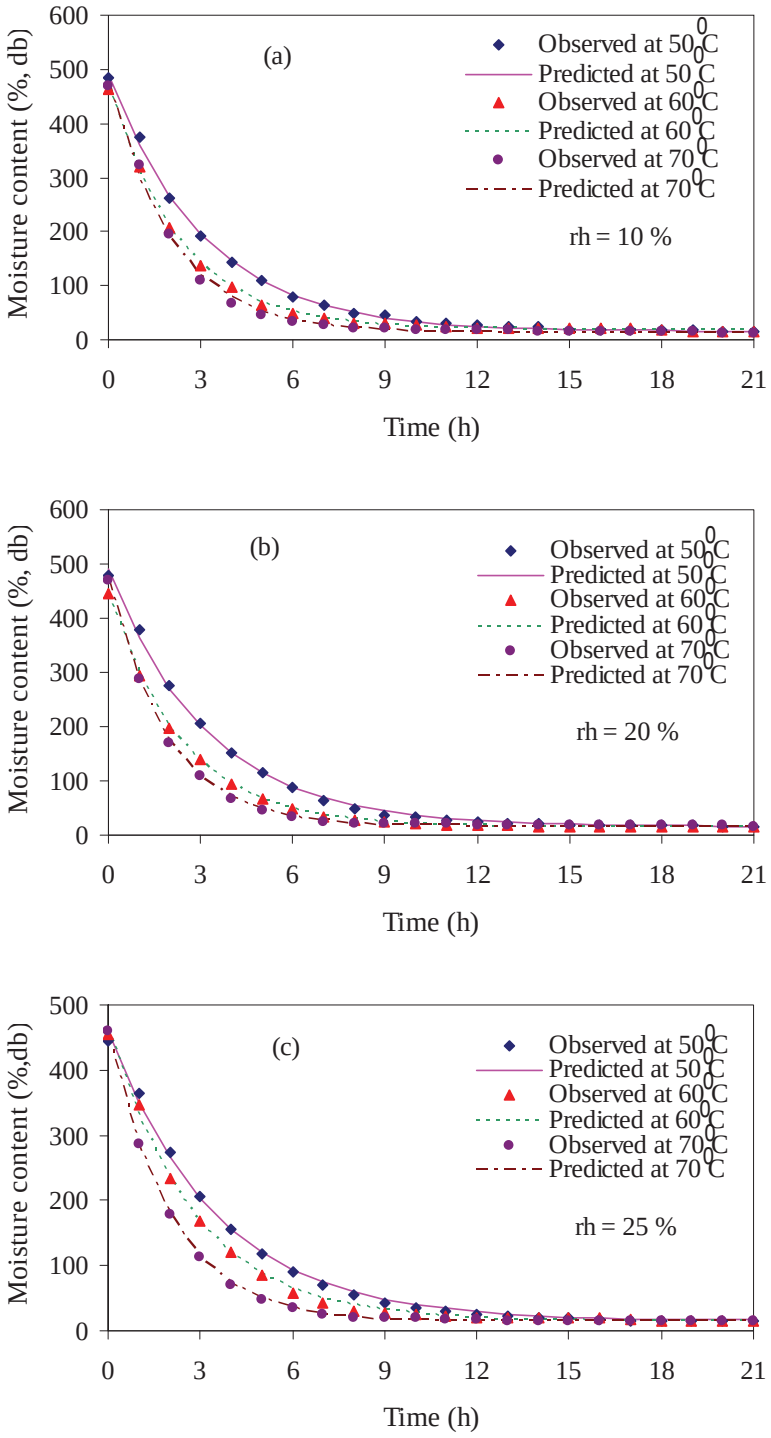

Fig. 8 Predicted and observed moisture content of peeled longan using modified Henderson and Pabis model for a) T = 50, 60 and 70ºC and rh = 10%, b) T = 50, 60 and 70 ºC and rh = 20% and c) T = 50, 60 and 70ºC and rh = 25%

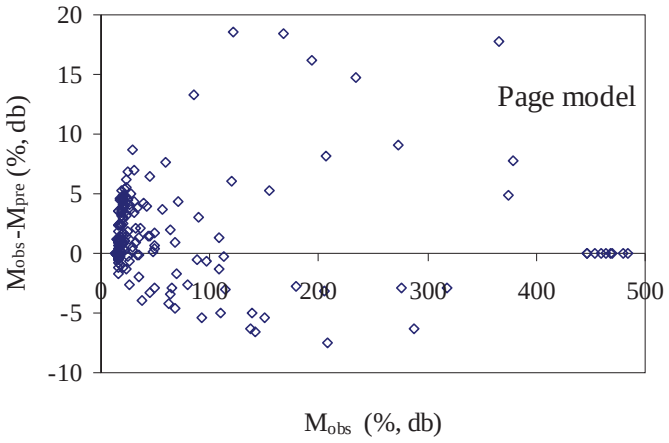

Fig. 9 Plot of residual between observed moisture content (M_{obs}) and predicted moisture content (M_{pre}) of peeled longan from Page model for different temperatures and relative humidities

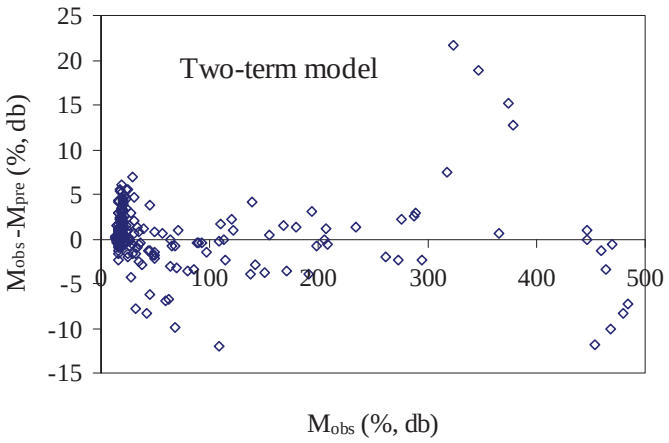

Fig. 10 Plot of residual between observed moisture content (M_{obs}) and predicted moisture content (M_{pre}) of peeled longan from Two-term model for different temperatures and relative humidities

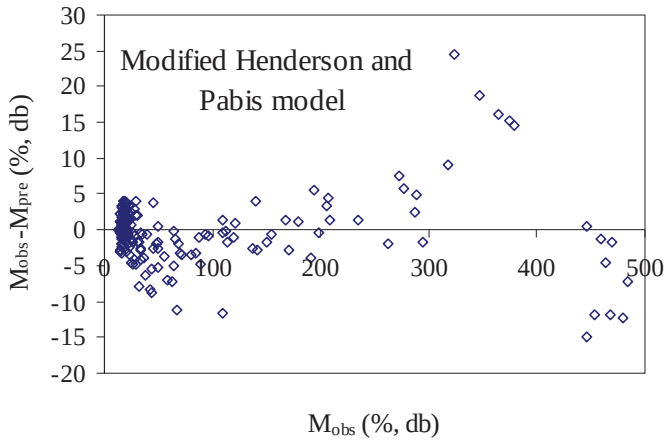

Fig. 11 Plot of residual between observed moisture content (M_{obs}) and predicted moisture content (M_{pre}) of peeled longan from modified Henderson and Pabis model for different temperatures and relative humidities

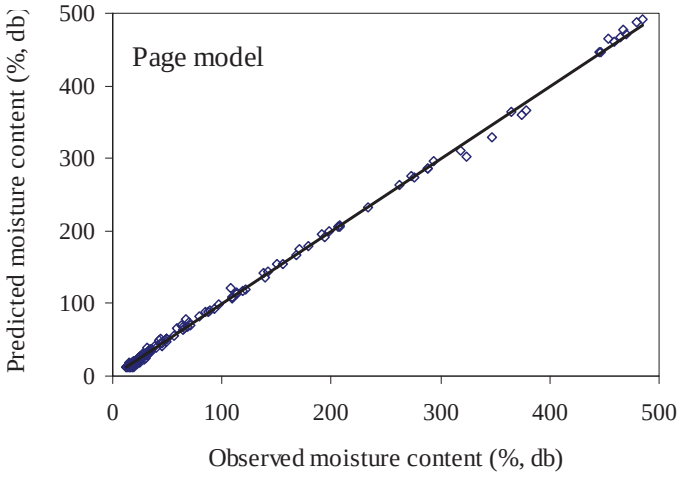

Fig. 12 Comparison of predicted moisture content from Page model and observed moisture content of peeled longan at different temperatures and relative humidities (R^2 = 0.9991)

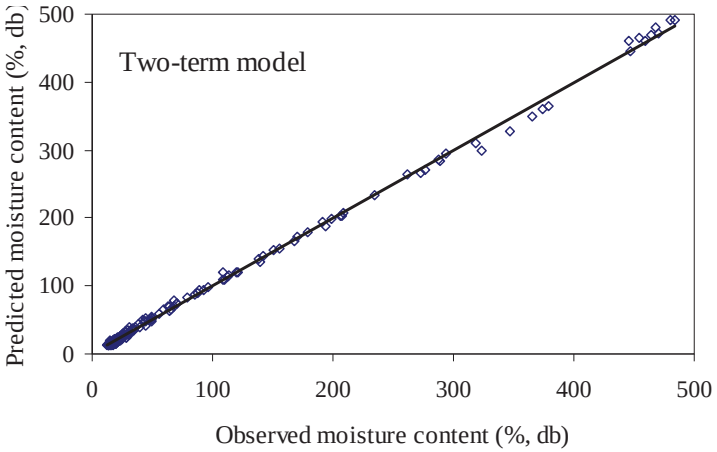

Fig. 13 Comparison of predicted moisture content from Two-term model and observed moisture content of peeled longan at different temperatures and relative humidities (R^2 = 0.9987)

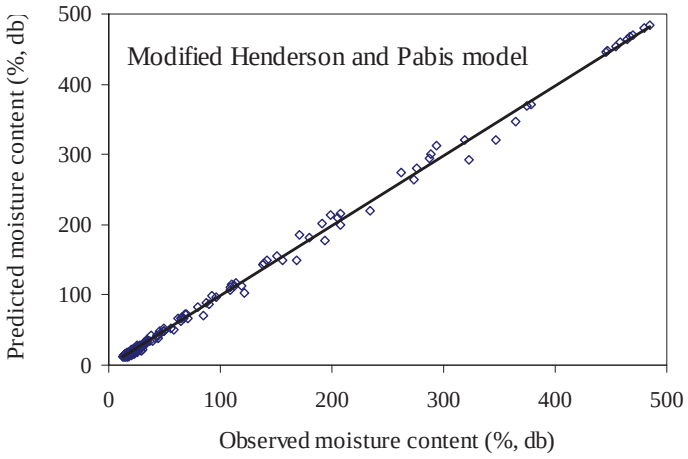

Fig. 14 Comparison of predicted moisture content from modified Henderson and Pabis model and observed moisture content of peeled longan at different temperatures and relative humidities (R^2 = 0.9985)

2.5.3 Colour change

The colour of peeled longan were measured before and after drying. Variations of colour of fresh and dried longan dried at different temperatures are shown in Table 4. The longan was dried to the desired moisture content at 50, 60 and 70ºC of drying temperatures and the colour indexes are shown in Fig. 15. From Table 4 and Fig. 15 it is observed that the lightness remains almost same for both fresh and dried longan. Drying increases the redness and more intensively the yellowness of longan which causes the golden colour of dried longan and it is a combination of L* (brightness), +a* (redness) and +b* (yellowness). The chroma (C*) of dried longan increases significantly (1.84 to

17.63-18.18) indicating colour saturation and this implies that the colour of dried longan was bright golden. Hue angles (h) of the dried longan decreases more significantly (232.43 to 50.31-52.760 and this implies that the colour of the peeled dried longan was golden brown for the temperature levels of 50, 60 and 70ºC which indicated the golden colour (mixture of large quantity of yellow and small quantity of red colour attributes) of the product. Thus, there is no difference in colour for dried longan for drying at 50 to 70 ºC. Achariyaviriya et al. (2001) reported that the maximum permissible air drying temperature for production of the desired golden brown colour of the peeled longan is 65ºC. But, this study supports that drying of peeled longan at 70 ºC does not affect the golden brown colour of dried longan.

Table 4. Colour variations of peeled longan dried at different temperatures.

Status	Treatments	Colour value				
		L*	a*	b*	C*	h
Fresh	Average of nine observations at ambient temperature	33.022	0.752	-0.663	1.843	232.43
Dried peeled longan	Average of three observations at 50 ºC	34.006	11.539	13.813	18.099	50.312
	Average of three observations at 60 ºC	34.583	11.128	14.213	18.177	51.679
	Average of three observations at 70 ºC	35.111	10.388	14.087	17.635	52.764

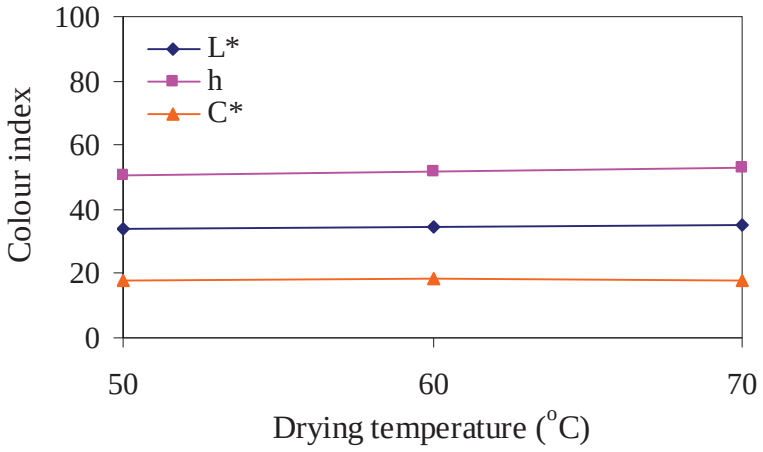

Fig. 15 Influence of drying temperature on lightness L*, hue angle (h) and chroma (C*) of peeled longan.

2.6 Conclusions

Thin layer drying of peeled longan was investigated in this study and the increase in drying air temperature from 50 to 70 ºC decreased the drying time from 21 hours to 10 hours. The entire drying process occurred in falling rate period and constant rate period was not observed. Drying rate is not affected by relative humidity in the range of 10% to 25%.

Eight thin layer drying models were fitted to the experimental data of peeled longan to describe the drying behaviour of peeled longan. Expressions of drying parameters with high coefficients of determination were developed. The Page model was the best followed by Two-term model and modified Henderson and Pabis model and the agreement between the predicted and experimental data was excellent for all these three models. Either one of these three models can be used to assess drying behaviour of peeled longan and also for simulation and optimization of the dryer for efficient operation. The colour of the peeled dried longan is golden brown for the temperature levels of 50, 60 and 70 ºC and there is no difference in colour for dried longan for drying at 50 to 70 ºC.

Chapter 3

Moisture Diffusivity Determination of Different Parts of Longan Fruit*

3.1 Introduction

The mature Longan fruit (*Dimocarpus Longan* Lour.) is a small (Ca. 1.5 – 2 cm diameter) conical, heart shaped or spherical in shape and light brown in color. It has a thin, leathery and indehiscent pericarp surrounding a succulent, edible white aril. The aril contains a relatively dark brown seed. Maturity can be determined on the basis of fruit weight, skin color, flesh sugar concentration, flesh acid concentration, sugar to acid ratio, flavor and/or days from an thesis. Longan fruits are non-climacteric with little change in soluble solid concentration (SSC) or titratable acidity (TA) after harvest. Longan fruits deteriorate rapidly unless proper handing and processing techniques are employed (Jiang el al., 2002).

Longan is an important commercial fruit in northern Thailand and it is widely processed as dried fruits for exporting to China. Conventional hot air dryer are widely used for the production of dried longan. Energy consumption and product quality are the prime concerns of drying of longan. To understand the transport processes during drying is of importance for production of better quality of dried product and knowledge of the moisture diffusivity of longan is essential to understand the transport processes during drying.

Longan is a complex fruit consisting of shell, flesh, seed coat, seed and seed stalk (Fig. 16). Because of their varying composition and microstructure, these components have different physical properties including moisture diffusivity. Moisture movement based on Fick's second law of diffusion can be used to interpret the phenomena of drying of longan fruit and the moisture diffusivities of longan fruit components are needed to accurately predict the moisture transfer during drying.

---

* This chapter has been published in Journal of Food Properties vol. 10, page 471-478. (2007)

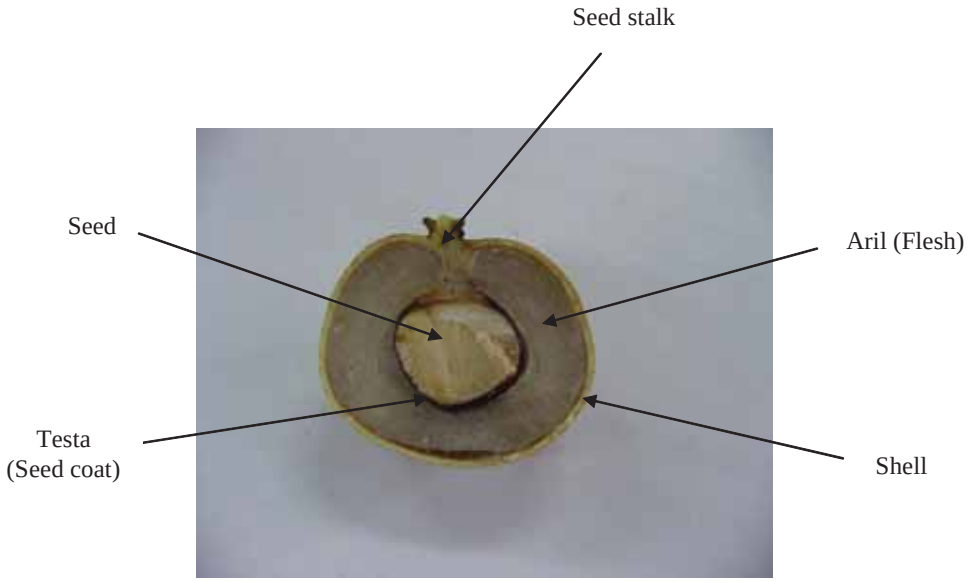

Fig. 16 Anatomy of longan fruit

Extensive research has been done on moisture diffusivity of single kernels and components of a kernel of different grains (Kang and Delwiche, 2000; Gaston et al., 2002; Giner and Mascheroni, 2002; Muthukumarappan and gunasekaran, 1994(a-c); Steffe and Singh, 1980(a-c)). Severed studies have been reported on moisture diffusivity of fruits, vegetables and spices (Azzouz el al., 2002; Babalis and Belessiotis, 2004; Sharma and Prasad, 2004; Doymaz, 2005; Nguyen et al., 2006; Kaleemullah and Kailappan, 2006). Panagiotou et al. (2004) reported moisture diffusivity of more than 100 food materials classified in 11 food categories and results concern the reported range of variation of moisture data together with corresponded range of variation of material moisture content and temperature. Limited studies have been on overall effective diffusivity of longan fruit (Achariyaviriya, 2003; Achariyaviriya et al., 2001; Achariyaviriya et al., 2003; Moreno-Castillo et al., 2005). But negligible study has been reported on the component diffusivities of the longan fruit. Purpose of this study is to determine the component diffusivities of the longan fruit.

3.2 Materials and methods

Longan fruit used in this investigation was collected from a fresh market of Chiang Mai, Thailand and it was stored at 5°C in the Department of Food Engineering, Silpakron University, Nakhon Pathom. The initial moisture content of fresh longan was about 84 % (wb). It was neither treated with chemicals or separated into components before conducting the experiment. Before starting an experiment the fruits were left in the room temperature in the laboratory in the Department of Physics, Silpakorn University, Nakhon Pathom, Thailand, and then single fruits were separated into shell, flesh, seed coat, seed and seed stalk. Each of the components was dried separately in a laboratory dryer in the Physics Department, Silpakorn University, Nakhon Pathom, Thailand, under controlled

conditions of temperature and relative humidity. The thin layer drying apparatus used is similar to that described by Guarte (1996). The laboratory drying apparatus consists of a centrifugal blower, a drying section, an electrical resistance air heating section, measurement sensors, and data recording and controlling system with a personal computer. The thin layer drying tests were conducted in the temperature range of 50°C to 80°C and the relative humidity of the drying air from 1.5 to 13.33 %. Four set of experiments was conducted for each of the components of the longan fruit.

Before starting an experiment the drying apparatus was allowed to run for one hour to obtain steady temperature. Thin layer drying of the longan component was conducted at a temperature of 50, 60, 70 and 80°C. For each experiment about 100 g of the components of the fresh longan fruit was spread in the drying chamber is a single layer. All the drying experiments were carried out at an air velocity of 0.2 m/s. The drying air temperatures were monitored using thermocouple (K type) connected to a personal computer using an interface at an interval of 5 min and the weights of longan components were recorded by an electronic balance (accuracy ± 0.01 g) at an interval of one hour. Removing, weighting and replacement needed about 2 min.

3.3 Theoretical consideration

Fick's second law of the unsteady state diffusion, neglecting the effects of temperature and total pressure gradient, can be used to describe the drying behavior of fruits (Bala, 1997).

$$\frac{\partial M}{\partial t} = \mathrm{Div}\left(D \ \mathrm{grad}\ M\right) \tag{1}$$

This equation can be solved for different standard shapes of the drying material. These equations are:

For sphere

$$\frac{M - M_e}{M_o - M_e} = \frac{6}{\pi^2} \sum_{n=1}^{\infty} \frac{1}{n^2} \exp\left(-n^2 \pi^2 \frac{D_{eff}\, t}{r_0^2} \right) \tag{2}$$

For cylinder

$$\frac{M - M_e}{M_o - M_e} = \sum_{n=1}^{\infty} \frac{4}{r^2 (\alpha_n)^2} \exp\left(-(\alpha_n)^2 \frac{D_{eff}\, t}{r^2} \right) \tag{3}$$

For slab of half thickness, z

$$\frac{M - M_e}{M_0 - M_e} = \frac{8}{\pi^2} \sum_{n=1}^{\infty} \frac{4}{(2n-1)^2} \exp\left(-(2n-1)^2 \frac{D_{eff} t}{z^2} \right) \quad (4)$$

Equations (2) to (4) can be fitted to the experimental data of the products if the products have the shapes of sphere, cylinder and slab and the diffusivity can be determined minimizing sum of squares of the deviations between the predicted and experimental data.

The following assumptions are made in solving the Equations (2) to (4):

(1) Drying is isothermal

(2) The fruit consists of five components: seed, seed stalk, flesh, seed coat and shell. The seed is spherical and the seed stalk is cylindrical in shape, and the flesh, seed coat and shell are cut into the shape of slab.

(3) Each component of the fruit is homogenous.

(4) Initial moisture content is uniform

(5) Moisture movement is one directional

(6) Diffusivity is constant for each component of the fruit

(7) Shrinkage is negligible.

3.4 Determination of diffusivities

Thin layer drying models of sphere for the seed, slab for flesh, seed coat and shell, and cylinder for the seed stalk were fitted to experimental data of thin layer drying of the components of the longan fruit. The suitability of the models was determined by using standard error of estimate and coefficient of determination. Equation (2) was fitted to the experimental data of seed, equation (3) was fitted to the experimental data of seed stalk and equation (4) was fitted to the experimental data of flesh, shell and seed coat. Moisture diffusivity of each of the components of the longan fruit was determined by minimizing the sum of square of derivations between the experimental and predicted values for thin layer drying of the components under controlled conditions of air temperature and relative humidity.

3.5 Results and discussions

The influences of drying air temperature on drying curves for different components are shown in Fig. 17. The drying rate of the different components of longan increased with the increase of drying air temperature. The agreement between the predicted and observed results of moisture content of different components of longan fruit was found to be excellent. The comparison of the predicted values

and experimental data of the moisture content for flesh of longan for different temperature are shown in Fig. 18 and the agreement between the predicted and experimental value is excellent (R^2=0.99).

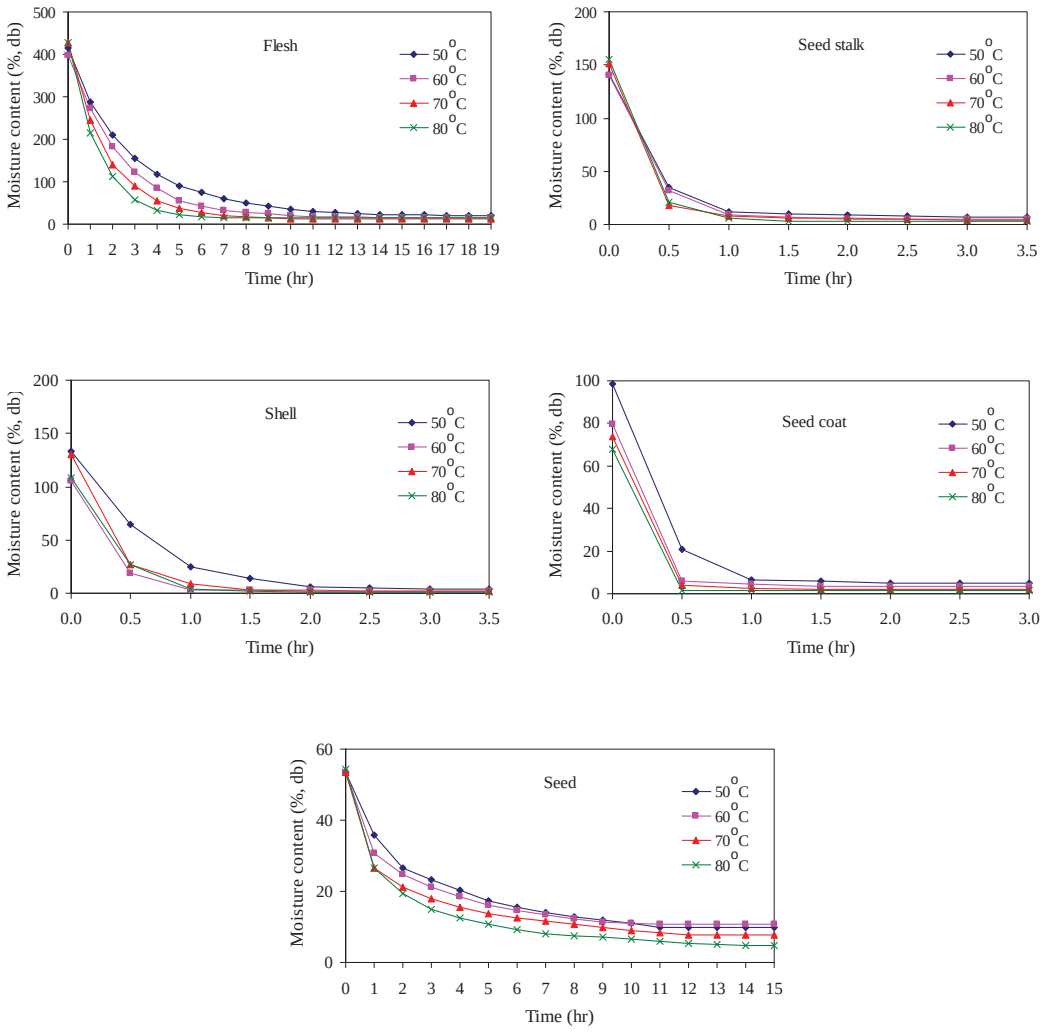

Fig.17 Influences of the drying air temperatures on drying curves for different components of longan fruit

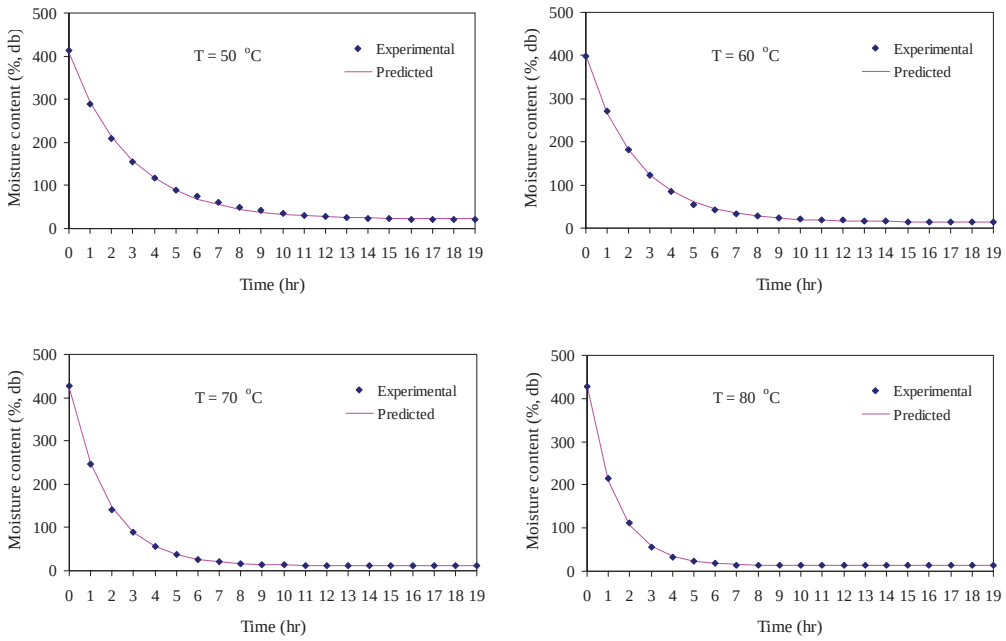

Fig. 18 Comparison of predicted values and experimental data of flesh of longan fruit for temperature of 50°C, 60°C, 70°C, and 80°C

The diffusivities of the different components of the longan are shown in Table 5. The diffusivity of the flesh of longan is highly temperature dependent but for other components the diffusivity is independent of temperature. The diffusivity of the flesh can expressed as a function of temperature using Arrhenius type equation as:

$$D_{flesh} = 5.0\times10^{-9} e^{\left(\frac{-0.2717}{T_{ab}}\right)} \qquad R^2 = 0.99 \qquad (5)$$

Table 5 Diffusivities of different components of longan fruit

Component	Diffusivity (m^2/s) at temperature: 50°C	60°C	70°C	80°C	Mean diffusivity (m^2/s)
Flesh	1.819×10^{-9}	2.431×10^{-9}	3.086×10^{-9}	4.156×10^{-9}	2.867×10^{-9}
Shell	2.524×10^{-11}	2.53×10^{-11}	1.97×10^{-11}	2.25×10^{-11}	2.32×10^{-11}
Seed stalk	$2{,}524\times10^{-9}$	2.56×10^{-9}	2.07×10^{-9}	2.42×10^{-9}	2.39×10^{-9}
Seed coat	5.133×10^{-12}	4.74×10^{-12}	4.61×10^{-12}	3.49×10^{-12}	4.49×10^{-12}
Seed	2.936×10^{-10}	3.14×10^{-10}	2.63×10^{-10}	3.34×10^{-10}	3.01×10^{-10}

Fig. 19 shows the variation of the moisture diffusivity of flesh of longan fruit as a function of the reciprocal of absolute drying air temperature. Achariyaviriya et al. (2001) reported the effective diffusivity of single longan fruit in the range of 1.389×10^{-11} to 3.750×10^{-10} m^2/s. The mean value of the components of the longan fruit in this study lies in the range of 4.494×10^{-12} to 2.867×10^{-9} m^2/s and it is within the range of effective diffusivity of single longan fruit reported by Achariyaviriya et al. (2001). The mean value of the diffusivity of mango lies within the range of 8.846×10^{-11} to 1.935×10^{-10} m^2/s, but the range is very narrow. This might be due to the difference in biological structure of longan and mango.

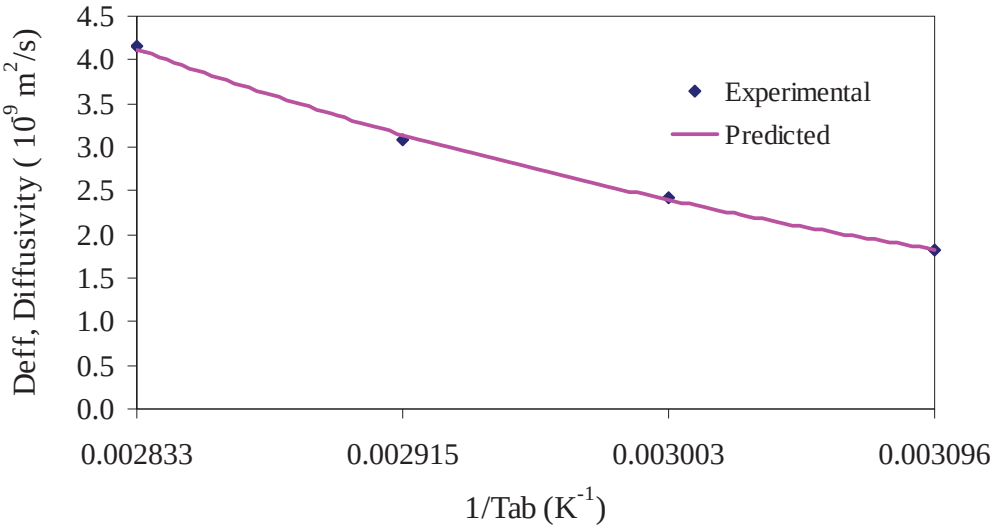

Fig. 19 Variation of the moisture diffusivity of flesh of longan fruit as a function of the reciprocal of absolute drying air temperature

3.6 Conclusions

Moisture diffusivity of flesh of longan fruit increased with air temperature. But the air diffusivities of shell, seed coat, seed and seed stalk were independent of temperature changes. Moisture diffusivities of shell and seed coat were much lower than those of the other components of longan fruit. Temperature dependence of the flesh of the longan fruit can be satisfactorily described by an Arrhenius-type equation. The mean value of the diffusivity of the components of the longan fruit in this study lies in the range of 4.494×10^{-12} to 2.867×10^{-9} m^2/s.

Chapter 4

Finite Element Simulation of Drying of Longan Fruit*

4.1 Introduction

Longan fruit is usually dried in convectional dryers. A knowledge of the transport processes is essential for the production of quality dried longan and energy conservation of the drying process. Understanding and controlling of the drying process are also important in establishing improved design guidelines for drying systems. This requires an accurate description of the drying mechanism (Mujumdar, 2000; Haghighi and Segerlind, 1988).

Considerable theoretical and experimental works have been carried out in the past decades to describe the drying of biological materials (Irudayaraj et al., 1990; Irudayaraj and Haghighi, 1993; Olivelra et al., 1995; Liu and Irudayaraj, 1995; Haghighi and Aguirre, 1999; Hawlader ey al., 2006; Ochoa-Martinez et al., 2007). Several studies have been conducted on finite element modelling of drying of cereal grains (Muthukumarappan et al., 1996; Sarker et al., 1996; Lan and Kunze, 1996; Kang and Delwiche, 1999; Neminyi et al., 2000; Gaston et al., 2002; Jia et al., 2002). A number of studies have been reported on finite element modelling of heating and drying of food materials (Haghighi, 1990; Bon et al., 2007; Zhou et al., 1995; Ranjan et al., 2004; Pandit and Prasad, 2004; Romano e al., 2005; Nguyen et al., 2006; Janjai et al., 2008). However, limited studies have been reported on modelling of drying of longan fruit (Achariyaviriya, 2001; Achariyaviriya et al., 2001). No study has been reported on finite element modelling of drying of longan fruit.

Longan fruit comprises five components: seed, flesh, shell, seed coat and seed stalk (Fig. 16). Moisture diffusivities of these components have been reported by Janjai et al (Janjai et al., 2007). Moisture diffusivities of the shell and seed coat are much lower than those of the flesh, seed stalk and seed. These components limit the movement of moisture while the diffusivities of flesh, seed stalk and seed are quite high and thus facilitate the transport of moisture. These facts make it worthwhile to investigate the drying behaviour of longan fruit using the different diffusivities for the different components. The purpose of this paper is to determine how we can simulate the moisture diffusion in longan fruit during drying using the different moisture diffusivities for the different components.

---

* This chapter has been published in Drying Technology vol. 26, page 666-674. (2008)

Among several numerical methods available in simulation study, two methods have been mainly applied to model heat and mass transfer: the finite difference method and the finite element method. The finite element method assumes that any continuous quantity such as moisture content can be approximated by a discrete model composed of a set of piecewise continuous functions defined over a finite number of sub-domains or elements (Segerlind, 1984). Elements are connected at nodal points along the boundaries and their equations are obtained by minimizing a function of the physical problem. The finite element method has been extensively used to solve problems having irregular geometrical configurations and material properties depending on the temperature and moisture. This study aims to use the finite element method to simulate the drying of longan fruit using the component diffusivities.

4.2 Materials and method

The longan fruit used in this investigation was stored at 50 °C. The initial moisture content of fresh longan was about 71% (wb). It was neither treated with chemicals nor separated into components before the experiment. Prior to an experiment, the fruits were left at room temperature in the laboratory for about 16 hours to attain a temperature in equilibrium with the room temperature. A single layer of longan fruit was dried in a laboratory dryer under controlled conditions of temperature and relative humidity. The laboratory dryer used is similar to that described by Guarte (1996). The schematic diagram of this laboratory dryer is shown in Fig. 20. The laboratory dryer consists of a ceramic packed-bed for producing saturated air at a given temperature, an electrical heater, a blower, a drying section, measurement sensors and a data recording and controlling system with a personal computer. In this laboratory dryer, the blower sucks ambient air to flow through a humid ceramic packed-bed. The air absorbs moisture while it passes through the packed-bed. At the top of the packed-bed, this air becomes saturated. The saturation is checked by using relative humidity sensor. Then this saturated air is heated by the air heater and blown to the product on the tray. Users can chose the through-flow drying mode or over-flow drying mode by closing or opening the air flaps to control the flow direction. The relative humidity and temperature of the drying air are controlled by adjusting the power of the air heater and the water heater using a psychometric chart as a guideline. In our experiments, the thin layer drying tests with the over-flow mode were conducted in the temperature range of 50 °C to 70 °C and the relative humidity of the drying air of 8-14 %.

Prior to an experiment the laboratory dryer was allowed to run for 0.5 hour to obtain steady temperature. For each experiment, about 500 g of fresh longan fruit was placed in the drying chamber in a single layer. All the drying experiments were carried out at an air velocity of 0.2 m/s. The low air velocity was used because this finite element model was planned to be used for deep-bed drying simulations of longan in the future and low air velocity will be used in the deep-bed drying simulations. The drying air temperatures were monitored using a thermocouple (K type) connected to a personal computer using an interface at an interval of 5 min and the weights of longan components were recorded by an electronic balance (accuracy ± 0.01 g) at an interval of one hour.

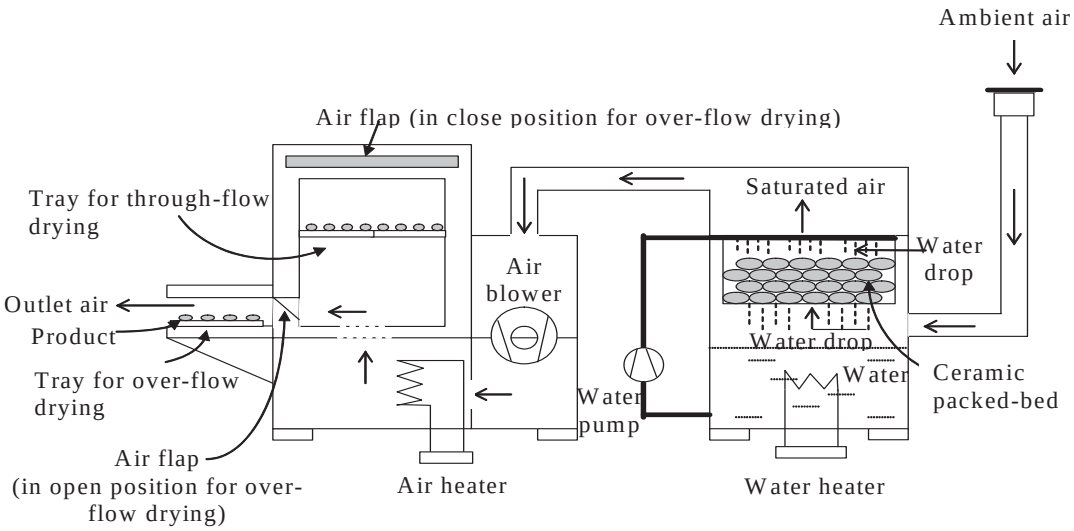

Fig. 20 Schematic diagram of the laboratory dryer

4.3 Finite element modeling of longan drying

Fick's law of diffusion is used in modelling the moisture movement within longan fruit during drying and the general equation which describes the moisture diffusion can be expressed as (Bala, 1998):

$$\frac{\partial M}{\partial t} = \nabla.(D \nabla M) \qquad (1)$$

where M is moisture content on a dry basis (%, db), D is moisture diffusivity and t is time.

The following assumptions are made in solving Eq. (1) for longan fruit using the finite element method:

1) Drying is isothermal.
2) The fruit consists of five components: seed, seed stalk, flesh, seed coat and shell. The fruit is spherical and the seed stalk is cylindrical in shape.
3) Each component of the fruit is homogenous.
4) Initial moisture content is uniform for each of the fruit components.
5) Moisture movement inside the longan fruit is two directional.
6) Shrinkage is mainly in the flesh of the fruit.

In two dimensions, the diffusion equation becomes:

$$\frac{\partial \mathrm{M}}{\partial \mathrm{t}} = \frac{\partial}{\partial \mathrm{x}}\left[\mathrm{D}\frac{\partial \mathrm{M}}{\partial \mathrm{x}}\right] + \frac{\partial}{\partial \mathrm{y}}\left[\mathrm{D}\frac{\partial \mathrm{M}}{\partial \mathrm{y}}\right] \tag{2}$$

with initial and boundary condition

$$\text{at t = 0} \qquad \mathrm{M} = \mathrm{M}_0 \tag{3}$$

$$\text{and} \qquad \text{at t>0} \qquad -D\frac{\partial M}{\partial n} = h_m\left(M_s - M_e\right) \tag{4}$$

where $\mathrm{h_m}$ is the mass transfer coefficient, $\mathrm{M_e}$ is the equilibrium moisture content on a dry basis (%, db), $\mathrm{M_s}$ is the surface moisture content on a dry basis (%,db) and *n* is the magnitude of a normal vector to the surface.

The finite element equations are obtained using Galerkin's formulation of the weighted residual method and Eq. (2) using Galerkin's method can be expressed as (Segerlind, 1984):

$$\int_{\Omega}[\mathrm{N}]^{\mathrm{T}}\left(\frac{\partial}{\partial \mathrm{x}}\left[\mathrm{D}\frac{\partial \mathrm{M}}{\partial \mathrm{x}}\right] + \frac{\partial}{\partial \mathrm{y}}\left[\mathrm{D}\frac{\partial \mathrm{M}}{\partial \mathrm{y}}\right] - \frac{\partial \mathrm{M}}{\partial \mathrm{t}}\right)\mathrm{d}\Omega = 0 \tag{5}$$

where [N] is a matrix of interpolating function and Ω is the fruit domain.

A system of equations is developed by evaluating the weighted residual integral. Using Green's theorem and simplifying the results, the following first order differential equation can obtained as:

$$[\mathrm{c}]\frac{\mathrm{d}\{\mathrm{M}\}}{\mathrm{dt}} + [\mathrm{k}]\{\mathrm{M}\} = \{\mathrm{f}\} \tag{6}$$

$$\text{where} \quad [\mathrm{c}] = \text{element capacitance matrix} = \int_{\Omega}[\mathrm{N}]^{\mathrm{T}}[\mathrm{N}]\mathrm{d}\Omega \tag{7}$$

$$[\mathrm{k}] = \text{element stiffness matrix} = \int_{\Omega}\mathrm{D}\left(\frac{\partial[\mathrm{N}]}{\partial \mathrm{x}}\frac{\partial \mathrm{N}}{\partial \mathrm{x}} + \frac{\partial[\mathrm{N}]}{\partial \mathrm{y}}\frac{\partial \mathrm{N}}{\partial \mathrm{y}}\right)\mathrm{d}\Omega \tag{8}$$

$\{\mathrm{M}\}$ = vectors of unknown which can be defined as

$$\mathrm{M} = [\mathrm{N}]\{\mathrm{M}\} \tag{9}$$

{f} = element force vector.

When the element matrices [c] are combined with the element matrices [k] using the direct stiffness procedure, the final result is a system of first order differential equations (Segerlind, 1984):

$$[C]\left\{\frac{\partial M}{\partial t}\right\} + [K]\{M\} - \{F\} = 0 \tag{10}$$

where [C] = global capacitance matrix
[K] = global stiffness matrix
{F} = load force vector

Eq. (10) in the finite difference form can be expressed as:

$$([C] + \Delta t[K])\{M\}_{t+\Delta t} = [C]\{M\}_t + \Delta t\{F\}_{t+\Delta t} \tag{11}$$

where Δt is the time step.
The final system of Eq. (11) has the following form

$$[A]\{M\}_{t+\Delta t} = [P]\{M\}_t + \{F_*\} \tag{12}$$

where
$$[A] = ([C] + \Delta t[K]) \tag{13}$$
$$[P] = [C]$$
$$\{F_*\} = \Delta t\{M_e\}_{t+\Delta t}$$

The longan fruit is considered as a spheroid embedded with a small cylindrical seed stalk at the top of the fruit as shown in Fig. 16 it is symmetrical around the central line of both the fruit and the seed stalk. Moisture moves from the interior of the fruit to the outward surface by diffusion and passes through different sections of the fruit having different diffusivities. The moisture diffusion is considered to be symmetrical from the common axis of the spherical fruit and cylindrical seed stalk. A two dimensional central axis symmetric finite element triangular grid is used to model the fruit and the only the half section of the domain in two dimensions is considered because of the geometric and transfer symmetries. This domain consists of seed stalk, shell, flesh, seed coat and seed. Fig. 21 shows finite element discrimination of half of the axis symmetric two dimensional section of a longan fruit and it consists of 78 nodes and 120 triangular elements. The moisture content of a longan fruit was computed using the method proposed by Haghighi and Segerlind (1988).

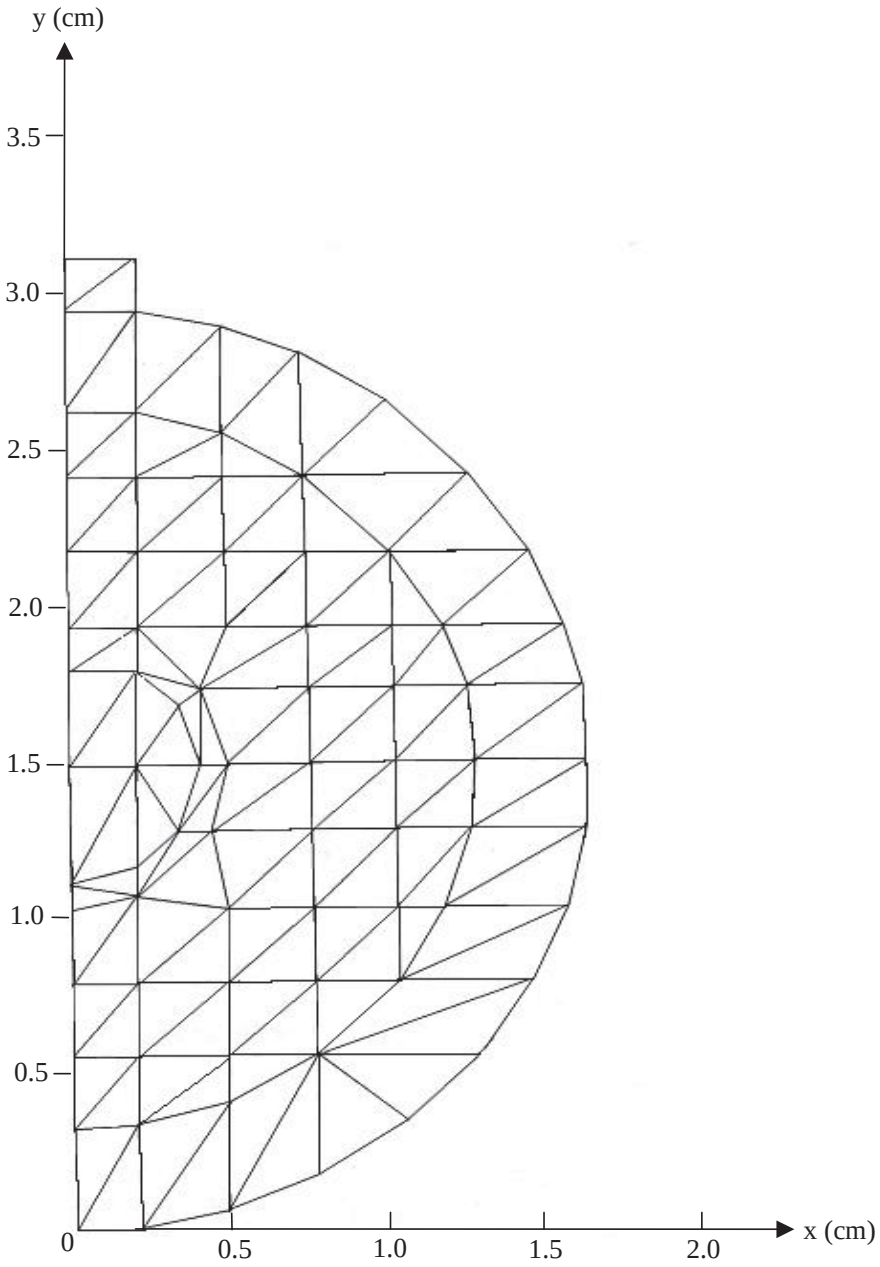

Fig. 21 Finite element grid for half of a single fruit of longan

4.4 Thermo-physical properties of longan

4.4.1 Moisture diffusivity of longan

Fick's law of diffusion incorporated with drying experiments has been widely used to determined moisture diffusivities of various fruits and other biological materials (Kechaou and Maalej, 2000; Achriyaviriya et al., 2000; Efremov and Hudra, 2000; Simal et al., 2006; Lagunez-Rivera et al., 2007). In this work, the moisture diffusivities of the components of longan fruit determined by Janjai et al (2007) were employed in the finite element model. They modeled the components of the longan fruit as a sphere for seed, cylinder for seed stalk and slab for seed coat, shell and flesh and the following analytical solutions were adopted:

For sphere of radius of r_0

$$\frac{M - M_e}{M_o - M_e} = \frac{6}{\pi^2}\sum_{n=1}^{\infty}\frac{1}{n^2}\exp\left(-n^2\pi^2\frac{Dt}{r_0^2}\right) \tag{14}$$

For cylinder of radius of r

$$\frac{M - M_e}{M_o - M_e} = \sum_{n=1}^{\infty}\frac{4}{r^2(\alpha_n)^2}\exp\left(-(\alpha_n)^2\frac{Dt}{r^2}\right) \tag{15}$$

For slab of half thickness, z

$$\frac{M - M_e}{M_o - M_e} = \frac{8}{\pi^2}\sum_{n=1}^{\infty}\frac{4}{(2n-1)^2}\exp\left(-(2n-1)^2\frac{Dt}{z^2}\right) \tag{16}$$

Then moisture diffusivities were determined by minimizing the sum of square of derivations between the predicted and experimental values of moisture content of thin layer drying under controlled conditions of air temperature and relative humidity. Experimental data were obtained from thin layer drying of the components in the form of sphere for seed, cylinder for seed stalk and slab for seed coat, shell and flesh. Air temperatures of 50°C, 60°C and 70°C and relative humidity in the range of 1.5-13.3% were used. The diffusivities of the components of the longan fruit are shown in Table 6. The diffusivity of flesh of longan fruit increased with temperature but the diffusivities of shell, seed coat, seed and seed stalk were independent of temperature. The diffusivity of the flesh (D_{flesh}) was expressed as a function of temperature (T_{ab}) using Arrhenius type equation as:

$$D_{flesh} = 0.3333\times10^{-6}e^{\left(\frac{-0.2718}{T_{ab}}\right)} \qquad R^2 = 0.99 \tag{17}$$

Table 6 Diffusivities of different components of longan fruit

Component	Diffusivity (m^2/hr) at temperature of			Mean diffusivity (m^2/hr)
	50°C	60°C	70°C	
Flesh	0.655×10^{-5}	0.875×10^{-5}	1.111×10^{-5}	1.032×10^{-5}
Shell	9.086×10^{-8}	9.112×10^{-8}	7.087×10^{-8}	8.346×10^{-8}
Seed stalk	9.086×10^{-6}	9.213×10^{-6}	7.466×10^{-6}	8.618×10^{-6}
Seed coat	1.848×10^{-8}	1.708×10^{-8}	1.658×10^{-8}	1.618×10^{-8}
Seed	1.057×10^{-6}	1.130×10^{-6}	0.948×10^{-6}	1.084×10^{-6}

The moisture diffusivities of the shell and the seed coat were much lower than those of the other components.

It was observed experimentally that there was no appreciable shrinkage of the shell and the seed. In addition, the flesh inside the shell had significant shrinkage and an air gap between the shell and the flesh was occurred during drying. Thus, the total volume of the combination of the air gap and the flesh inside longan fruit remained the same and the volume shrinkage in the flesh (Δs) is equal to the volume increase in the air gap.

The effective diffusivity (D_{eff}) of the combination of the flesh with the thickness of Δx_{fr} and the air gap (Δx_{ar}) between the shell and the flesh is computed from the relation:

$$D_{eff} = \frac{\left[\left(D_{flesh}\Delta x_{fr}\right)+\left(D_{air}\Delta x_{ar}\right)\right]}{\Delta x_{fr}+\Delta x_{ar}} \qquad (18)$$

where $\Delta x_{fr} = \Delta x_f - \Delta s$

and $\Delta x_{ar} = \Delta x_a + \Delta s$

where Δx_f and Δx_a are the recent thicknesses of the flesh and the air gap, respectively and Δs is the shrinkage of the flesh.

The effective diffusivity is used to compute the moisture movement between the shell and the seed coat.

4.4.2 Shrinkage of Longan

To develop a mathematical model of volumetric shrinkage of longan flesh the following hypotheses are considered (Talla et al., 2004):

1) The volume change due to the shrinkage of the product is equal to the volume of water evaporated.
2) The pores in the product are occupied by water with density ρ_w.

Let us now consider the mass of the product at a given time to be m and while the mass of dry matter is m_d and that of water is m_w. The volume of dry matter is V_d, the volume of water in the pores is V_w and the volume of the product is V. Now we can write

$$m = m_w + m_d; \qquad V = V_w + V_d \tag{19}$$

Furthermore, it can be written as:

$$\rho = \frac{m}{V}, \ \rho_d = \frac{m_d}{V_d} \ \text{and} \quad M = \frac{m_w}{m_d} \tag{20}$$

where ρ is density of the product, ρ_d is density of dry matter and M is the moisture content of the product on a dry basis.

The development of Eqs. (19) and (20) gives the following expression:

$$V = V_0(A + \beta M) \tag{21}$$

where

$$A = \frac{1}{1 + aM_0}; \qquad \beta = \frac{a}{1 + aM_0} \qquad \text{and} \quad a = \frac{\rho_d}{\rho_w} \tag{22}$$

where M_0 is the initial moisture content , V_0 is initial volume and β is shrinkage coefficient
If $(M_0\text{-}M)$ is chosen to quantify the moisture removed at a time t, expression in Eq. (21) becomes:

$$V_r = 1 - \beta(M_0 - M) \tag{23}$$

where $V_r = \frac{V}{V_0}$

Drying experiments to determine shrinkage of longan flesh were carried out on thin layer under controlled conditions. The dimension of longan flesh was measured during drying.

4.4.3 Equilibrium moisture content

Janjai et al. (2006) fitted five models to the isotherm data of longan. The GAB model fitted the best to the experimental data of longan and the modified Oswin model was the next to the GAB model. The agreement between the best-fitted models and experimental data was excellent. For simplicity and consistency effect of temperature, Oswin model was selected for use in this simulation. The equilibrium moisture content model used is:

$$a_w = \frac{1}{1+\left[\frac{b_o + b_1 T}{M_e}\right]^{b_2}} \tag{24}$$

where b_0 = 79.9826, b_1 = - 0.8277, b_2 = 2.1867. T is temperature (°C) and a_w is water activity (decimal). The water activity is equal to the relative humidity (%) divided by 100.

4.4.4 Surface Mass Transfer Coefficient

The surface mass transfer coefficient of longan (h_m) was computed using the relation developed by Patil (1988):

$$h_m = \frac{D_{air}}{d}(2.0 + 0.522\,Re^{0.5}\,Sc^{0.33}) \tag{25}$$

where D_{air} is diffusivity of air, (d) is diameter of longan, Re is Reynolds number and Sc is Schmidt number.

The Reynolds number (Re) and Schmidt number (Sc) are defined as:

$$Re = \frac{u\,d\,\rho_{air}}{\mu} \tag{26}$$

$$Sc = \frac{\mu}{\rho_{air}\,D_{air}} \tag{27}$$

where u is air velocity, ρ_{air} is density of air and μ is viscosity of air.

4.5 Results and discussions

Shrinkage of longan flesh was determined experimentally and it was found to be a function of moisture removal. The following equation was developed for volume shrinkage of longan flesh:

$$\frac{V}{V_0} = 1 - 0.181\,(M_0 - M) \qquad R^2 = 0.99 \tag{28}$$

Ochoa et al. (2002) and Talla et al.(2004) also studied shrinkage in biological materials and they found that the volume shrinkage is a function of the moisture content.

The simulated moisture contents were compared with the measured values to build up confidence in the model. The comparison was aimed at showing the performance of the finite element model for the prediction of the moisture content of longan fruit during drying. First comparison was made using the measured values of the moisture content of the longan taken from the thin layer drying of longan under controlled conditions of temperature and relative humidity by Phupaichitkun et al. (2005). Fig. 22 shows the comparison of the predicted moisture contents using component diffusivities with the experimental data from Phupaichitkun et al. (2005). The mean bias error and the root mean square error of the prediction of the model were used to determine the prediction accuracy of the model developed. The mean bias error and the root mean square error between the predicted results and the data obtained from Phupaichitkun et al. (2005) are 2.0% and 2.8%, respectively.

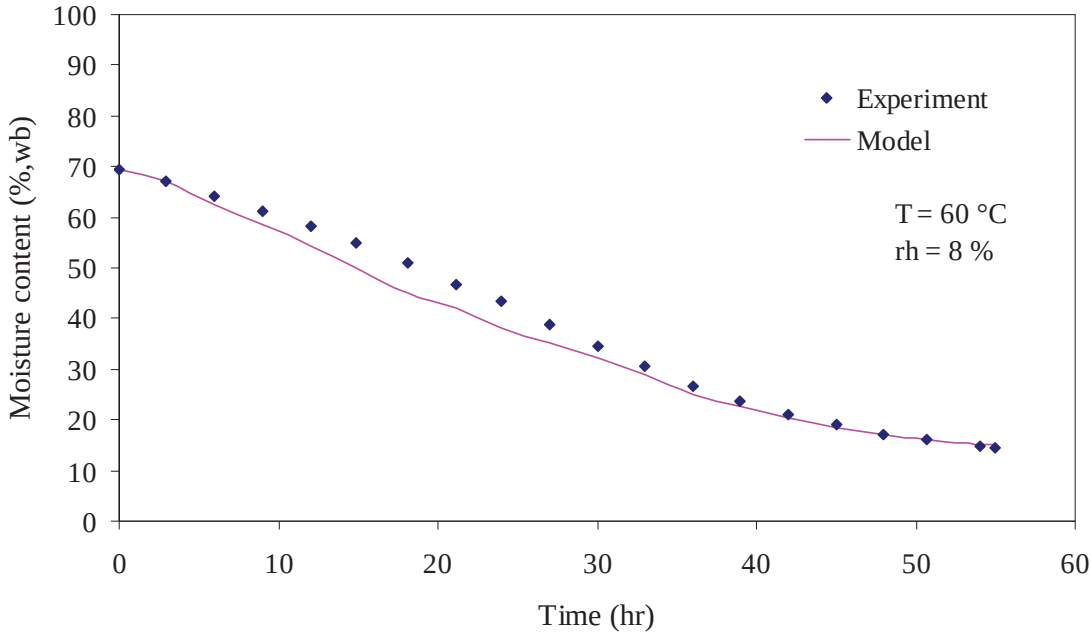

Fig. 22 Comparison of the predicted moisture contents on a wet basis of longan fruit with the experimental data obtained from Phupaichitkun et al. (2005)

Fig. 23 shows the comparison of the predicted moisture contents using component diffusivities with the experimental data from this study. The mean bias error and the root mean square error between the predicted results and the measured values are 1.8% and 2.1%, respectively.

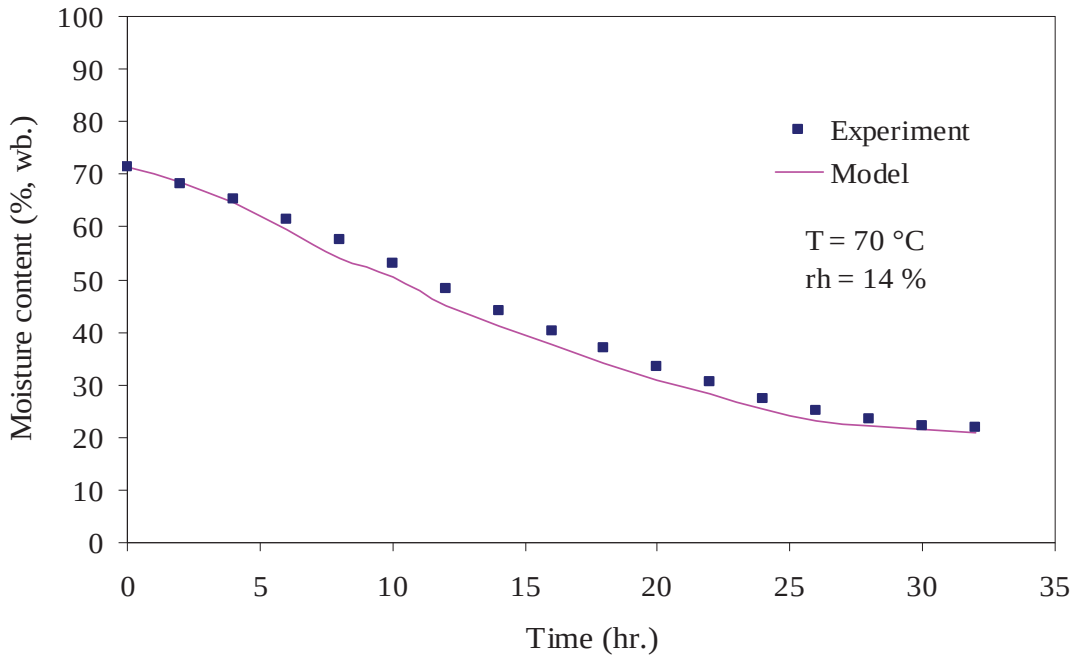

Fig. 23 Comparison of the predicted moisture contents on a wet basis of longan fruit with the experimental data from this study

Thus, the finite element model predicts the moisture contents very well. This is because individual component diffusivities of longan fruit were considered and another reason may be that the finite element model is 2-D which has more flexibility to describe the geometry of the components. Similar finite element studies have also been reported for wheat, barley, corn and soybean kernels using constant average and component diffusivities. Some researchers (Giner and Mascheroni, 2002; Gaston et al., 2004) have shown that moisture diffusivity also has the Arrhenius type dependency of temperature with pre-exponential factor that depends linearly on initial moisture content. Although the use of the diffusivity as a function of temperature in the finite element simulation predicts the drying of longan well, the use of diffusivity as a function of temperature and initial moisture content would make the finite element model more flexible for any initial moisture content to predict drying of longan more accurately.

Fig. 24 shows the variations of the predicted moisture contents with time in the different components of the longan fruit. The variations of the moisture content in the different components of the longan fruit may be explained as follows: The different components of the longan fruit have different initial moisture contents with the highest for the flesh and the lowest for the seed and the seed coat. The flesh has the highest diffusivity and is confined between two very low diffusivity components i.e. the shell and the seed coat. Also the seed has high diffusivity and is covered by very low diffusivity seed coat. As a result, the moisture from these two major sources moves into the drying environment

mainly through the high diffusivity seed stalk. The flesh possessing the largest source of moisture is dominant in the moisture diffusion through the seed stalk. This might have caused similar drying patterns in the flesh and the seed stalk. Since the flesh has the highest diffusivity and the largest area exposed to the seed stalk and in addition, moisture from the flesh is partly diffused through the shell to the environment, probably these result in a high drying rate of the flesh. Of course, the drying rate of the seed is relatively lower than those of the flesh and seed stalk due to the lower diffusivity of the seed.

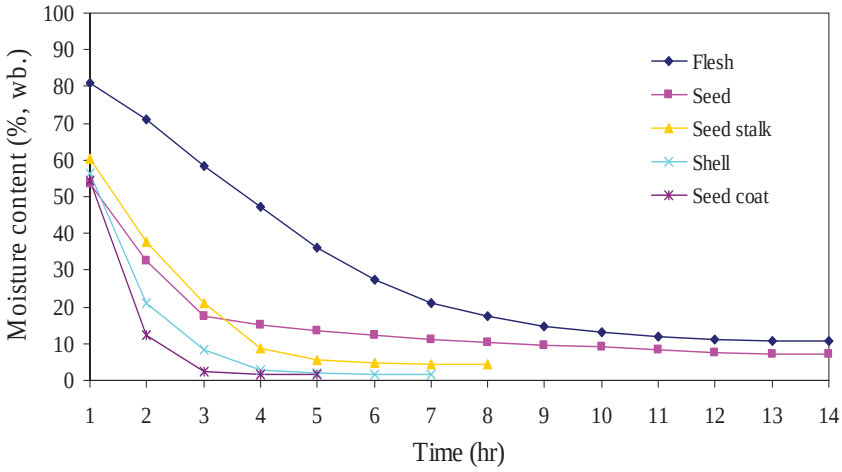

Fig. 24 Variations of the moisture contents on a wet basis with time in the different components of the longan fruit

The shell is thin and the seed coat is extremely thin. Both the shell and the seed coat are minor sources of moisture with a high internal resistance to moisture diffusion. Again, the shell is directly exposed to the drying environment through a large surface area and of course the seed coat is exposed to the flesh and the seed through a large area. This in fact probably caused the moisture to diffuse into the drying environment from the shell directly and from the seed coat into the flesh and then through the seed stalk into the drying environment.

It is clear from the results discussed above that moisture diffusion in the longan fruit is complex phenomena and the seed stalk controls the drying of the longan fruit. Finally it may be concluded that these complex phenomena might be related to nonhomogeneity and interfaces between different components of the longan fruit.

The finite element model predicted the nodal moisture contents which were transformed to contour plots using the Surfer software. The contour plots show the regions of equal moisture contents. The moisture profiles after 1, 5, 10 and 15 hours of drying at a temperature of 70°C are presented in Fig. 25. The moisture content decreases from the centre towards the surface resulting in steeper moisture content gradient and exhibits a similar pattern for all the elapsed times but the level of moisture content decreases with an increase in drying time. The moisture content is also symmetrical

circumferentially except the seed stalk where it is also symmetrical around the central axis of the seed stalk with a higher moisture profile in the outer regions of the seed stalk. This indicates that the seed stalk controls the moisture movement from the flesh into the drying environment. This symmetry is logical because of the symmetry of the geometry of the different components of the fruits although the moisture diffusivities of the different components of the longan are different.

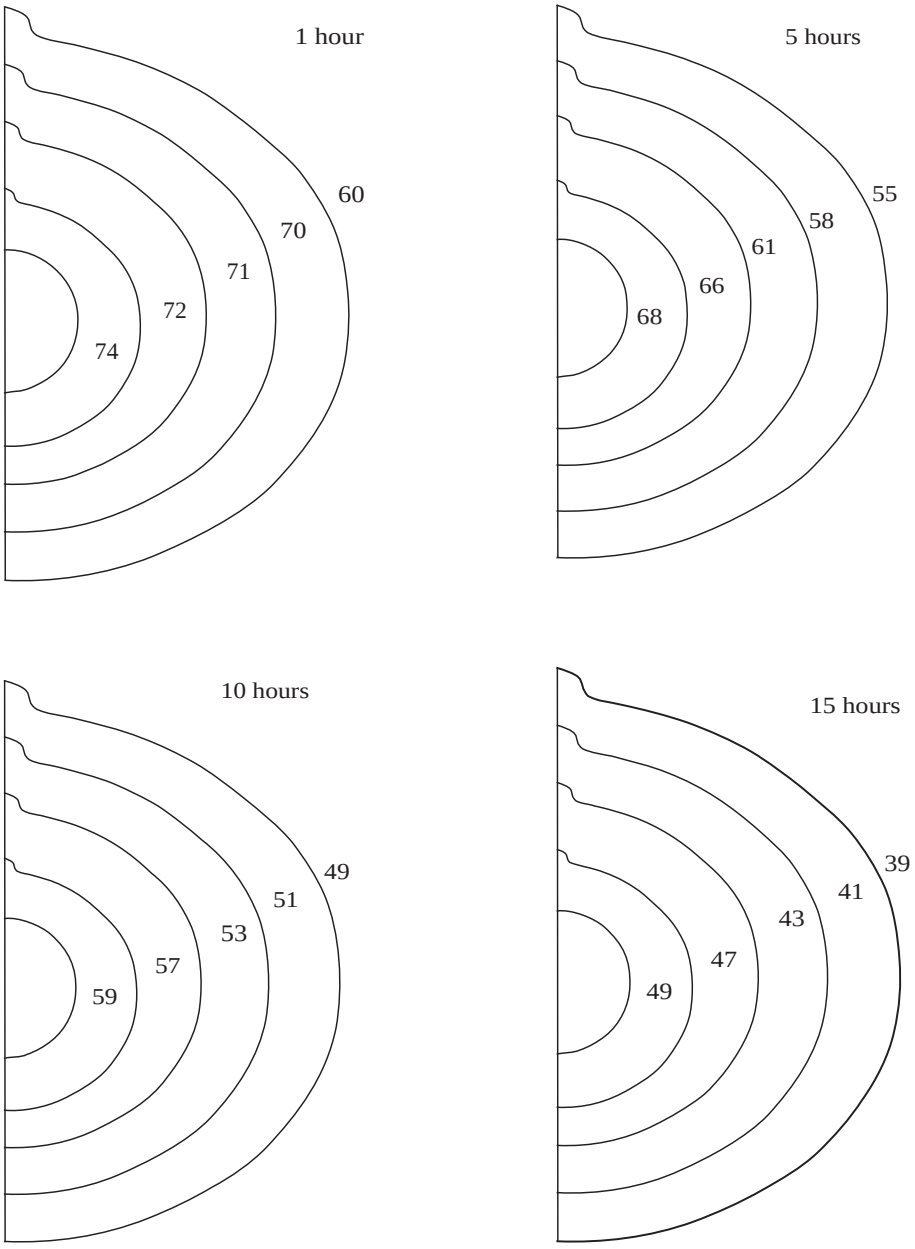

Fig. 25 Moisture within the longan fruit after 1, 5, 10 and 15 hours after drying at the drying air temperature of 70 °C and relative humidity of 14%. Values in the contour represent the moisture contents in %, wb.

In this work, the experimental validation of the moisture profile in longan fruit predicted by the finite element was not conducted, due to the lack of advanced equipment for the moisture profile measurement. However, several researchers reported similar distribution and gradients of moisture developed inside kernel of corn, wheat and soybean using finite element technique. Thus, the finite element prediction agrees with the reported predictions qualitatively.

4.6 Conclusions

A two dimensional finite element model for drying of longan fruit has been developed and it is programmed in Compaq Visual FORTRAN version 6.5. The finite element model predicts the moisture contents very well during drying. This model provides information on the dynamics of the moisture movement without actual measurements and the use of this mathematical model is of great potential benefit to the longan fruit drying industry. Furthermore, the model provides a better understanding of the transport processes in the different components of the longan fruit.

Chapter 5

Solar Drying of Peeled Longan Using a Side Loading Type Solar Tunnel Dryer: Experimental and Simulated Performance*

5.1 Introduction

Drying is one of the oldest methods for preservation of fruits and vegetables and it also an energy intensive operation. Improved drying technology is needed for improvement of the quality of dried products for value addition, reduction of post harvest losses, and also for conservation of energy.

Mechanical hot air drying is a common method for drying of whole longan fruit for large scale drying for export industries and peeled longans derived from broken shell longans are also dried in small to medium scale mechanical dryers. Most of the peeled longan are dried in a large open flat bed using hot stoves burning fuel wood and charcoals. This procedure results in poor quality dried product due to dirt and dust from the burning stoves. Some peeled longans are also dried under the sun on mats. During sun drying, peeled longan fruits on mats are exposed to the open environment and are contaminated by dust and insects, resulting in poor quality dried fruits with less value addition.

Thailand, located at the tropical regions of the Southeast Asia, receives annual average daily solar radiation of 18.2 $MJm^{-2}day^{-1}$ (Janjai et al., 2005). Thus, utilization of solar energy to produce quality solar dried peeled longan has been considered to be the most promising option. Furthermore, solar energy is a renewable and environmental friendly energy source.

Solar drying can be considered as an elaboration of sun drying and is an efficient system of utilizing solar energy (Bala, 1998; Muhlbauer, 1986; Parker and Mujumdar, 1991). Many studies have been reported on natural convection solar drying of agricultural products (Excell and Hornsakoo, 1978; Zaman and Bala, 1989; Oosthuizen, 1995; Sharma et al., 1995; Weitz et al., 1990; Simate, 2001; Vlachos et al., 2002; Yaldyz and Ertekyn, 2001). Considerable studies on simulation of natural convection solar drying of agricultural products and optimization have also been reported (Bala and Wood, 1994; Bala and Wood, 1995; Simate, 2003; Forson et al., 2007). The success achieved by natural convection solar dryers has been limited due to low buoyancy induced air flow. These prompted researchers to develop forced convection solar dryers. Many researches and performance studies have been reported on forced convection solar dryers (Oosthuizen, 1996; Karin and Hawlader, 2005; Ratti and Mujumdar, 1997; Bose and Ojha, 1983; Raouzeos and Saravacos, 1986; Rossello et al., 1990; Janjai and Tung, 2005; Janjai et al., 2008). Studies on simulation and optimization of forced convection solar dryers have also been reported (Jamjai and Guevezov, 1986; Smitabhindu et al., 2008). Numerous tests of forced convection solar tunnel dryers were carried out in the different regions of the tropics and subtropics. The results of the tests have shown that fruits, vegetables, cereals, grain,

---

* This chapter has been published in Drying Technology vol. 27, page 595-605. (2009)

legumes, oil seeds, spices, fish and even meat can be dried properly in the UV resistant plastics covered solar tunnel dryer (Eissen, 1985; Lutz and Muhlbauer, 1986; Esper and Muhlbauer, 1993; Esper and Muhlbauer, 1994; Schirmer et al., 1996; Bala and Mondol, 2001; Bala et al., 2003; Hossian and Bala, 2007; Bala and Janjai, 2005; Esper and Muhlbauer, 1996). The UV resistant plastics covered solar tunnel dryer suffers from several drawbacks. The plastic cover lasts for only few months during drying season. The loading and unloading of the products in this type of dryer are also not convenient since it requires the opening of the plastic cover over the drying section. This prompted to develop the side loading type glass covered solar tunnel dryer at Silpakorn University in which the loading and unloading are conducted through the windows at one side of the dryer (Janjai et al., 2006; Janjai and Keawprasert, 2006).

Solar drying systems must be properly designed in order to meet particular drying requirements of specific products and to give satisfactory performance. Designers should investigate the basic parameters such as dimensions, temperature, relative humidity, airflow rate and the characteristics of products to be dried. However, full-scale experiments for different products, drying seasons and system configurations are sometimes costly and not possible. The development of a simulation model is a valuable tool for predicting the performance of solar drying systems. Again, simulation of solar drying is essential to optimize the dimensions of solar drying systems and optimization technique can be used for optimal design of solar drying systems.

Although many studies have been reported on solar drying of fruits and vegetables, limited studies have been reported on drying of longan fruit (Achariyaviriya, 2001; Achariyaviriya et al., 2001). Achariyaviriya et al. (2001) reported quality tests of dried peeled longan. Recently Varith et al. (2007) reported drying of peeled longan using combined microwave-hot air and also reported drying kinetics using Sherwood's exponential equation, quality indices and specific energy consumption.

Very limited studies have been reported on drying of longan fruit and no systematic experimental and simulated study on solar drying of peeled longan has been reported. This paper presents a systematic experimental and simulated study of solar drying of peeled longan using side loading type glass covered solar tunnel dryer.

5.2 Experimental study

The new version of the solar tunnel dryer (side loading and unloading through windows with glass cover type) was constructed at Silpakorn University, Nakhon Pathom, Thailand. It consists of two parts: a solar air heating collector and a drying unit. Both parts have similar structures and connected in series. The top sides of both parts are covered by glass plates fixed with silicon glue to the aluminium frames. These glass plates with the frames can be easily removed from the dryer when the dryer is needed to be cleaned. The bottom side of the dryer is made of high density foam sandwiched between two galvanized iron sheets which functions as back insulator to reduce heat losses. The upper surface of this back insulator was painted black which functions as a solar radiation absorber. The side walls of the dryer are made of galvanized iron sheet. They were designed in such a manner that they are

supported by the back insulator at the bottom side and the side walls also support the glass plates which cover the dryer, as shown in Fig. 26. The two side walls have different height, so that the glass plates make a tilted angle of 10° to facilitate drainage of water in case of rain. The higher side wall has windows, each of which has the dimension of 20 cm x 80 cm for loading and unloading products. Each window has a galvanized sheet cover to prevent rain and air leakage. The top glass cover, the bottom insulator and the side walls were made in modules. Each module can be inter-locked at the junction to prevent air leakage and to facilitate the construction and transportation.

For a ventilation system, a dc fan driven by a 15 W solar cell module was installed at the collector to suck ambient air into the dryer (Fig. 26).

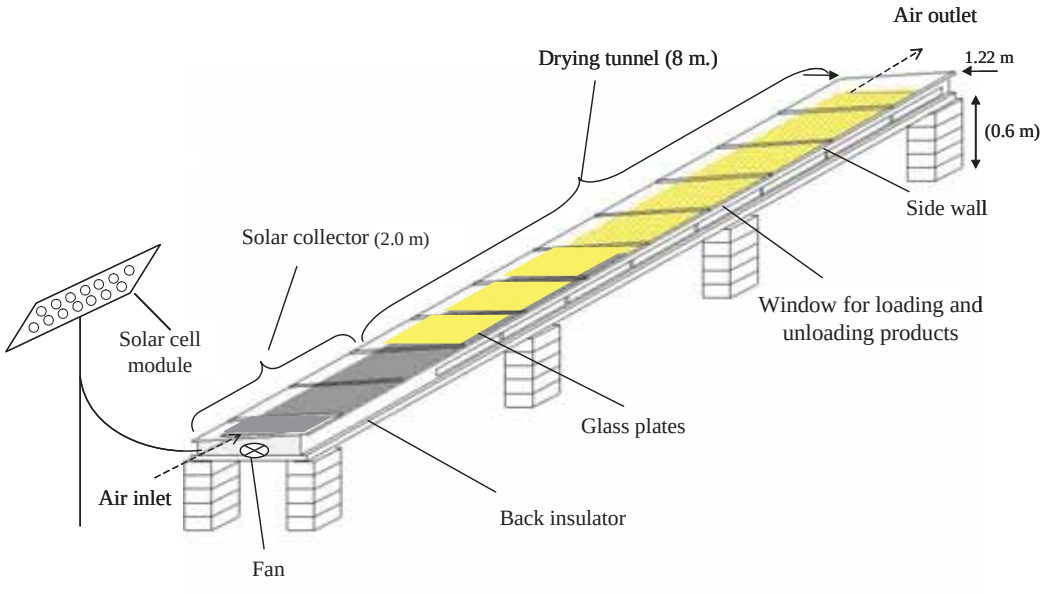

Fig.26 Schematic diagram of the side loading type solar tunnel dryer

Solar radiation passing through the glass cover heats the absorber. Ambient air is forced through the collector and while passing it the collector gains heat from the absorber. This heated air while passing through the drying unit absorbs moisture from the peeled longan. The product receives heat from solar passing through the glass cover of the drying unit in addition to the heat received from the collector and this enhances the drying rate of the product.

A total of five full scale experimental runs were conducted and the dryer was loaded to a capacity of 100 kg of peeled longan for each experimental run. The drying was started at 8 am and continued till 6 pm. The control sample was also dried naturally under the same weather conditions.

To investigate the dryer performance, various sensors were placed at the dryer. Solar radiation was measured by a pyranometer (Kipp & Zonen model CM 11, precision ± 0.5%) and this was placed on the roof of the dryer. Thermocouples of type K were used to measure the air temperatures in the collector and drying unit (precision ± 2%). The positions of the thermocouples for the measurements of

temperatures in the collector and drying unit are shown in Fig. 27. Hot wire anemometer (Airflow, model TA5, precision ± 2%) were employed to monitor the air speed in the collector and drying unit. This anemometer was also used to monitor the wind speed. Relative humidities of ambient air and drying air were periodically measured with hygrometers (Electronik, model EE23, precision ± 2%).

Voltage signals from the pyranometer, hygrometers and thermocouples were recorded every 10 minutes by a 40-channel data logger (Yokogawa, model DC100). The air speeds in the solar collector and drying unit were also manually read and recorded every hour during the drying experiments. Samples of products in the dryer were weighed at 2-hour intervals using a digital balance (Satorius, model E2000 D, precision ± 0.0001 g). The positions of the measurements of the sample weights in the drying unit are also shown in Fig. 27. Before the installations, the pyranometer for measuring solar radiation was calibrated against a new pyranometer recently calibrated by Kipp&Zonen, the manufacturer. For the hygrometers, they were calibrated using standard saturated salt solutions supplied by the manufacturer. Before being used, the thermocouples were also tested by measuring the boiling and freezing temperatures of water to ensure the accuracy.

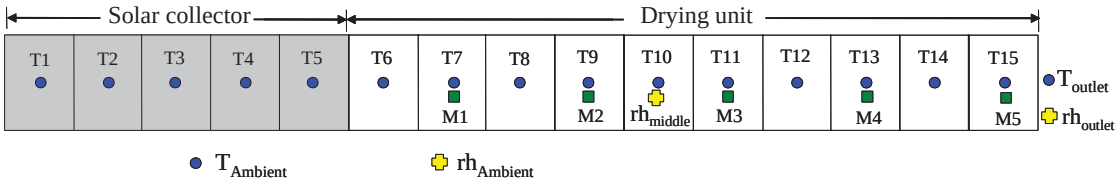

Fig. 27 Positions of the thermocouples (T) and hygrometers (rh) and product sample for moisture determination (M).

For the drying tests, 100 kg of peeled longan was used for each experimental run. The experiments were started at 8.00 am and continued till 6.00 pm. During night time, the products were kept in the dryer. The process was repeated until the desired moisture content (about 12% on a wet basis) was reached. This final moisture content corresponds to the moisture content of high quality dry product in local markets. About 100 g of the product sample was taken from the dryer and weighed at 2-hour intervals. The moisture content during drying was estimated from the weight of the product samples and the estimated dried solid mass of the samples. At the end of the drying process, the exact dry solid mass of the product samples was determined by using the air oven method. The samples were placed in the oven at the temperature of 103°C for 24 hours (precision ± 0.5%).

5.3 Mathematical modeling

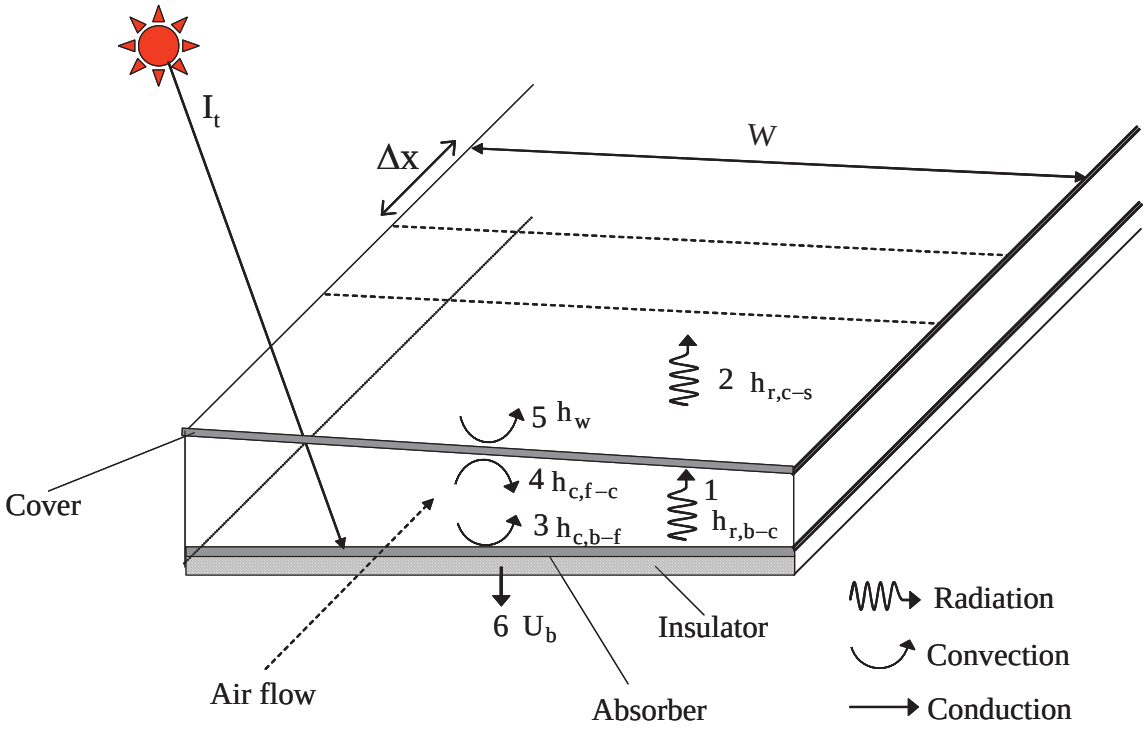

Fig. 28 Heat transfer in the solar collector: 1. radiative heat transfer between absorber and cover 2. radiative heat transfer between cover and sky 3. convective heat transfer between absorber and air 4. convective heat transfer between cover and air 5. convective heat transfer of cover due to wind 6. conduction loss through back insulator

5.3.1 Energy balances in the collector (see Fig. 28)

- **Energy balance for glass cover**

The energy balance for the glass cover is as follows:

Rate of thermal energy accumulation in the cover = rate of radiative heat transfer between the absorber and the cover + rate of the convective heat transfer between the cover and air in the collector + rate of the convective heat loss from the cover due to the wind +rate of radiative heat transfer between the cover and the sky +rate of solar radiation absorption in the cover.

This energy balance can be formulated as:

$$\rho_c \delta_c C_c \frac{dT_c}{dt} = h_{r,b-c}(T_b - T_c) + h_{c,f-c}(T_f - T_c) + h_w(T_a - T_c) + h_{r,c-s}(T_s - T_c) + \alpha_c I_t \quad (1)$$

- **Energy balances in the air steam**

The energy balance in the air stream in the collector can be written as:

Rate of enthalpy change in the air stream = convective heat transfer between the air steam and the cover + convective heat transfer between the air stream and the absorber

This energy balance can be expressed mathematically as:

$$D_c G C_f \frac{dT_f}{dx} = h_{c,c-f}(T_c - T_f) + h_{c,b-f}(T_b - T_f) \quad (2)$$

- **Energy balance for the absorber**

The energy balance for the absorber is considered as follows:

Rate of thermal energy accumulation in the absorber = rate of convective heat transfer between the absorber and the air stream + rate of radiative heat transfer between the cover and the absorber + rate of the heat loss from the absorber through the back insulator to ambient air + rate of solar radiation absorbed by the absorber

This energy balance can be written as:

$$\rho_b \delta_b c_b \frac{dT_b}{dt} = h_{c,b-f}(T_f - T_b) + h_{r,b-c}(T_c - T_b) + U_b(T_a - T_b) + (\tau\alpha)I_t \quad (3)$$

The radiative heat transfer coefficient $(h_{r,c-s})$ from the cover with temperature of T_c to the sky with the equivalent temperature T_s was computed as (Duffie and Beckman, 1991):

$$h_{r,c-s} = \varepsilon_c \sigma (T_c^2 + T_s^2)(T_c + T_s) \quad (4)$$

where ε_c is the emissivity of the cover, σ is Stefen-Boltzmann constant.

The sky temperature (T_s) was computed from

$$T_s = 0.552 T_a^{1.5} \quad (5)$$

where T_a is the ambient temperature in K.

The radiative heat transfer coefficient $(h_{r,b-c})$ between the absorber with the temperature of T_b and the cover with temperature T_c was computed as (Duffie and Beckman, 1991):

$$h_{r,b-c} = \frac{\sigma(T_b^2 + T_c^2)(T_b + T_c)}{\frac{1}{\varepsilon_b} + \frac{1}{\varepsilon_c} - 1} \quad (6)$$

where ε_b is the emissivity of the absorber

The convective heat transfer coefficient from the cover to the ambient air due to wind (h_w) was calculated from (Duffie and Beckman, 1991):

$$h_w = 5.7 + 3.8 V_a \tag{7}$$

where V_a is the wind speed in m/s.

The convective heat transfer coefficient inside the collector for either the cover $h_{c,c-f}$ or absorber $h_{c,b-f}$ was computed from the following relationship:

$$h_{c,b-f} = h_{c,c-f} = \frac{Nu\, k_a}{D_h} \tag{8}$$

where Nu is the Nusselt number, k_a is thermal conductivity of the air and D_h is the hydraulic diameter of the collector.

Nusselt number, Nu was computed from the following relationship (Kays and Crawford, 1980):

$$Nu = 0.0158 Re^{0.8} \tag{9}$$

where Re is the Reynolds number which is given by:

$$Re = \frac{D_h V \rho_a}{\nu} \tag{10}$$

where V is the air speed in the collector, ρ_a is air density and ν is the viscosity of the air.

Over all heat loss coefficients from the bottom of the absorber (U_b) was computed from the following relation:

$$U_b = \frac{k_b}{L_b} \tag{11}$$

where k_b and L_b are the thermal conductivity and the thickness of the back insulator, respectively.

The systems of equations (1–3) were solved numerically using the finite difference technique. The length of the collector is divided into a number of sections with the section length of Δx so that the properties of the materials are constant or nearly so within each section. The time interval should be small enough for the air conditions to be constant over the distance Δx. A compromise between the computing time and precision must be considered for the economy of computing.

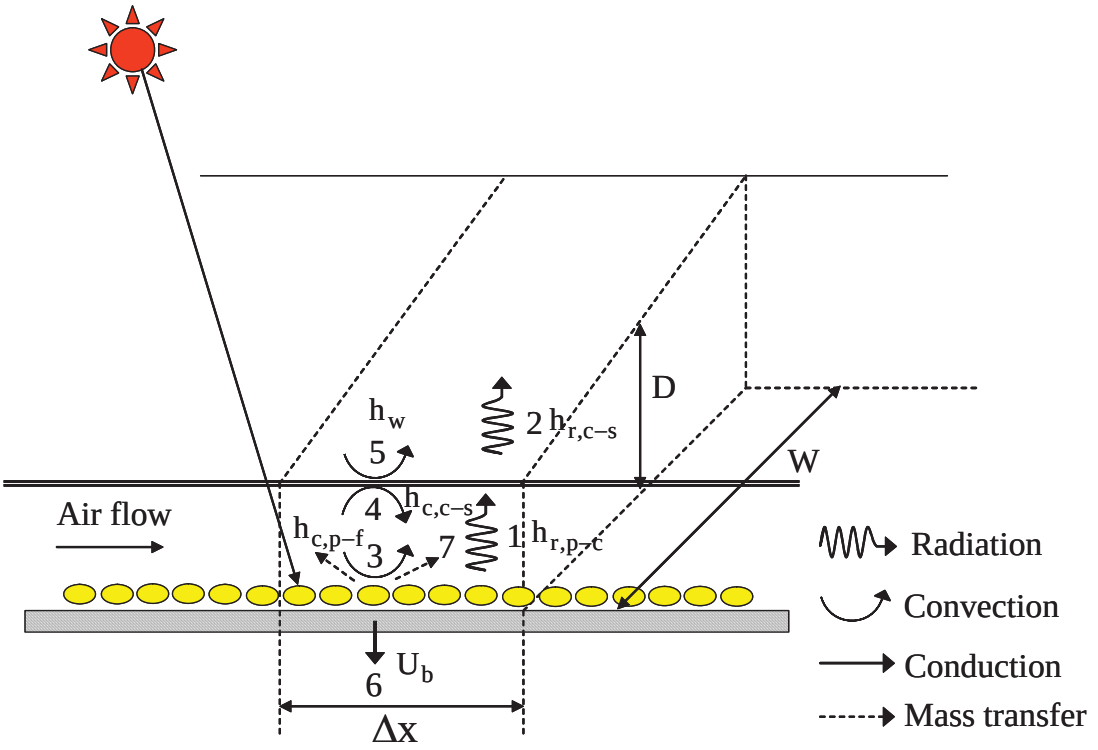

Fig. 29 Energy balances in the drying unit: 1. radiative heat transfer between the product and the cover 2. radiative heat transfer between cover and sky 3. convective heat transfer between the product and air 4. convective heat transfer between cover and air 5. convective heat transfer of cover due to wind 6. heat loss through back insulator 7. mass transfer

5.3.2 Energy and mass balances in the drying unit (see Fig. 29)

For each component of the drying unit, the energy balances and mass balances were written as the followings.

- **Energy balance for the cover of the drying unit**

Rate of energy accumulation in the cover = rate of the radiative heat transfer between the cover and the product (peeled longan) + rate of the convective heat transfer between the moist air steam in the drying unit and the cover + rate of heat loss from the cover due to wind + rate of radiative heat loss from the cover to the sky + rate of solar energy absorption by the cover

This energy balance can be expressed mathematically as:

$$\rho_c \delta_c C_c \frac{dT_{c1}}{dt} = h_{r,p-c}(T_p - T_{c1}) + h_{c,f-c}(T_f - T_{c1}) + h_w(T_a - T_{c1}) + h_{r,c-s}(T_s - T_{c1}) + \alpha_c I_t \quad (12)$$

- **Energy balance for the moist air steam in the drying unit**

Rate of enthalpy change of the moist air steam = rate of the convective heat transfer between the product and the moist air steam + rate of convective heat transfer between the moist air steam and the cover

This energy balance can be written as:

$$DG(C_f + C_v H)\frac{dT_{f1}}{dx} = h_{c,p-f}(T_p - T_{f1}) + h_{c,f-c}(T_c - T_{f1}) \quad (13)$$

- **Energy balance for the product (peeled longan)**

Rate of enthalpy change of the product = rate of the sensible and latent heat for the evaporization of the moisture from the product + rate of the convective heat transfer between the air steam and the product +rate of the radiative heat transfer between the cover and the product+ rate of heat loss through the back insulator from the product to ambient air + rate of solar radiation absorbed by the product

This energy balance can be represented mathematically as follows:

$$\begin{aligned}\rho_{s,p}(C_p + C_w M)\frac{dT_p}{dt} = {} & [h_{fg} + C_v(T_p - T_f)]DG\frac{dH}{dx} \\ & + h_{c,p-f}(T_f - T_p) + h_{r,p-c}(T_c - T_p) + U_b(T_a - T_p) + \tau_c \alpha_p I_t\end{aligned} \quad (14)$$

- **Mass balance equation**

The rate of moisture transfer between the product and the air steam can be written as:

$$DG\frac{dH}{dx} = -\rho_{s,p}\frac{dM}{dt} \quad (15)$$

- **Thin layer drying equation of the product**

To obtain the thin layer drying equation, thin layer drying experiments of peeled longan were conducted under controlled conditions of the drying air in a laboratory dryer (Janjai, 2007). A number of experiments were carried out for different values of the temperature (T) and relative humidity (rh). For each experiment, the temperature and relative humidity were fixed and the weight of the peeled longan in this laboratory dryer was measured during drying. Afterwards, this weight was used to determine the moisture content (M) of peeled longan.

The following thin layer drying model based on Page's equation was used to fit the drying data obtained from these experiments :

$$\frac{M - M_e}{M_0 - M_e} = \exp(-kt^n) \quad (16)$$

where

$$k = -0.213788 + 0.0101640T - 0.001372rh \quad (17)$$

$$n = 1.108816 - 0.0005210T - 0.000061rh \quad (18)$$

The equilibrium moisture content of peeled longan (M_e) proposed by Janjai et al (2006) was used in this work.

Radiative heat transfer coefficient $(h_{r,p-c})$ between the cover with temperature T_c and the product with temperature T_p was computed as (Duffie and Beckman, 1991):

$$h_{r,p-c} = \frac{\sigma(T_p^{\,2} + T_c^{\,2})(T_p + T_c)}{\frac{1}{\varepsilon_p} + \frac{1}{\varepsilon_c} - 1} \tag{19}$$

where ε_p is the emissivity of the product.

The system of Eqs. (12-14) was solved numerically using the finite difference technique.

On the basis of the drying air temperature and relative humidity for all the sections of the drying unit, the constants k and A were computed from Eqs. (17-18) and equilibrium moisture content (M_e) of the peeled longan was calculated by using the model proposed by Janjai et al. (2006). Using the k, n and M_e values, the change in moisture content of peeled longan ΔM for all the sections for a time interval Δt were calculated using Eq. (15). Next the system of finite difference equation derived from Eqs. (12), (13), and (14) for the interval Δt for the entire length of drying unit was formulated. This system of equations is a set of implicit equations and was solved using the Gauss–Jordan elimination method. Using the recent value of drying air temperature and relative humidity for the different sections of the entire length of drying unit, the change in moisture content of peeled longan, ΔM for next time interval for the different sections of the entire length of drying unit was calculated and the process was repeated until the final time was reached. The numerical solution was programmed in Compaq Visual FORTRAN version 6.5.

5.4 Results and discussion

5.4.1 Experimental results

Full scale tests of the side loading type solar tunnel dryer for drying of peeled longan were carried out in the months of August to September, 2007. The typical results for drying of peeled longan are shown in Fig 30-35. Fig. 30 shows the variations of solar radiation during a typical experimental run of solar drying of peeled longan in a side loading type solar tunnel dryer. The solar radiation varied between 0-1,108 W/m^2 during the drying period. There were some fluctuations in solar radiation due to clouds and rain fall. In the early part of the first and second days of the drying test, there were clouds which resulted in fluctuations in solar radiation and later part of the second day, there was a rainfall which also resulted in fluctuations in solar radiation. However, the overall tendency of the patterns of changes in solar radiation was sinusoidal.

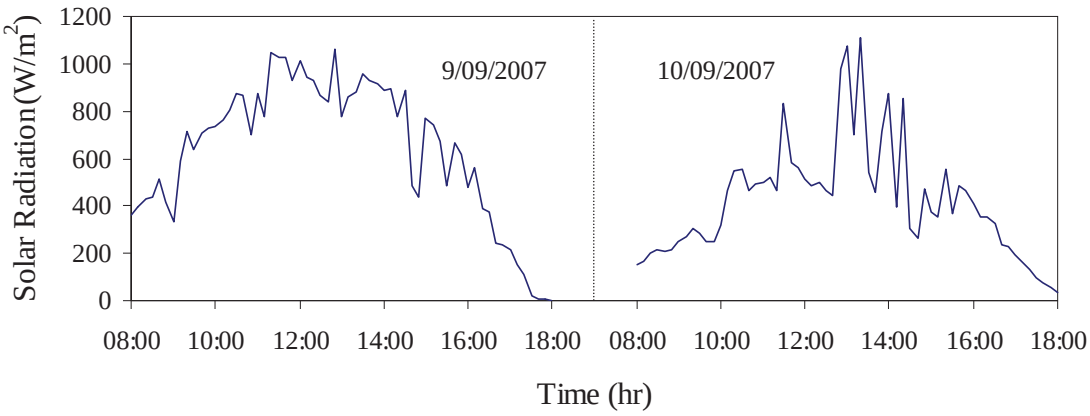

Fig.30 Variations of the solar radiation during a typical experimental run

Figure 31 shows the comparison of the temperature changes at different positions inside the collector for a typical experimental run of solar drying of peeled longan in the side loading tunnel dryer. The temperatures in the different positions increase till noon and then again decrease in the afternoon. The patterns of temperature changes are almost similar for all the days and the temperature increased with the increase in distance from inlet inside the collector. There was a significant difference in temperature levels in the different positions of the collector at a significance level of 5%. The temperature at outlet of the collector increased up to 72°C.

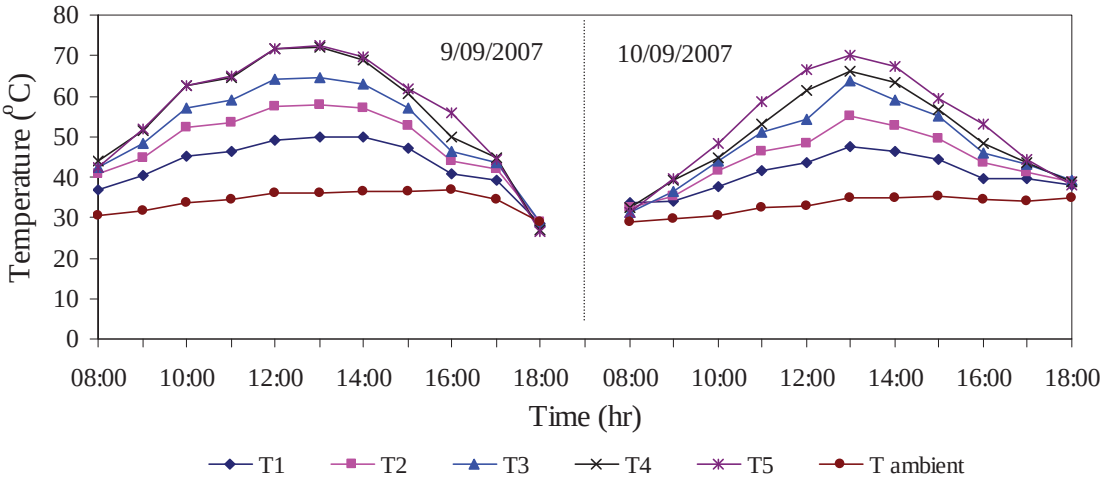

Fig. 31 The variations of the temperatures (T) at different positions inside the collector (see Fig. 27)

Figure 32 shows the variations of the temperatures at different positions inside the drying unit for a typical experimental run of solar drying of peeled longan in a side the dryer. The temperatures in the different positions increased till noon and then again decreased in the afternoon. Temperatures in

the different positions inside drying unit changed within narrow band for the positions T6 to T15 and are different at a significance level of 5%.

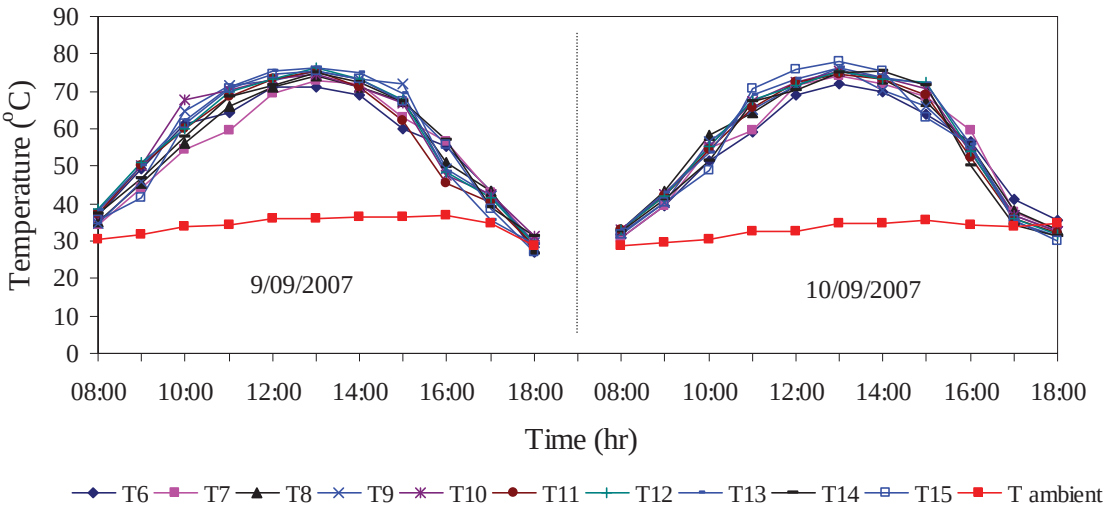

Fig. 32 The variations of the temperatures at different positions inside the drying unit (see Fig. 27)

Figure 33 shows relative humidities at three different positions inside the dryer for a typical experimental run during solar drying of peeled longan in the side loading type solar tunnel dryer. The relative humidities in the different locations decreased in the early part of the day because of the decreased level of the ambient relative humidity and increased level of the drying air temperature with time while the relative humidities in the different locations increased in the later part of the day because of the increased level of the ambient relative humidity and decreased level of the drying air temperature with time in later part of the day. The relative humidity at difference positions inside the drying unit depends on the moisture released from the product and the air temperature. For most cases, the relative humidity at the outlet of the dryer was higher than that at the middle of the dryer.

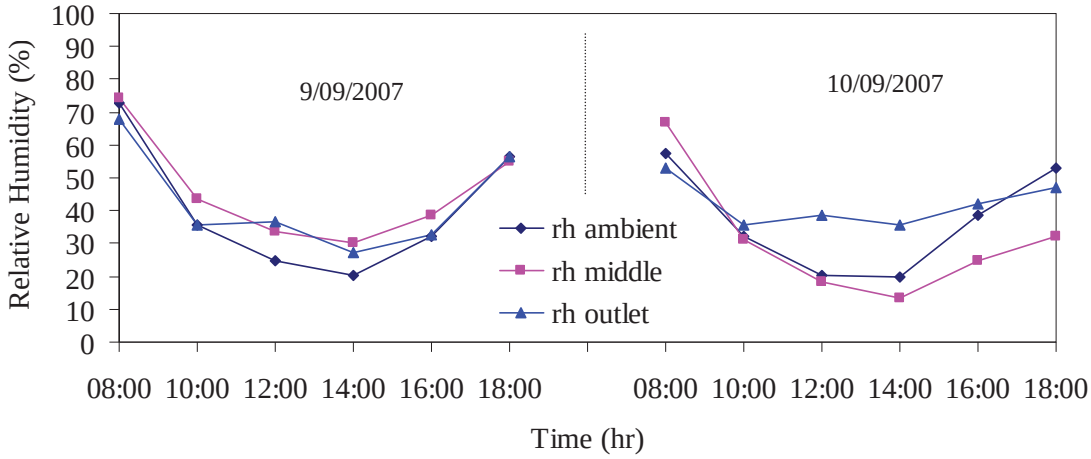

Fig. 33 Variations of relative humidities (rh) at three different positions inside the drying unit during a typical experimental run (see Fig. 27)

Figure 34 shows mass flow rate inside dryer of a typical experimental run. The mass flow rate inside dryer increased till noon and then decreased in the afternoon. The pattern of changes in mass flow rate followed the pattern of the changes in solar radiation (Fig. 30). This is due to the fact that the mass flow rate was provided by a dc fan operated by a solar cell module and the output power of the module depended strongly on solar radiation. However, there was a threshold value of solar radiation for the operation of the dc motor used to run the fan to provide the mass flow rate in the dryer.

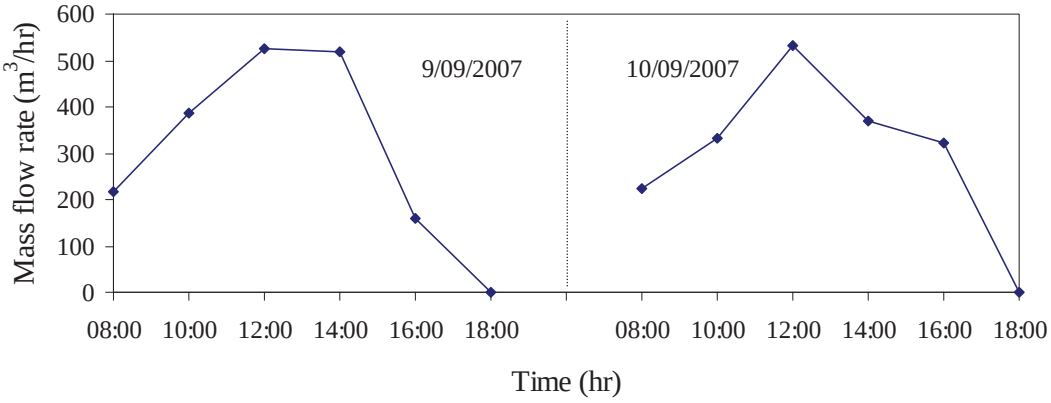

Fig. 34 Variations of mass flow rate inside the dryer during a typical experimental run

Figure 35 shows the variations of the moisture contents of peeled longan in 5 different positions inside dryer and of the control sample for a typical experimental run of the experiments. The moisture content of peeled longan in the solar dryer was reduced from an initial value of 84 % (wb) to

the final value of 12 % (wb) within 16 hours whereas the moisture content of the sun dried samples was reduced to 40 % (wb) within the same period under similar conditions.

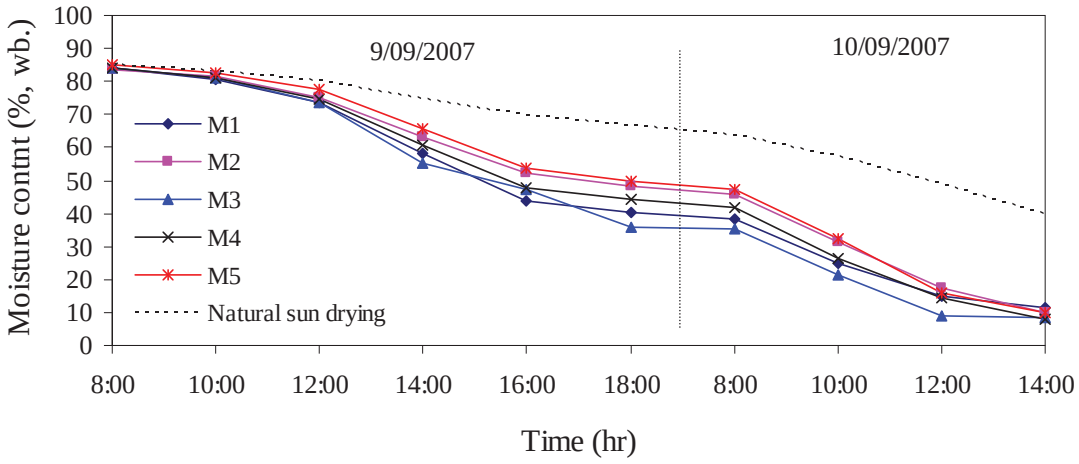

Fig. 35 Variations of the moisture contents (M) in the different locations of the drying unit for a typical experimental run during drying of peeled longan. The positions of the measurement of moisture contents are shown in Fig. 27.

Statistical analysis shows that there is no significant difference in solar drying of peeled longan in the different locations of the side loading type solar tunnel dryer at a significance level of 10%, but there is a significant difference in drying after hours of initial drying between drying inside the solar dryer and sun drying of peeled longan.

Thus, the drying in the side loading type solar tunnel dryer resulted in reduction in drying time and production of better quality dried product. The colour of the dried peeled longan was comparable to that of a high quality dried peeled longan in markets when the colour was tested.

For the economic analysis, it was assumed that the dryer is used to dry peeled longan during the harvest season and to dry off-season longan. Based on production of dried longan and the capital and operating cost of the drying system, the payback period of this system was estimated to be 2.9 years.

5.4.2 Simulated results

To validate the model, the predicted air temperatures at collector outlet and moisture contents of peeled longan during drying were compared to the experimental values. Fig. 36 shows a typical comparison between the predicted and experimental values of the temperatures at the outlet of the collector for consecutive 2 days starting from September 09, 20007 to September 10, 2007. Predicted temperature shows plausible bahaviour and the agreement is good. Figure 37 shows a typical

comparison of the predicted and observed moisture contents of peeled longan inside the dryer and the model predicts well the moisture content changes during drying.

The model predictions were evaluated on the basis of Root Mean Square difference (RMSD). RMSD of the prediction of the collector outlet temperatures was 4%. This indicates that the model can predict the temperature with a reasonable accuracy. RMSD of the prediction of the moisture contents was 4.1%. Thus, the model predictions are reasonably good. Furthermore, predictions are within the acceptable limit (10%) (O'Callaghan et al., 1971).

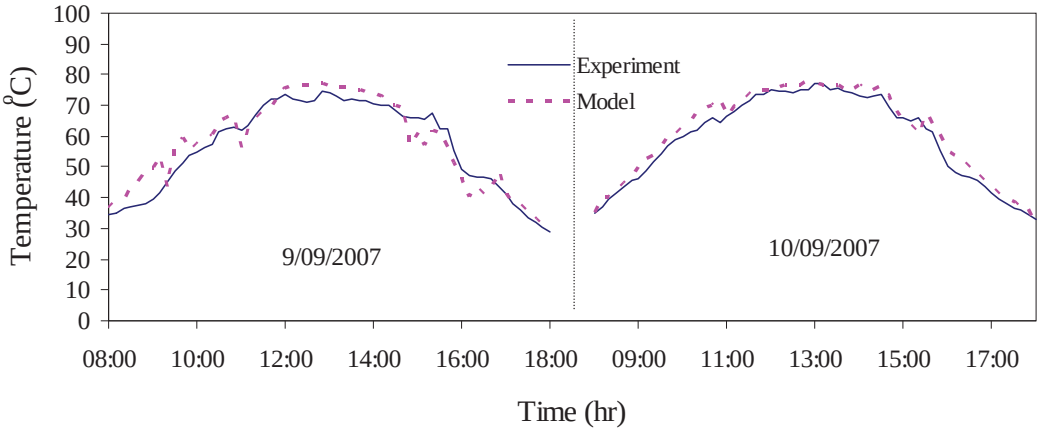

Fig. 36 Comparison of the simulated and observed collector outlet temperature during drying of peeled longan for a typical full scale experimental run

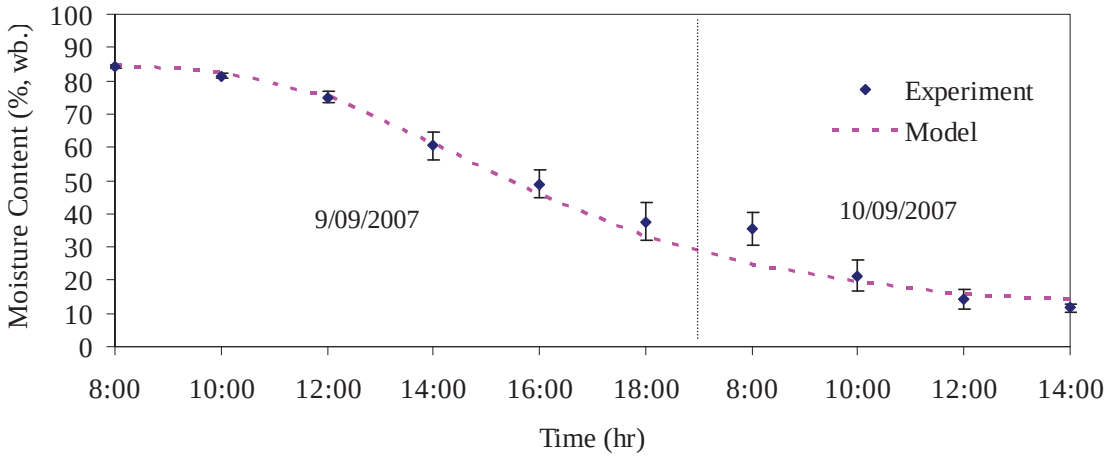

Fig. 37 Comparison of the simulated and observed moisture content during drying of peeled longan for a typical full scale experimental run

5.5 Conclusions

From the drying experiments of peeled longan in the side-loading type tunnel dryer, the temperature inside the collector varied with the positions but it varied within a narrow band for the positions starting from the middle of the dryer to exit of the dryer in the middle of the day. Pattern of changes of air velocity inside the solar tunnel dryer followed the pattern of changes in the solar radiation. Field level tests demonstrate the potentiality of solar drying of peeled longan in the side loading type solar tunnel dryer. Solar drying of peeled longan in the side loading type solar tunnel dryer resulted in considerable reduction in drying time as compared to the natural sun drying and the products dried in the solar tunnel were quality dried products. The payback period of the side loading type solar tunnel dryer is 2.9 years.

A system of partial differential equations for heat and moisture transfer was developed for solar drying of peeled longan in a side loading type solar tunnel dryer and the model was programmed in Compaq Visual FORTRAN version 6.5. The simulated air temperatures at the collector outlet agreed well with the observed data on temperatures. Good agreement was found between the experimental and simulated moisture content of peeled longan during drying and the precision was reasonable. This model can be used for providing design data for side loading type solar tunnel dryer and also for optimization of side loading type solar tunnel dryer.

Chapter 6

Experimental and Simulated Performances of a Batch Type Longan Dryer with Air Flow Reversal Using Biomass Burner as a Heat Source*

6.1 Introduction

Drying of longan is an energy-intensive process (Nathakaranakule etal., 2010). Majority of dryers are manually operated batch dryers where fresh longans are placed in a deep bed on one large tray. Commonly used longan dryers have a loading capacity of about 2000 kg of fresh longan per batch. Heat is supplied to drying air by LPG burner and the heated air is forced by means of a ducted fan operated by an electric motor into the dryer. One batch of drying takes about 48–72 hours. Long drying time is usually required to achieve the desired 'golden brown' color. Normally, non-uniform drying is obtained. To ensure uniformly dried product, drying operators usually turn the fruit layer upside down and inside out thoroughly in 12 hours intervals and this causes damage and cracks of a significant fraction of dried longan during drying (Achariyaviriya et al., 2007).Also the turning of the bed is a labour intensive operation.

In the recent years, drying cost of longan has increased considerably due to the increase in the price of LPG. Thailand is located in the tropics, there are sufficient biomass potentials. Furthermore, longan farmers have to do thinning operations of longan tree annually to promote flowering of longan. Therefore, utilization of biomass to dry longan may be considered as a possible alternative fuel to LPG for drying of longan.

Temperature and moisture content during deep bed drying of agricultural products change with time and position. Many mathematical models have been proposed to simulate the deep bed drying of agricultural products. Models of deep bed dying may be classified as (i) graphical and logarithmic models, (ii) heat and mass balance models and (iii) partial differential equation models (Bala, 1997). McEwen and O'Callaghan (1954) were the first to propose that deep bed drying can be represented by a number of thin layers in series and developed a semi-graphical method of solution. About the same time Van Arsdel (1955) developed partial differential equation models and solved these equations by the predictor-corrector methods. About decade after the publications of these models, Boyce (1965&1966) was the first to develop a digital computer model and later on Bakker-Arkema et al. (1967) proposed a set of partial differential equation models. Several studies have been on simple heat and mass balance models (Thomson et al., 1967; Bloome and Shove, 1971; Abu-Hamdeh and Othman, 2004). Although these are based on some assumptions of the dominant mechanisms of heat and mass transfers. However, many studies have been reported on modeling batch dryer using partial differential equation models even including momentum transfer(Berbert et al., 1994; Ratti and Mujumdar, 1995; Nafle et al., 2010; Ruiz-Lopez et al., 2008; Achariyaviriya et al., 2007; Tippayawong et al., 2008&2009; Phaphuangwittayakul et al., 2004; O'Callaghan et al., 1971; Baka and Wood, 1984;

* This chapter has been accepted to publish in Journal of Drying Technology, 2011 (in press)

Bala, 1990; Sun and Wood, 1997; Mandas and Habit, 2002; Srivastava and John, 2002; Sitompul et al., 2003; Tang et al., 2004).

Several studied have also been reported on modeling of deep bed drying of agricultural products with air flow reversal (Berbert et al., 1994; Ratti and Mujumdar, 1995; Nafle et al., 2010; Ruiz-Lopez et al., 2008). Recently, Ruiz-Lopez et al. (2008) reported a partial differential equation model based on heat and mass transfer mechanism between the air and the product in a fixed bed drying of food materials with and without periodical reversals of the air flow direction.

Moisture content gradients normally develop inside the batch dryers during the drying of agricultural products (Berbert et al., 1994; Ratti and Mujumdar, 1995).The product near the air inlet dries faster while the product next to exit dries less and this may not only cause drying stress in the product and inefficiency in drying but also degrade product quality near the exit. The possible options are interchanging layers of the products or reversing the air flow inside the dryer at regular intervals of time. The interchanging layers of the product which is practiced now for drying of longan is inconvenient and labour intensive. But using air flow reversal, a more uniform product in a fixed bed can be obtained (Ruiz-Lopez et al., 2008; Achariyaviriya et al., 2007). Basically, this method consists of applying the drying airflow in one direction for some time and then reversing the direction of the flow for the next period; the process may be repeated several times before drying is complete although not many reversals are needed to uniform the profiles.

Convective batch drying of longan in batch dryers is a complex process which involves simultaneous heat and mass transfer. To provide design data for the dryer and understand the drying process with air reversal, it is essential to predict temperature and moisture changes with time and position inside the dryer. Many studies have been reported on modeling of deep bed drying of cereal grains (Zare et al., 2006; Aregba and Nadeau, 2007; Hemis et al., 2009; Ratti and Crapiste, 2009) and several studies have been reported on drying of vegetables and fruits.

Limited studies have been reported on modeling of deep bed drying of vegetables and fruits with air reversal. Although several studies have been reported on batch drying of longan with recirculation, no detailed study has been reported on batch drying of longan with reversal of air flow. The purpose of this study is to design a biomass fuelled indirect heating batch type dryer with arrangement for air flow reversal for drying of longan and also assess the experimental and simulated performances of biomass fuelled indirect heating batch type dryer with air flow reversal for drying of longan fruit.

6.2 Materials and methods

6.2.1 Experimental study

The biomass fuelled batch type longan dryer with an arrangement for air reversal was constructed and installed at Silpakorn University, Nakhon Pathom, Thailand. The longan dryer consists of a biomass furnace with a cross flow heat exchanger, a drying bin to contain longan, an electric motor operated axial fan to provide the required air flow and an arrangement for air reversal. The biomass

furnace is designed for fuel wood and the cross flow heat exchanger permits indirect heating of the drying air so that the product is not contaminated by the dust from the biomass furnace. The arrangement for air reversal permits reversal of air flow in the static product bed. The designed batch type longan dryer is shown in Fig 38-39. The drying bin is essentially a deep bed dryer. The bin has the width of 1.8 m, the length of 3.0 m and the height of 01.2 m. The inlet of the bin has the width of 0.4 m and the height of 0.4 m whereas the outlet of the bin has the width of 0.6 m and the height of 0.2 m. The glass wool sandwiched between two parallel galvanized iron sheets is used as the side walls, the cover and bottom side of the drying bin.

Fig. 38 Pictorial view of the longan dryer

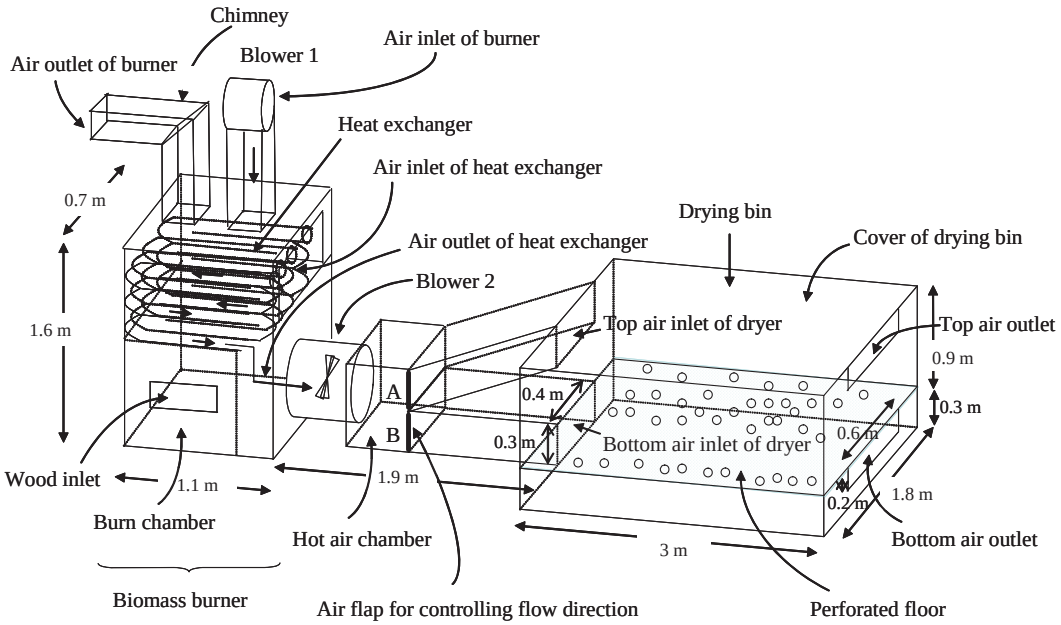

Fig. 39 The structure and dimension of the longan dryer

The three tests were carried out during the period of July - September, 2010. Longans for the experimental runs were purchased from markets at Chiang Mai, northern Thailand. The initial moisture content was 74% (wb) at start of drying and the drying was continued until final moisture content reduced to 14% (wb).

To investigate the dryer performance drying air temperature, air flow rate, relative humidity and weight of longan were monitored during drying. Thermocouples of type K were used to measure the air temperatures in the drying bin (precision ± 2%). The positions of the thermocouples for the measurements of temperatures in the drying bin are shown in Fig. 40. Hot wire anemometer (Airflow, model TA5, precision ± 2%) were employed to monitor the air speed in the drying bin. The direction of air flow was reversed periodically. Relative humidity of ambient air and drying air were periodically measured with hygrometers (Electronik, model EE23, precision ± 2%).

Voltage signals from the hygrometers and thermocouples were recorded every 10 minutes by a 40-channel data logger (Yokogawa, model DC100). Samples of products in the dryer were weighed at 3-hour intervals using a digital balance (Satorius, model E2000 D, precision ± 0.0001 g). The positions of the measurements of the sample weights in the drying bin are also shown in Fig. 40. Before the starting the experimental runs, the hygrometers were calibrated using standard saturated salt solutions with the guideline provided by the manufacturer. Before being used, the thermocouples were also tested by measuring the boiling and freezing temperatures of water to ensure the accuracy. All the drying experiments were carried out at an air velocity entering the drying bed of 3 m/s.

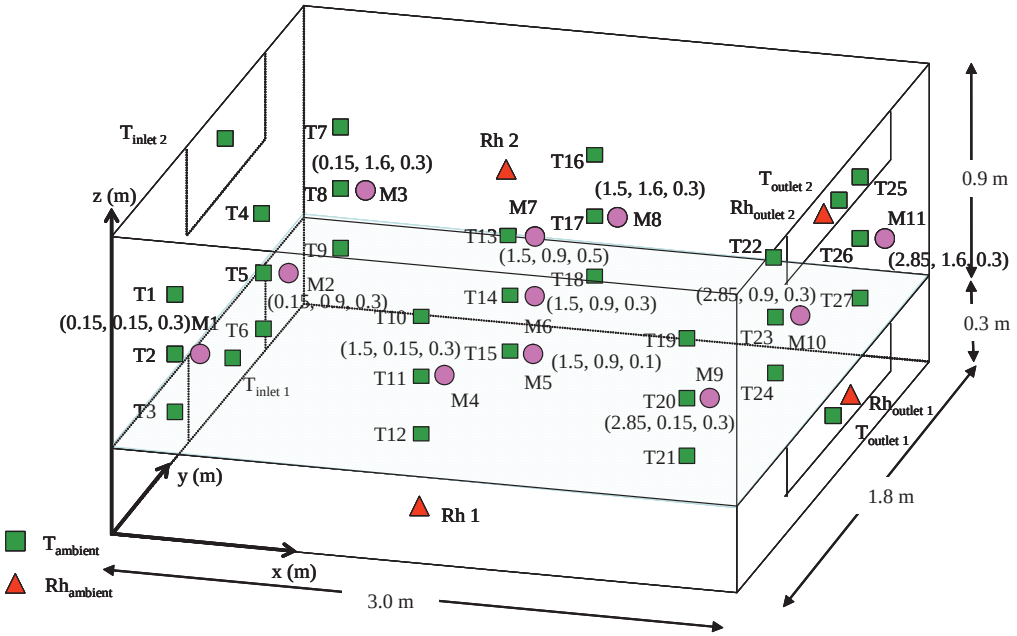

Fig. 40 Positions of the thermocouples (T), hygrometers (rh) and product samples for weights (M). x, y and z are the axis of reference

For the drying tests, 2000 kg, 1500 kg and 1000 kg of whole longan were loaded in the drying bin for each experimental run. For reversal of air flow inside bed, air flap A is closed and air flap B is kept open to pass hot air from the bottom to the top through longan bed from biomass burner while the air flap B is closed and air flap A is kept open to reverse the air flow through longan bed (see Fig. 39). The process was repeated at an interval of 3-hours until the desired moisture content (about 14% on a wet basis) was reached. The moisture content during drying was estimated from the weight of the product samples and the estimated dried solid mass of the samples. At the end of the drying process, the exact dry solid mass of the product samples was determined by using the air oven method. The samples were placed in the oven at the temperature of 103°C for 72 hours (Achariyaviriya et al., 2001).

6.2.2 Uncertainty analysis

Uncertainty analysis refers to the uncertainty or error in experimental data. A systematic error in the experimental data is a repeated error of constant value and the random error is due to an imprecision. The systematic error can be removed by a calibration but the random error can not be removed. The imprecision due to the random error can be defined numerically by a calibration. The measured data on temperature and relative humidity were recorded during the calibration. The mean value of the measurements and standard deviation of the random errors of the data on temperature and relative humidity were determined. The variable x_i which has an uncertainty δx_i is expressed as (Doiebelin, 1976; Holman, 1978; Schenck and Hawks, 1979):

$$x_i = x_{mean}(\text{measured}) \pm \delta x_i \quad (1)$$

where x_i is actual value of the variable, x_{mean} is mean value of the measurements and δx_i is the uncertainty in the measurement.

There is an uncertainty in x_i that may be as large as δx_i. The value of δx_i is the precision index which is taken as 2 times the standard deviation and it encloses approximately 95% of the population for a single sample analysis.

Statistical analysis (analysis of variance) was carried out to assess whether there exists any significant difference in the temperature inside the dryer and the ambient temperature as well as the humidity inside dryer and the ambient relative humidity.

The suitability of the model was evaluated using the value of the root mean square difference (RMSD) and it is measure of the average discrepancy between the experimental points and the fitted curve. It measures the goodness of fit in the unit of the dependent variable. The root mean square difference (RMSD) was calculated using the following equation:

$$\text{RMSD} = \frac{\sqrt{\frac{\sum_{i=1}^{N}(y_{pre,i} - y_{meas,i})^2}{N}}}{\frac{\sum_{i=1}^{N} y_{meas,i}}{N}} \times 100 \quad (2)$$

where $y_{pre,i}$ and $y_{meas,i}$ are the predicted and measured values of variable y, respectively and N is total number of data points.

6.2.3 Water activity measurement of dried longan

The water activity of dried longan samples were measured by a water activity meter (thermoconster, Novasina Co. Ltd., Switzerland). The removal of moisture content reduces the water activity of the product during drying. In general, the water activity (a_w) in most dried food is relatively low, typically less than 0.6, which is the recommended level for safe storage. Low water activity inhibits the growth of various microorganisms and prevents oxidation and enzymatic reactions. Table 7 shows typical water activity values which prevent growth of some common microorganisms (Rahman, 2005; Krokida et al., 2998; Lozano and Ibarz, 1997; Maskan, 2001; Zhang et al., 2003; Lopez Camelo and Gomez, 2004; Jangan et al., 2010).

Table 7 Critical water activity to inhibit microorganisms

Microorganisms	a_w (Critical range)
Bacteria	< 0.85 – 0.86
Yeasts and moulds	< 0.62

6.2.4 Colour measurement of dried longan

The colour of dried longan samples were measured by a chromometer (CR-400, Minolta Co. Ltd., Japan) in CIE (Commission Internationale l'Eclairage) chromaticity coordinates. L^*, a^* and b^* represent black to white (0 to 100), green to red (-60 to +60) and from blue to yellow (-60 to +60) colour respectively. Out of five available colour systems, the L*a*b* and L*C*h systems were selected because these are the most used systems for evaluation of the colour of dried food materials. The instrument was standardized each time with a white ceramic plate. Three readings were taken at each place on the surface of samples and then the mean values of L*, a* and b* were averaged. The different colour parameters were calculated using the following equations.

Hue angle (h) indicating colour combination i.e. browning, is defined as:

$$h = \begin{cases} \tan^{-1}(b^*/a^*) & (\text{when } a^* > 0) \\ 180° + \tan^{-1}(b^*/a^*) & (\text{when } a^* < 0) \end{cases} \quad (3)$$

Chroma (C*) indicating colour intensity or saturation is defined as:

$$C^* = (a^{*2}+b^{*2})^{1/2} \quad (4)$$

and the total colour change (ΔE) is defined as:

$$\Delta E = \sqrt{(L^* - L^*_{ref})^2 + (a^* - a^*_{ref})^2 + (b^* - b^*_{ref})^2} \quad (5)$$

6.2.5 Economic evaluation

The total capital cost for the dryer (C_T) is given by the following equation:

$$C_T = C_m + C_l \quad (6)$$

where C_m is the material cost of the dryer and C_1 is the cost for the construction.

The annual cost calculation method proposed by Audsley and Wheeler (1978) yields:

$$C_{annual} = \left[C_T + \sum_{i=1}^{N} (C_{main,i} + C_{op,i})\omega^i \right] \left[\frac{\omega - 1}{\omega(\omega^N - 1)} \right] \quad (7)$$

where C_{annual} is the annual cost of the system. $C_{main,i}$ and $C_{op,i}$ are the maintenance cost and the operating cost at the year i, respectively. ω is expressed as

$$\omega = (100 + i_{in}) / (100 + i_f) \quad (8)$$

where i_{in} and i_f are the interest rate and the inflation rate in percent, respectively.

The operating cost consists of the wood consumption cost, electricity consumption cost and the labor cost for operating the dryer. This cost can be written as follows;

$$C_{op} = C_{wood} + C_{electric} + C_{labour,op} \quad (9)$$

The maintenance cost was assumed to be 1% of the capital cost.

The annual cost per unit of dried product is called the drying cost (Z, USD/kg). It can be written as

$$Z = \frac{C_{annual}}{M_{dry}} \tag{10}$$

where M_{dry} is the dried product obtained from this dryer per year.

$$\text{Payback period} = \frac{C_T}{M_{dry} P_d - M_f P_f - M_{dry} Z} \tag{11}$$

where M_{dry} is annual production of dry product (kg), M_f is the amount of fresh product per year (kg), P_d is the price of the dry product (USD/kg) and P_f is the price of the fresh product (USD/kg).

6.3 Mathematical modeling

The following assumptions are made in deriving the equations: The volume shrinkage, the temperature gradients within the individual particles and the particle-to-particle conduction during the drying are negligible. Bin walls are adiabatic with negligible heat capacity. The heat capacities of moist air and of longan are constant and heat and mass transfer is one-dimensional.

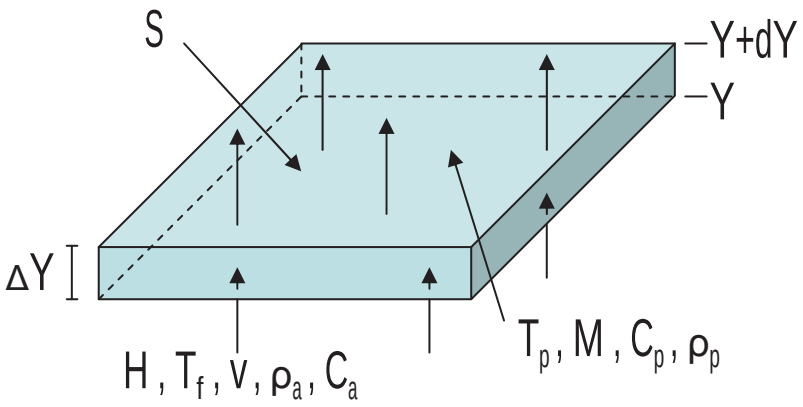

Fig.41 Element of the bed

Moisture content and temperature change with position and time during deep-bed drying of longan. Consider an element of the bed of the dryer (Y, Y+dY) and S is the cross-sectional area with air speed (v) from Y to Y+dY (Fig. 41). There are four unknowns: moisture content (M), humidity ratio (H), drying air temperature (T_f), and product temperature (T_p). Thus, two conservation equations and two rate equations are made, resulting in four equations to solve the problem.

- Energy balance equation

Change of enthalpy of air = Sensible heat transfer from the air to moisture prior to evaporation - Change in sensible heat of the moist product + Enthalpy in evaporated moisture

Mathematically this can be expressed as:

$$m_a(C_a + C_v H)\frac{\partial T_f}{\partial Y} = \rho_p C_v (T_f - T_p)\frac{\partial M}{\partial t} - \rho_p (C_p + C_f M)\frac{\partial T_p}{\partial t} + \rho_p L_p \frac{\partial M}{\partial t} \quad (12)$$

- Heat transfer rate equation

Change in enthalpy of the product = Convective heat transfer between the air and the product + Enthalpy in evaporated moisture

Mathematically this can be expressed as:

$$\rho_p (C_p + C_f M)\frac{\partial T_p}{\partial t} = h_v (T_f - T_p) + \rho_p L_p \frac{\partial M}{\partial t} \quad (13)$$

where h_v is the volumetric heat transfer coefficient and it is computed from the following relationship (Bakker-Arkema and Hall, 1974).

$h_v = 8.69 \times 10^4 m_a^{1.3}$ (14)

- Mass balance equation

The mass balance equation gives that the moisture lost by product is equal to moisture gained by the air. Mathematically it can be expressed as:

$$m_a \frac{\partial H}{\partial Y} = -\rho_p \frac{\partial M}{\partial t} \quad (15)$$

- Thin layer drying equation of the product

The rate of change of moisture content of a product in the dryer can be expressed by an appropriate thin layer drying equation. Thin layer drying equation in the form of Page equation developed by Phupaichitkun et al. (2008) was used in this study and the equation used is:

$$\frac{M - M_e}{M_0 - M_e} = \exp(-At^B) \quad (16)$$

where A is a function of drying air temperature (T, °C), relative humidity (rh, decimal), air speed (v, m/s) and radius of longan fruit (r_l, m) and B is a constant. The parameters A and B were obtained by fitting the Page equation to the experimental data using MATLAB (MathWork, Inc.). The details are given in Phupaichitkun et al. (2008) A and B are expressed as:

$$A = \frac{179.907 - 0.0569\left(\frac{rh}{v}\right) - 7182\exp\left(\frac{-455.2}{T + 273.15}\right)}{r_l^2} \quad (17)$$

B = 1.0829.

Equilibrium moisture contents for whole longan were determined experimentally in the Department of Physics, Silpakorn University, Nakhon Pathom, Thailand using the dynamic method. To determine the equilibrium moisture contents, three sets of equipment were constructed and each set consists of a hot air chamber containing six sample boxes in three trays. The sample box was essentially an airtight plastic box containing saturated salt solution to maintain constant relative humidity inside the sample box show in Fig. 42. Each sample box is divided by plastic wall into two sections for holding two samples separately and simultaneously. The sample boxes were half filled with salt solution. The samples were placed inside the perforated sample containers of 8 cm in width, 12 cm in length and 3 cm in height and the sample boxes were placed on the perforated plastic supports just above the salt solution. Two small electric fans were fitted to circulate the air inside the sample box to accelerate moisture transfer between the samples and air inside the sample box. The sample boxes were placed inside the hot air chamber. The hot air chamber was equipped with a 3 kW electrical heater and an electronic temperature controller to maintain the temperature and the relative humidity was maintained by saturated salt solution.

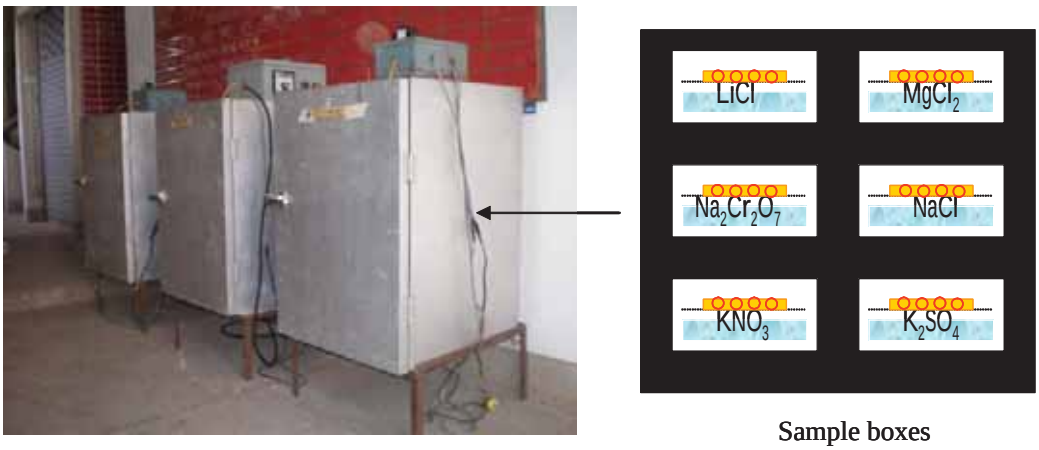

Fig. 42 Show the hot air chamber and sample boxes

In conducting the experiments, eight whole longan fruits were placed inside the sample containers located inside the sample boxes and the sample boxes were placed inside the hot air chamber. The samples were weighed regularly until they reached equilibrium. The final moisture contents of the product were determined by the standard oven method (temperature of 103 °C for 24 hours). Details of experiments and modeling are similar to those for the case of longan fresh reported in

Janjai et al. (2006). The results of the experiments and modeling of the equilibrium moisture content obtained from this work are shown in the next section.

To obtain the numerical solution of the longan deep bed model, the whole longan bed is divided into a number of layers ($Y = j.\Delta Y$) along the depth of the dryer. The drying time is also divided into a number of intervals ($t = i.\Delta t$). On the basis of the air temperature, air velocity and relative humidity, the drying content (A, B) and dynamic equilibrium moisture content (M_e) of the whole longan were computed. Using the A, B and M_e values, the changes of moisture content of whole longan, ΔM, for a time interval, Δt, were calculated using Eq. (16-21). Using the recent value of drying air temperature and drying rate, the product temperature of first layer of the dryer was computed using Eq. (13). On the basis of the recent value of the product temperature, the air temperature inside the first layer of drier was estimated using Eq. (12). The change in air humidity was computed using Eq. (15). This process was repeated layer-by-layer until the top of the bed was reached. This process was then repeated for each time increment. When air relative humidity exceeds 98%, the condensation routine deposits back the moisture from the saturated air. Air and whole longan temperatures are adjusted for this condensation. The numerical solution was programmed in Compaq Visual FORTRAN version 6.5.

6.4 Results and discussions

6.4.1 Experimental results

Three tests were carried out for drying of whole longan in the longan batch dryer in the months of July to September, 2010 and the loading capacities were 1000 kg, 1500 kg and 2000 kg.

Fig. 43 shows ambient, inlet and outlet air temperature during drying of whole longan for the loading capacity of 1000 kg. The inlet air temperature was maintained almost constant level of 80 °C and the outlet temperature was slightly lower than this for most of the drying period. Thus, outlet air appears to have sufficient drying potentials which can be recycled when more than one dryer are in operation. Similar results were found for the case of 1500 kg and 2000 kg because of the fact that the inlet temperature was maintained constant and the outlet air left the dryer with some drying potentials in all these cases.

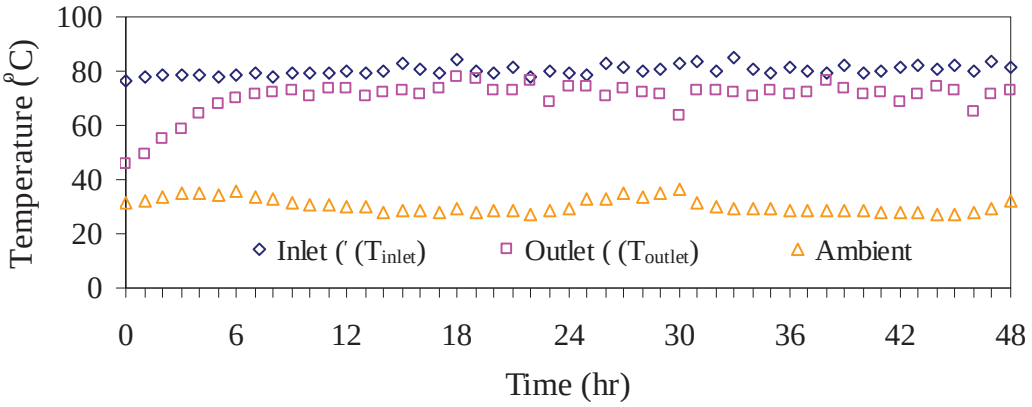

Fig. 43 Variations of inlet temperature and outlet temperature of the dryer and ambient temperature during a typical experimental run of a loading capacity of 1000 kg

Fig. 44 shows temperature at the bottom, middle and top of the drying bed for periodic air reversal. When the air enters at the bottom, the exhaust temperature at top is low and the reverse true when the air enters at the top of the bed resulting a constant temperature of 65 °C in the middle of the bed which is the optimum temperature for drying of longan. Basically, the drying airflow is in one direction for some time and then the direction of the air flow is reverse for the next period; the process is repeated several times until the drying is complete. The cyclic variation of the air flow rates causes the cyclic variation of the inlet and outlet temperatures. However, the temperature inside the dryer is almost same during air flow reversal periods. Similar results were found for the case of 1500 kg and 2000 kg because of the fact that the inlet temperature was maintained constant and the air flow was reversed in the same cyclic patterns in all these cases.

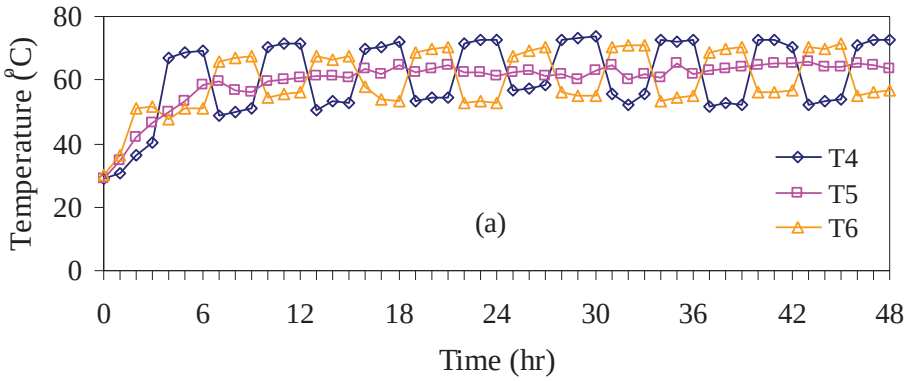

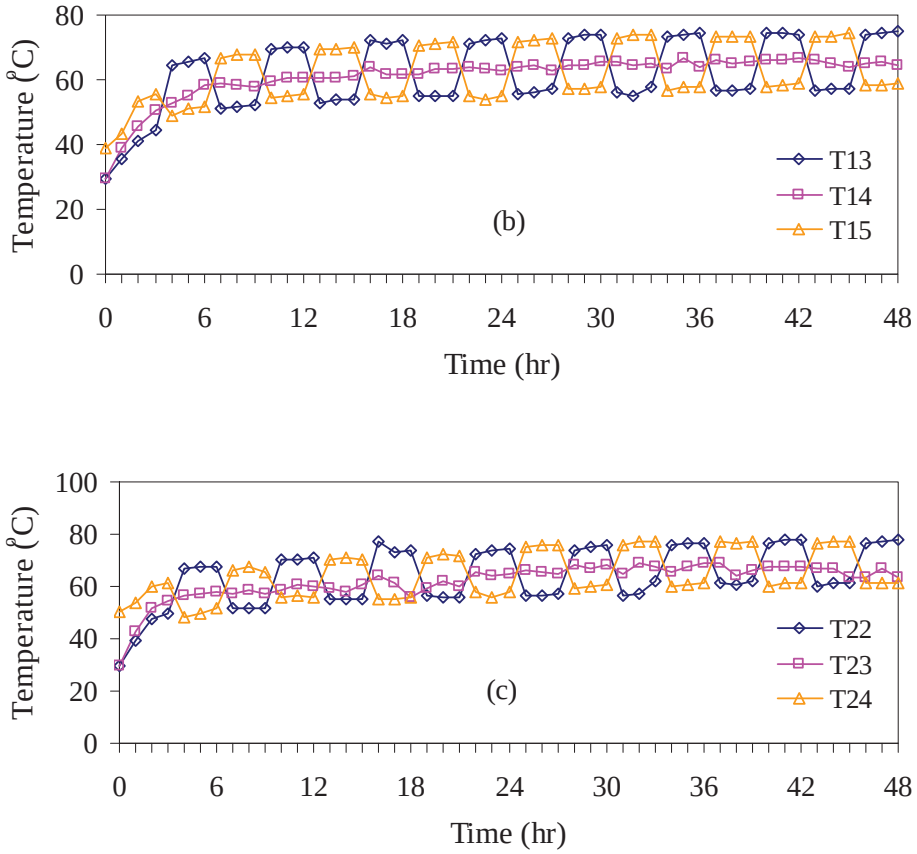

Fig. 44 Variations of the temperatures at bottom, middle and top positions of the dryer a) front section, b) middle section and c) behind section (see Fig. 40)

Fig. 45 shows the temperatures at different positions (except inlet and outlet) inside the drying bed for periodic air reversal. Analysis of variance (ANOVA) in Table 8 shows that the calculated $F_{0.05}$ is 0.472 which is less than the tabulated F value of 1.94. Hence there is no significant difference in temperatures in the different positions inside the dryer ($p<0.05$). Thus, the periodic reversal of the air flow air removes the temperature gradients inside the dryer. Similar results were found for the case of 1500 kg and 2000 kg because of the fact that the inlet temperature was maintained constant and the air flow was reversed in the same cyclic patterns in all these cases.

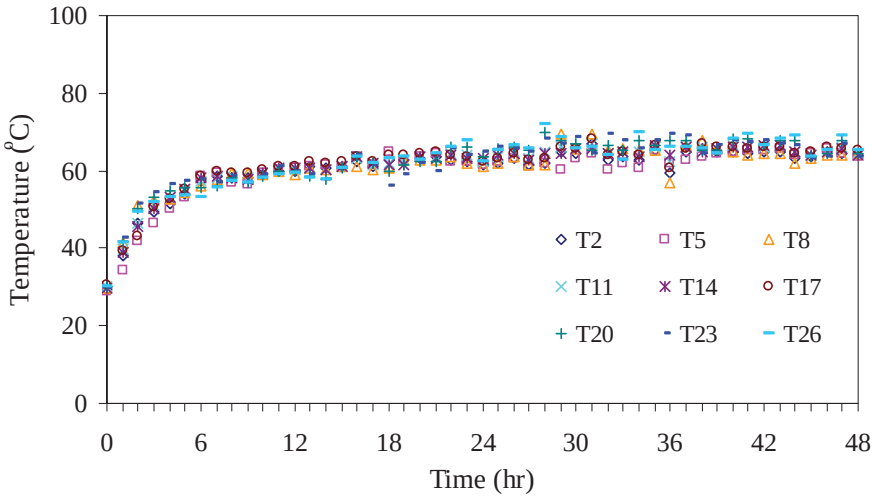

Fig. 45 Temperatures at different positions inside the drying bed for periodic air reversal of a loading capacity of 1000 kg

Fig. 46 shows relative humidity of ambient, inlet and outlet air. The inlet air relative humidity was almost constant and the outlet relative humidity decreased with time. The relative humidity of the outlet air decreased little towards the end of the drying indicating that it is approaching the inlet humidity. Thus, the exhaust air which is leaving the dryer at much higher temperature (Fig. 6.6) and at a lower relative humidity in comparison to the ambient air has sufficient drying potentials and can be recycled when more than one dryers are in operation. Similar results were found for the case of 1500 kg and 2000 kg because of the fact that the inlet relative humidity was low and the inlet temperature was maintained constant while the outlet air leaving the dryer was never saturated in all these cases.

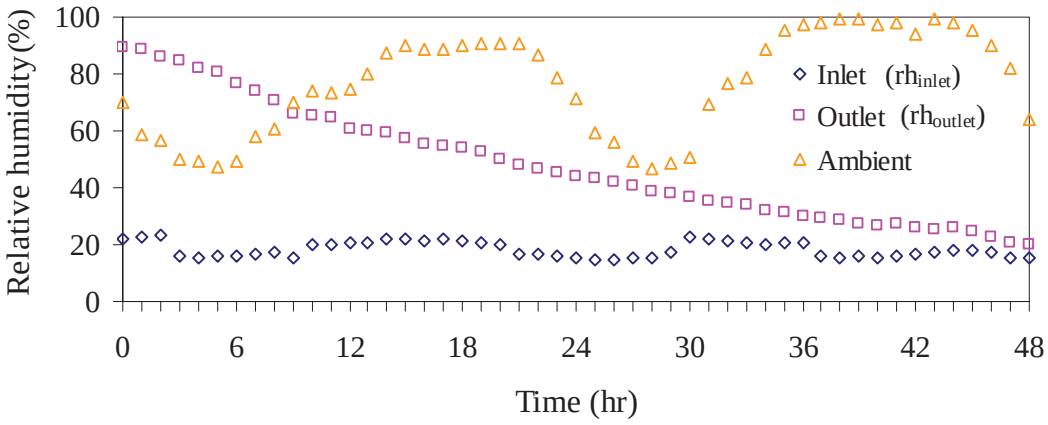

Fig. 46 Variations of ambient, inlet and outlet relative humidity during a typical experimental runs of a loading capacity of 1000 kg

Fig. 47 shows the moisture content changes at different positions (middle, sides and corners) inside the drying bed. Analysis of variance in Table 9 shows that the calculated $F_{0.05}$ is 0.005 which is less than the tabulated F value of 1.91. Hence there is no significant difference in moisture content in the different positions inside the dryer ($p<0.05$). Thus, the periodic reversal of the air flow removes the moisture content gradients inside the dryer. Similar results were found for the case of 1500 kg and 2000 kg because of the fact that the inlet temperature was maintained constant and the air flow was reversed in the same cyclic patterns in all these cases.

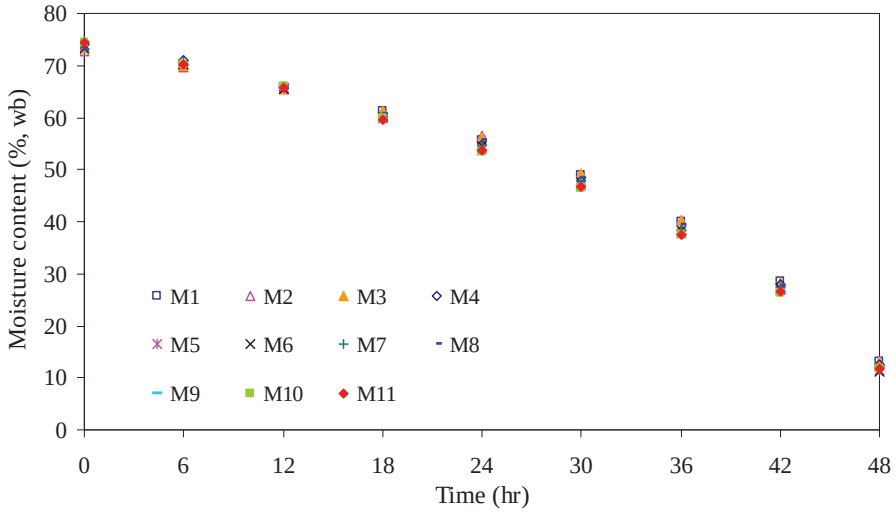

Fig. 47 Moisture content changes at different positions (middle, sides and corners) inside the drying bed

Fig. 48 shows that the moisture content of longan inside dryer during a typical drying run and it reduces from 74% (wb) to about 14% (wb) within 48 hours, 54 hours and 60 hours for loading capacity of 1000 kg, 1500 kg and 2000 kg respectively. The higher is the loading, the lesser is the percentage of the exposure of the products to higher temperature resulting higher drying time.

The operating costs of 1000 kg, 1500 kg and 2000 kg of loading capacity of the dryer are 0.052 USD/kg, 0.039 USD/kg and 0.031 USD/kg, respectively. Operating costs were estimated from the amount of electricity consumed and fuel wood used and unit prices of electricity and fuel wood. The drying behaviors of whole longan for loading capacity of 1000 kg, 1500 kg and 2000 kg were similar. But the operating cost decreases with the increase of the loading capacity. This suggests that batch dryer with air flow reversal should be operated at the full loading capacity for economic operation of dryer.

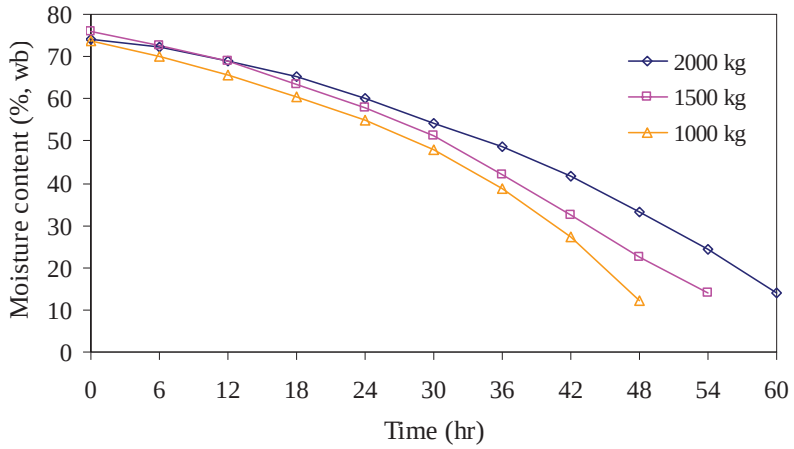

Fig. 48 Moisture content of longan inside dryer during typical drying runs

Table 8 The analysis of Variance (ANOVA) for temperature distributions in different positions inside the dryer

	Sum of squares	df	Mean square	Calculated F	Tabulated F
Between positions	195.784	8	24.473	0.477	1.94
Within positions	22160.552	432	51.298		
Total	22356.336	440			

Table 9 The analysis of Variance (ANOVA) for moisture content distributions in different positions inside the dryer

	Sum of squares	df	Mean square	Calculated F	Tabulated F
Between positions	22.078	10	2.208	0.005	1.91
Within positions	37662.515	88	427.983		
Total	37684.593	98			

6.4.2 Results of equilibrium moisture content

Sorption isotherms of whole longan at three temperature levels of 40, 50 and 60 °C, in the range of 11.6 - 96.2% relative humidity values are shown in Fig. 49. The isotherm curves have sigmoid shape and similar patterns. Fig. 49 show that the EMC values decreased with the increase in temperature at all levels of relative humidity.

These experimental results were fitted with existing equilibrium moisture content models. It was found that the GAB equation fitted best to experimental data. The equation is given by:

$$M_e = \frac{b_0 b_1 b_2 a_w}{(1-b_2 a_w)(1-b_2 a_w + b_1 b_2 a_w)} \quad (18)$$

where

$$b_0 = 0.21599 \exp\left(\frac{13662.7534}{R_0 T_{ab}}\right) \quad (19)$$

$$b_1 = -37.21382 \exp\left(\frac{31969.5594}{R_0 T_{ab}}\right) \quad (20)$$

$$b_2 = 1.27174 \exp\left(\frac{-906.6819}{R_0 T_{ab}}\right) \quad (21)$$

where a_w is water activity (decimal), T_{ab} is drying air temperature (K) and R_0 is universal gas constant (J/mol-K).

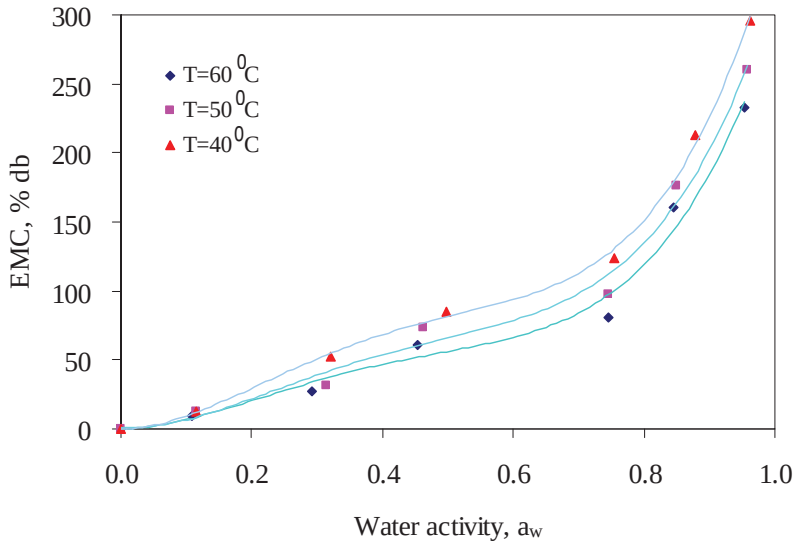

Fig. 49 Measured sorption isotherms (points) for whole longan at the temperature levels of 40°C, 50°C and 60°C

6.4.3 Simulated results

To validate the model, the predicted results during drying of whole longan at the middle of the drying bed were compared to the experimental values. Fig. 50 shows a typical comparison between the predicted and experimental values of the predicted and observed moisture contents of whole longan inside the dryer and the model predicts well the moisture content changes during drying.

The model predictions were evaluated on the basis of root mean square difference (RMSD). RMSD of the prediction of the moisture contents for the loading capacity of 1000, 1500 and 2000 was

3.7%, 4.9% and 4.7%, respectively. Thus, the model predictions of the moisture contents are reasonably good. Furthermore, predictions are within the acceptable limit (10%).

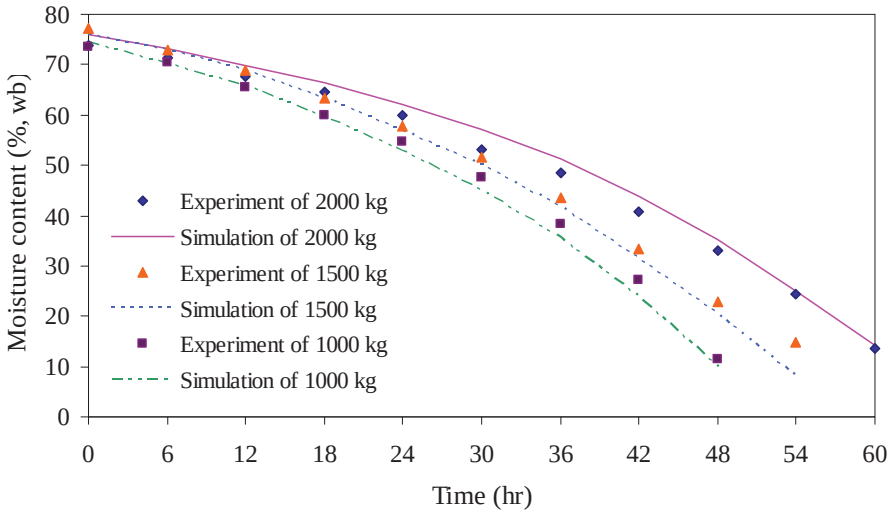

Fig. 50 Comparison of the simulated and observed moisture content during drying of whole longan 1000 kg, 1500 kg and 2000 kg

Simulated results of drying air temperature and relative humidity at the middle of drying bed were also compared with the observed values (Fig. 51 and Fig. 52) and the model predicts well the drying air temperature and relative humidity. RMSD of the prediction of the drying air temperature and relative humidity was 5.0% and 11.0%, respectively. These predictions are also within the acceptable limit (10%). Fig. 53 shows the simulated product temperature and the model predicts plausible behavior of the product temperature. Although there is no direct comparison between the simulated and observed values, the model predicts the product temperature reasonably well at least qualitatively.

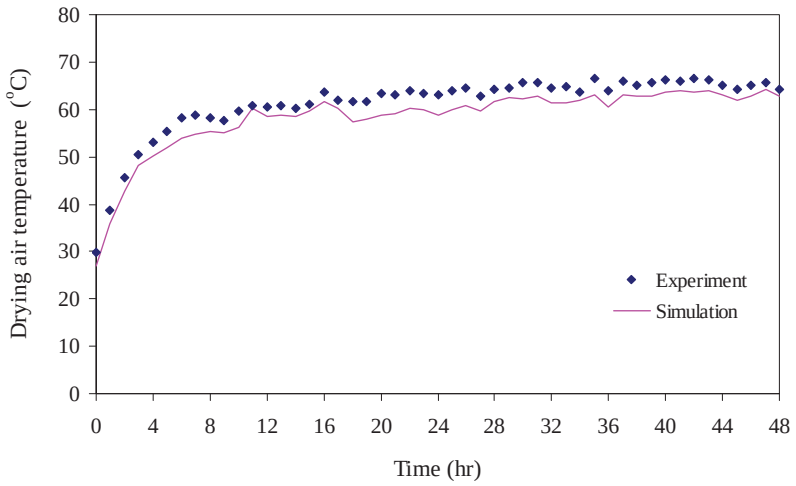

Fig. 51 Comparison of the simulated and observed drying air temperature (T_f) during drying for 1000 kg of whole longan

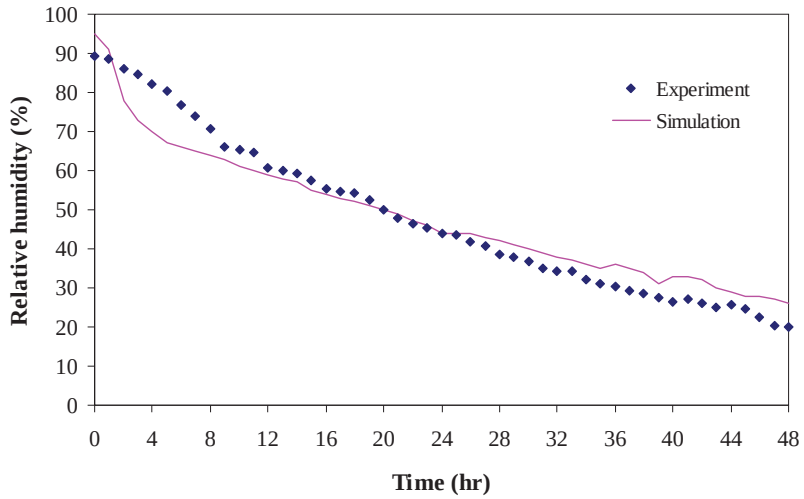

Fig. 52 Comparison of the simulated and observed relative humidity during drying for 1000 kg of whole longan

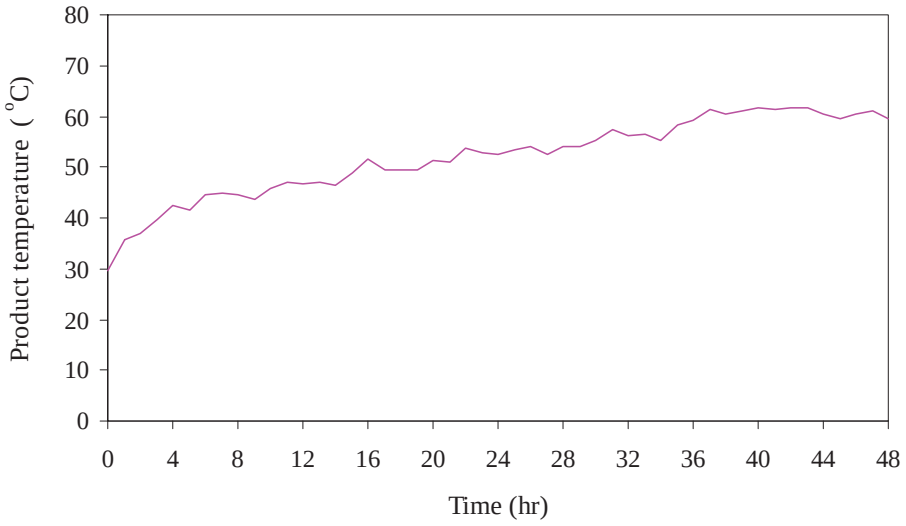

Fig. 53 The simulated result of product temperature (T_p) during drying for 1000 kg of whole longan

6.4.4 Qualities of dried whole longan

The average water activity (a_w) of dried whole longan for the drying tests of 2000 kg, 1500 kg and 1000 kg of whole longan was about 0.58 which is lower than the standard (a_w=0.60).

The results of colour measurements of whole longan are shown in Table 10. Drying of flesh of longan resulted in increase in the values of a* from 0.75 to 10.95, b* from -0.66 to 9.60 and chroma C* from 1.85 to 14.63. But L decreases from 33.02 to 22.78 and hue angle (h) decreased from 232.43 to

40.56. Nathakaranakule et al. (2010) also reported similar color changes. This implies that drying of logan flesh results in bright golden brown color. However, Varith et al. (2007) and Tippayawong et al. (2009) found golden brown, and golden and light reddish yellow color, respectively. Thus, the present findings agree with the results reported. Again, drying of shell of longan increases the values of a* from 8.76 to 10.88, b* from 16.52 to 19.82 and chroma C* from 18.70 to 22.63. But L decreases from 45.86 to 42.82 and hue angle (h) decreased from 62.06 to 61.20. This causes the color of shell to change into more golden brown. The total colour change of fresh longan was 18.0 which indicates a large difference in color while the total change of shell of longan is 4.9 which indicates an appreciable color difference. The colour change is more incase of longan flesh and this color is the acceptable color in the dried longan markets and to the consumers for dried longan.

Table 10 Colour variations of fresh and dried whole longan

Status	Treatments	Colour Value					
		L*	a*	b*	C*	h	ΔE
Fresh flesh of longan	Average of nine observations	33.023	0.752	-0.661	1.847	232.43	-
Dried flesh of longan	Average of nine observations	22.779	10.954	9.604	14.627	40.564	18.0
Fresh shell of longan	Average of nine observations	45.865	8.762	16.523	18.702	62.068	-
Dried shell of longan	Average of nine observations	42.821	10.882	19.821	22.625	61.203	4.9

6.4.5 Economic result

The capital cost for construction and installation of the longan dryer is 4,300 USD and capacity of dryer is 2,000 kg. The harvesting season is three months for whole longan and approximately 15,840 kg of dry whole longan are produced annually. The information for the computation of the payback period are given in Table 11. The labour and labour costs were estimated from usual construction costs of conventional longan dryers. The prices of fresh and dried longan were obtained from local markets in Chiang Mai. Based on these information on production scales, capital and operating costs of the drying system and price of the dried products, the payback period of the longan dryer for drying whole longan is estimated to be 2.6 years.

Table 11 Computation of payback period

Items	Costs and economic parameters
Materials of constructions	1,800 USD*
Biomass burner and blower	1,500 USD
Labour costs for constructions	1,000 USD
Repair and maintenance cost	1% of capital cost per year
Wood consumption: (a) Quantity of fuel wood (b) Price of fuel wood	 1200 kg per batch 37 USD per 1000 kg
Electricity consumption: (a) Amount of electricity (b) Price of electricity	 60 kWh per batch 0.114 USD per kWh
Labor cost for operating the dryer: (a) Labour cost (b) Number of labour per batch	 5.7 USD per person 2 person
Operating cost: (a) fuel wood (b) electricity (c) labour (d) number of batch (e) total operating cost	44.4 USD per batch 6.84 USD per batch 11.4 USD per batch 24 batch per year 1,503 USD per year
Price of fresh longan	0.4 USD
Price of dried longan	1.4 USD
Expected life of the dryer	15 years
Interest rate	7%
Inflation rate	3.5%

* (1USD = 35 Baht)

6.5 Conclusions

A biomass fueled batch type longan dryer with arrangement for periodic air flow reversal was designed and tested. The airflow reversals were found to give more uniform moisture and temperature distributions in the longan bed. It is also economical to use the dryer for a full loading capacity of 2000 kg of whole longan per batch. The quality of dried longan was good in comparison to the high quality product in markets.

A set of partial differential equations were developed and the equations were solved using finite difference technique. The numerical solution was programmed in Compaq Visual FORTRAN version 6.5. The simulated moisture contents agreed well with the experimental data. This model can be used to provide the design data and it is also essential for optimal design of the dryer.

Chapter 7
Conclusions

In this work, the drying kinetics of longan drying, diffusivities of longan fruit, finite element simulation of longan fruit and performance of two longan dryers have been investigated and the results can be concluded as follows:

1) Drying air temperature has a great influence on the drying rate of peeled longan and there is no difference in colour for longan dried between 50 to 70 °C. In addition, Page model was found to be the best model to predict the moisture content of thin layer drying peeled longan.
2) Moisture diffusivity of different parts of longan fruit has been determined. It was found that the diffusivity of the flesh of longan fruit increased with temperature but the diffusivities of shell, seed coat, seed and seed stalk were temperature independent. Additionally, moisture diffusivities of shell and seed coat were much lower than those of the other parts of the longan.
3) A two-dimensional finite element model has been developed to simulate moisture diffusion in longan fruit during drying. The simulation results revealed the moisture content inside the longan fruit. These results indicated that the seed stalk controlled the moisture movement from the flesh into the drying environment.
4) The performance of a side loading type solar tunnel dryer for drying peeled longan has been evaluated. The experimental results showed that the drying time of peeled longan in this solar tunnel dryer is significantly shorter than that of the natural sun drying and good quality dried product was obtained. Additionally, a system of partial differential equations describing heat and moisture transfer during drying of peeled longan was developed and the simulated results agreed well with the experimental data. This type of dryer has high potential for drying peeled longan in a commercial scale.
5) Experimental and simulated performance of a batch type longan dryer with air flow reversal using biomass burner as a heat source has been carried out. It was found that the air flow reversal gave uniform moisture and temperature distributions in the longan bed. In addition, the drying model developed for this dryer predicted well the moisture content of longan during drying process. This proposed dryer has high potential for drying longan fruit in commercial scale.

As the moisture profiles in longan fruit predicted by the finite element model could not be measured in this work, it is suggested that these profiles must be experimentally validated by using advanced instruments, such as nuclear magnetic resonance imager (NMRI) for a further work. It is also recommended that the side loading tunnel dryer and the reversal flow longan dryer should be tested in the fields and further developed.

References

Abu-Hamdeh, N.H.; Othman, A.M. An experimental study and mathematical simulation of wheat drying. Drying Technology, 22(3), 491-506, 2004.

Achariyaviriya, S.; Soponronnarit, S.; Terdyothin, A. Diffusion models of papaya and mango GLACE' drying. Drying Technology, 18(7), 1605-1615, 2000.

Achariyaviriya, A. Simulation and optimization of the drying strategy for longan drying; Ph.D. Dissertation. King Mongkut's University of Technology Thonburi, Thailand, 2001.

Achariyaviriya, A.; Soponronnarit, S.; Tiansuwan, J. Study of longan flesh drying. Drying Technology, 19(9), 2315-2329, 2001.

Achariyaviriya, A.; Punyabute, T. Drying kinetics of longan fruit without stone. In Proceedings of the international conference on crop harvesting and processing, 9 – 11 February, Louisville, Kentucty, USA, 2003.

Achariyaviriya, S.; Puttakarn, B. A mathematical model of moisture diffusivity lychee drying. Proceedings of the International Conference on Crop Harvesting and Processing, 9 -11 February, (Louisville, Kentucky, USA). ASABE Paper No. 701P1103e, 2003.

Achariyaviriya, A.; Maneeboon, K.; Jeorentong, W. Performance of a batch type dryer for longan fruits drying. In: 21st mechanical engineering network conference of Thailand, 17-19 October, Pattaya, Thailand, 2007.

Akpinar, E. K.; Bicer, Y.; Yildiz, C. (a). Thin layer drying of red pepper. Journal of Food Engineering, 59, 99-104, 2003.

Akpinar, E. K.; Midilli, A.; Bicer, Y. (b). Single layer drying behavior of potato slices in a convective cyclone dryer and mathematical modeling. Energy Conversion and Management, 44, 1689-1705, 2003.

Aregba, A.W.; Nadeau, J.P. Comparison of two non-equilibrium models for static grain deep-bed drying by numerical simulations. Journal of Food Engineering, 78, 1174-1187, 2007.

Audsley, E.; Wheeler, J. The annual cost of machinery calculated actual cash flows. Journal of Agricultural Engineering Research, 23,189-201, 1978.

Azzouz, S.; Guizani, A.; Jomma, W.; Belghith. Moisture diffusivity and drying kinetic equation of convective drying of grapes. J. Food Eng., 55, 323-330, 2002.

Babalis, S. J.; Belessiotis, V. G. Influence of the drying conditions on the drying constants and moisture diffusivity during thin layer drying of figs. J. Food Eng., 65, 449–458, 2004.

Bakker-Arkema, F.W.; Bricket, W.G.; Patterson, R.J. Simultaneous heat and mass transfer during the cooling of a deep bed of biological products under varying inlet air conditions. Journal of Agricultural Engineering Research, 12(4), 2197-307, 1967.

Bakker – Arkema, F.W.; Hall, C.W. Drying Cereal Grains. Westport, Connecticut: AVT, 1974.

Bala, B.K.; Woods, J.L. Simulation of deep bed malt drying. Journal of Agricultural Engineering Research, 30, 235-244, 1984.

Bala, B.K.; Woods, J.L. Simulation of the indirect natural convection solar drying of rough rice. Solar Energy, 53, 259-266, 1994.

Bala, B.K.; Woods, J.L. Optimization of a natural convection solar drying system. Energy, 20, 285-294, 1995.

Bala BK. Drying and Storage of Cereal Grains. Oxford & IBH Publishing Co., New Delhi, India, 1997.

Bala, B.K. Solar Drying Systems; Udaipur: Agrotech Publishing Academy, 1998.

Bala, B.K. Mathematical modeling of deep bed drying of agricultural crops. Journal of Agricultural Engineering, 27(1-4), 54-65, 1990.

Bala, B.K.; Mondol, M.R.A. Experimental investigation on solar drying of fish using solar tunnel drier. Drying Technology, 19, 1-10, 2001.

Bala, B.K.; Mondol, M.R.A.; Biswas, B.K.; Das Choudhury, B.L.; Janjai, S. Solar drying of pineapple using solar tunnel drier. Renewable Energy, 28, 183-190, 2003.

Bala B.K.; Janjai S. Solar drying of fish (Bombay Duck) using solar tunnel dryer. International Energy Journal, 6, 91-102, 2005.

Baini, R.; Langrish, T. A. G. Choosing an appropriate drying model for intermittent and continuous drying of bananas. Journal of Food Engineering, 79, 330-343, 2006.

Berbert, P.A.; Queiroz, D.M.; Silva, J.S.; Pinheiro, J.B. Drying of coffee (Coffea Arabica L.) in a fixed bed with a simulated periodic airflow reversal. Journal of Agricultural Engineering Research, 59, 195-202, 1994.

Bloome, P.D.; Shove, G.E. Near equilibrium simulation of shelled corn drying. Transactions of the ASAE, 14(4), 709-712, 1971.

Bon, J.; Rosselló, C.; Femenia, A.; Eim, V.; Simal, S. Mathematical modeling of drying kinetics for apricots: Influence of the external resistance to mass transfer. Drying Technology, 25(11), 1829-1835, 2007.

Bose, A.S.C.; Ojha, T.P. An integrated solar drying system for agricultural crop drying. Drying Technology, 2, 61-95, 1983.

Boyce, D.S. Grain moisture and temperature changes during through drying. Journal of Agricultural Engineering Research, 10(4), 333-341, 1965.

Boyce, D.S. Heat and moisture transfer in ventilated grain. PhD thesis. Newcastle upon Tyne, UK, University of Newcastle upon Tyne, 1966.

Chen, X.D. Moisture diffusivity in food and biological materials. Drying Technology, 25, 1203-1213, 2007.

Chen, J.Y.; Isobe, K.; Zhang, H.; Matsunaga, R. Hot-air dryimg model for udon noodles. Food Science and Technology Research, 6(4), 284-287, 2000.

Diamante, L.M.; Munro, P.A. Mathematical modelling of the thin layer solar drying of sweet potato slices. Solar Energy, 51, 271-276, 1993.

Doiebelin, E.O. Measurement Systems. McGraw Hill. New York, 1976.

Doymaz, I. Drying Charateristics and kinetics of okra. J. Food Eng., 69,275-279, 2005.

Duffie, J.A.; Beckman, W.A. Solar Engineering of Thermal Processes, New York, John Wiley and Sons, 1991.

Efremov, G.; Kudra, T. Model-based estimate for time-dependent apparent diffusivity. Drying Technology, 23, 2513-2522, 2005.

Eissen, W.; Mühlbauer, W.; Kutabach, H.D. Solar drying of grapes. Drying Technology, 3, 63-74, 1985.

El Fadil, A.A.B. Solar drying of sliced onion and quality attrinutes as affected by the drying process and storage condition. Ph.D Dissertation, Institute for Agricultural Engineering in the Tropics and Subtropics, The University of Hohenheim, Stuttgart, Germany, 1998.

Erenturk, S.; Gulaboglu, M.S.; Gultekin, S. The thin-layer drying characterisitics of rosehip. Biosystems Engineering, 89(2), 159–166, 2004.

Ertekin, C.; Yaldiz, O. Drying of eggplant and selection of a suitable thin layer drying model. Journal of Food Engineering, 63, 349-359, 2004.

Esper, A.; Mühlbauer, W. Development and dissemination of solar tunnel drier. In proceedings of ISES Solar World Congress. Budapest, 22, 1993.

Esper, A.; Mühlbauer, W. Solar tunnel dryer for fruits. Plant Research and Development, 44, 61-80, 1996.

Esper, A.; Mühlbauer, W. PV-driven solar tunnel drier. In Proceeding of Agricultural Engineering Conference, Bangkok, Thailand, December 6-9, 1994.

Exell, R.H.B.; Kornsakoo, S. A low-cost solar rice dryer. Appropriate Technology, 5, 23-24, 1978.

Exell, R.H.B.; Kornsakoo, S. Basic design theory for a simple solar rice dryer. Renewable Energy Review Journal, 1, 1-14, 1980.

Forson, F.K.; Nazha, M.A.A.; Rajakaruna, H. Modeling and experimental studies on a mixed-mode natural convection solar crop-dryer. Solar Energy, 81, 346-357, 2007.

Gaston, A. L.; Abalone, R. M.; Giner, S. A. Wheat drying kinetics for sphere and ellipsoid by finite element. J..Food Eng., 52, 313-322, 2002.

Gaston, A.L; Abalone, R.M.; Giner, S.A.; Bruce, D.M. Effect of modeling assumptions on the effective water diffusivity in wheat. Biosystems Engineering, 86, 175-185, 2004.

Giner, S.A.; Mascheroni, R.H. Diffusive drying kinetics in wheat, part II : applying the simplified analytical solution to experimental data. Biosystems Eng., 81(1), 85-97, 2002.

Goyal, R. K.; Kingsley, A. R. P.; Manikantan, M. R.; Ilyas, S. M. Thin-layer drying of raw mango slices. Biosystems Engineering, 95(1), 43-49, 2006.

Guarte, R. Modeling the drying behavior of copra and development of a natural convection dryer for production of high quality copra in the Philippines. PhD Dissertation, Institute for Agricultural Engineering in the Tropics and Subtropics, The University of Hohenheim, Stuttgart, Germany, 1996.

Guarte, R. C.; Muhlbauer, W.; Kellert, M. Drying characteristics of copra quality of copra and coconut oil. Postharvest Biology and Technology, 9, 361-372, 1996.

Haghighi, K.; Segerlind, I.J. Modeling simultaneous heat and mass transfer in an isotropic sphere - a finite element approach. Transactions of the ASAE, 31(2), 629-637, 1988.

Haghighi, K. Finite element simulation of the thermo-hydro stresses in a viscoelastic sphere during drying. Drying Technology, 8(3), 451-464, 1990.

Haghighi, K.; Aguirre, C.G. Adaptive and stochastic finite element analysis in drying. Drying Technology, 17, 2037-2053, 1999.

Hashimoto, A.; Kameoka, T. Water sorption analysis in vegetables using a modified dubinin-astakhov equation. Food Science and Technology Research, 4(3), 227-229, 1998.

Hawlader, M.N.A.; Perera, C.O.; Min, T.; Yeo, K.L. Drying of guava and papaya: Impact of different drying methods. Drying Technology, 24, 77-87, 2006.

Hemis, M.; Bettahar, A.; Singh, C.B.; Bruneau, D.; Jayas, D.S. An experimental study of wheat drying in thin layer and mathematical simulation of a fixed-bed convection dryer. Drying Technology, 27, 1142-1151, 2009.

Henderson, S.M. Progress in developing the thin layer drying equation.Transactions of the ASAE, 17, 1167-1172, 1978.

Holman, J.P. Experimental Method for Engineers. McGraw Hill, New York, 1978.

Hossain, M.A.; Bala, B.K. Drying of hot chilli using solar tunnel drier. Solar Energy, 81, 85-92, 2007.

Hossain, M. A.; Bala, B. K. Thin-layer drying characteristics for green chilli. Drying Technology, 20(2), 489-505, 2002.

Irudayaraj, J.; Haghighi, K.; Stroshine, R.L. Nonlinear finite element analysis of coupled heat and mass transfer problems with an application to timber drying. Drying Technology, 8, 731-749, 1990.

Irudayaraj, J.; Haghighi, K. I. Theory and finite element formulation. Drying Technology, 11, 900-927, 1993.

Jain, D.; Pathare, P. B. Selection and evaluation of thin layer drying models for infrared radiative and convective drying of onion slices. Biosystems Engineering, 89(3), 289–296, 2004.

Jangam, S.V.; Law, C.L.; Mujumda, A.S. Drying of food, vegetable and fruits-volume 1, Ed. ISBN-978-981-08-6759-1, Published in Singapore, 2010.

Janjai S.; Guevezov V.; Daguenet M. Technico-economic feasibility of solar-assisted Virginia tobacco curing. Drying Technology, 4, 605-632, 1986.

Janjai, S.; Laksanaboonsong, J.; Nunez, M.; Thongsathiya, A. Development of a method for generating operational solar radiation maps from satellite data for a tropical environment. Solar Energy, 78, 739-751, 2005.

Janjai S.; Tung P. Performance of a solar dryer using hot air from roof-integrated solar collectors for drying herbs and spices. Renewable Energy, 30, 2085-2095, 2005.

Janjai, S.; Intawee, P.; Chaichoet, C.; Sittiamnuay, P. Field experiments of the Silpakorn type solar tunnel dryers in northern Thailand. In Proceedings of Energy Conference, Phuket, Thailand, 2006.

Janjai, S.; Keawprasert, T. Design and performance evaluation of a solar tunnel dryer with polycarbonate cover. International Energy Journal, 7, 187-194, 2006.

Janjai, S.; Bala, B.K.; Tohsing, K.; Mahayothee, B.; Haewsungcharern, M.; Muhlbauer, W.; Muller, J. Equlibrium moisture content and heat of sorption of londan (Dimocarpus longan Lour.). Drying Technology, 24, 1691-1696, 2006.

Janjai, S., Tohsing, K. and Bala, B.K. Moisture sorption isotherms of lincheu mushroom (Ganoderma lucidum). Food Science and Technology Research, 13(4), 315-320, 2007.

Janjai, S.; Lambert, N.; Intawee, P.; Mahayothee, B.; Haewsungcharern, M.; Bala, B.K.; Müller, J. Finite element simulation of drying of mango. Biosystems Engineering, 2007.

Janjai, S.; Bala, B.K.; Lamlert, N.; Mahayothee, B.; Haewsungcharern, M. Muhlbauer, W.; Muller, J. Moisture diffusivities of the components of longan fruit. International Journal of Food Properties, 10, 471-478, 2007.

Janjai, S. Thin layer drying model of peeled longan, Research Report, Department of Physics, Silpakorn University. 2007.

Janjai, S.; Bala, B. K.; Lamlert, N.; Boonlot, Y.; Mahayothee, B.; Haewsungcharern, M.; Nagle, M.; Leis, M. H.; Muller, J. Finite element simulation of longan fruit. Drying Technology, 26, 666-674, 2008.

Janjai S.; Srisittipokakun N.; Bala B.K. Experimental and modeling performances of a roof-integrated solar drying system for drying herbs and spices. Energy, 33, 91-103, 2008.

Janjai, S.; Lamlert, N.; Mahayothee, B.; Thamrongmas, C.; Bala, B.K.; Precooe, M.; Müller, J. Thin Layer Drying of Peeled Longan *(Dimocarpus longan Lour.)*. Journal of Food Science and Technology Research, 17, 4, 2011.

Janjai, S.; Lamlert , N.; Mahayothee, B.; Sruamsiri, P.; Thamrongmas, C.; Precoppe, M.; Nagle, M.; Bala, B.K.; Müller, J. Experimental and Simulated Performances of a Batch Type Longan Dryer with Air Flow Reversal Using Biomass Burner as a Heat Source. Drying Technology, 2011. (in press)

Jia, C. C.; Yang, W.; Siebenmorgen, T. J.; Cnossen, A. G. Development of computer simulation software for single kernel drying, tempering and stress analysis. Transactions of the ASAE, 45(5), 1485-1492, 2002.

Jiang, Y.; Zhang, Z.; Joyce, D. C.; Kesta, S. Postharvest biology and handling of longan fruit (Dimocarpus Longan Lour). Postharvest Biology and Technology, 26, 241-252, 2002.

Kaleemullah, S.; Kailappan, R. Modeling of thin layer drying kinetics of red chiliies. J. Food Eng., 76, 531-537, 2006.

Kang, S.; Delwiche, S.R. Moisture diffusion modeling of wheat kernel during soaking. Transactions of the ASAE, 42(5), 1359-1365, 1999.

Kang, S.; Delwiche, S.R. Moisture diffusivity coefficients of single wheat kernels with assumed simplified geometries, analytical approach. Transactions of the ASAE, 42(6), 1653-1659, 2000.

Karathanos, V.T. Determination of water content of dried fruits by drying kinetics. Journal of Food Engineering, 39, 337-344, 1999.

Karim, M.A.; Hawlader, M.N.A. Mathematical modeling and experimental investigation of tropical fruits drying. International Journal of Heat and Mass Transfer, 48, 4914-4925, 2005.

Kashaninejad, M.; Mortazavi, A.; Safekordi, A.; Tabil, L.G. Thin-layer drying characteristics and modeling of pistachio nuts. Journal of Food Engineering, 78, 98-108, 2007.

Kays, W.M.; Crawford, M.E. Convective Heat and Mass Transfer; McGraw Hill; New York, 1980.

Kechaou, N.; Maâlej, M. A simplified model for determination of moisture diffusivity of date from experimental drying curves. Drying Technology, 18 (4&5), 1109-1125, 2000.

Kiranoudis, C. T.; Tsami, E.; Maroulis, Z. B.; Marinos-Kouris, D. Drying kinetics of some fruits. Drying Technology, 15(5), 1399-1418, 1997.

Krokido, M. K.; Karathanos, V. T.; Maroulis, Z. B.; Marinos-Kouris, D. Drying kinetics of some vegetables. Journal of Food Engineering, 59, 391-403, 2003.

Krokida, M.K.; Tsami, E.; Maroulis, Z. B. Kinetics on color changes during drying of some fruits and vegetables. Drying Technology, 16(3–5), 667–685, 1998.

Lan, Y.; Kunze, O.R. Moisture adsorption rates by different forms of rice. Transactions of the ASAE 1996, 39(3), 1035-1038.

Lagunez-Rivera, L.; Ruiz-López, I.I. García-Alvarado, M.A.; Salgado-Cervates, M.A. Mathematical simulation of the effective diffusivity of water during drying of papaya. Drying Technology 2007, 25, 1633-1638.

Li, Z.; Kobayashi, N.; Hasatani, M. Modeling of diffusion in ellipsoidal: A comparative study. Drying Technology, 22, 649-675, 2004.

Liu, Q.; Irudayaraj, J. Finite element analysis of a moving boundary value problem. Drying Technology, 13, 99-123, 1995.

Lopez Camelo, A. F.; Gomez, P. A. Comparison of colour indexes for tomato ripening. Horticultural Brassica, 22(2): 534-537, 2004.

Lozano, J. E.; Ibarz, A., Colour changes in concentrated fruit pulp during heating at high temperatures. Journal of Food Engineering, 31(3), 365–373, 1997.

Lutz, K.; Mühlbauer, W. Solar tunnel dryer with integrated collector. Drying Technology, 4, 583-603, 1986.

Mandas, N.; Habte, M. Numerical simulation static-bed drying of barley. Biosystems Engineering, 82(3), 313-319, 2002.

Maskan, M. Kinetics of colour change of kiwifruits during hot air and microwave drying. Journal of Food Engineering, 48(2), 169–175, 2001.

McEwen, E.; O'Callaghan, J.R. Through drying of wheat grain. Part III: deep beds of wheat grain. The Engineer, 10, 817-819, 1954.

Menges, H. O.; Ertekin, C. Mathematical modeling of thin layer of golden apples. Journal of Food Engineering, 77, 119-125, 2006.

Midilli, A.; Kucuk, H. Mathematical modeling of thin layer drying of pistachio by using solar energy. Energy Conversion and Management, 44(7), 1111-1122, 2003.

Moreno-Castillo, E.J.; Gonzalez-Garcia, R.; Grajales-Lagunes, A.; Ruiz-Cabrera, M. A.; Abud-Archila, M. Water diffusivity and color of cactus pear fruits (Opuntia Ficus Indica) subjected to osmotic dehydration. International J.Food Properties, 8(2), 323-336, 2005.

Muhlbauer, W. Present status of solar crop drying. Energy in Agriculture, 5, 121-137, 1986.

Mujumdar, A.S. "Handbook of industrial drying." New York: Marcel Dekker, 1987.

Mujumdar, A.S. Fundamental Principle of Drying in S. Devahastin (Ed) Mujumdar's Practical Corporation, Montreal, Canada, 1-22, 2000.

Murata, S.; Amaratunga, K.S.P.; Tanaka, F.; Shibuya, K.; Koide, S.; Uchino, T. Simulation of moisture adsorption by polished rice in deep-bed. Food Science and Technology Research, 2(2), 86-91, 1996.

Muthukumarappan, K.; Gunasekaran, S. Finite element simulation of cron moisture adsorption. Transactions of the ASAE, 39(6), 2217-2222, 1996.

Muthukumarappan, K.; Gunasekaran, S. Moisture diffusivity of corn kernel components during adsorption part I: Germ. Transactions of the ASAE, 37(4), 1263-1268, 1994.

Muthukumarappan, K.; Gunasekaran, S.. Moisture diffusivity of corn kernel during adsoption part II: pericarp. Trans. ASAE, 37(4), 1269-1274, 1994.

Muthukumarappan, K.; Gunasekaran, S. Moisture diffusivity of corn kernal components during adsorption part III: Soft and hard endosperms. Trans. ASAE, 37(4), 1275-1280, 1994.

Nafle, M.; Gonzalez Azcarraga, J.C.; Mahayothee, B.; Haewsungcharern, M.; Janjai, S.; Muller, J. Improved quality and energy performance of a fixed-bed longan dryer by thermodynamic modifications. Journal of Food Engineering, 99, 392-399, 2010.

Nathakaranakule, A.; Jaiboon, P.; Soponronnarit, S. Far-infrared radiation assisted drying of longan fruit. Journal of Food Engineering, 100, 662-668, 2010.

Neminyi, M.; Czaba, I.; Kovacs, A.; Jani, T. Investigation of simultaneous heat and mass transfer within the maize kernels during drying. Computers and Electronics in Agriculture, 26, 123-135, 2000.

Nguyen, T.A.; Verboven, P.; Scheerlinck, N.; Vandewalle, S.; Nicolai, B.M. Estimation of effective diffusivity of pear tissue and cuticle by means of a numerical water diffusivity model. Journal of Food Engineering, 72, 63-72, 2006.

Nuthong, P.; Achariyaviriya, A.; Namsanguan, K.; Achariyaviriya, S. Kinetics and modeling of whole longan with combined infrared and hot air. Journal of Food Engineering, 102, 233-239, 2010.

Ochoa, M.R.; Kesseler, A.G.; Piron, B.N.; Marquez, C.A.; De Michelis, A. Shrinkage during convective drying of whole rose hip (Rosa rubiginosa L.) fruits. Lebensm.-Wiss.u.-Technol, 35, 400-406, 2002.

Ochoa-Martinez, C.I.; Ramaswamy, H.S.; Ayala-Aponte, A.A. ANN-based models for moisture diffusivity coefficient and moisture loss at equilibrium in osmotic dehydration process. Drying Technology, 25, 775-783, 2007.

Office of Agricultural Economics, Thailand. Import-export statistics, http://www-oae.go.th. (September 25, 2007).

Olivelra, L.S.; Adriana, S.; Haghighi, K. An adaptive approach to finite element modeling of drying problems. Drying Technology, 13, 1167-1185, 1995.

Oosthuizen, P.H. The design of indirect solar rice dryers. Journal of Engineering for International Development, 2, 20-27, 1995.

Oosthuizen, P.H. Experimental study of simulated indirect solar rice dryer fitted with a small fan. Journal of Engineering for International Development, 3, 22-29, 1996.

O'Callaghan, J.R.O.; Menzies, D.J.; Bailey, P.H. Digital simulation of agricultural drier performance. Journal of Agricultural Engineering Research, 16, 223-244, 1971.

O'Callaghan, J.R.O.; Menzies, D.J.; Bailey, P.H. Digital simulation of agricultural drier performance. Journal of Agricultural Engineering Research 1971, 16, 223-244. Pal, U. S. and Chakraverty, A. Thin layer convention drying of mushrooms. Energy Conversion and Management, 38(2), 107-113, 1997.

Paitil, N.D. Evaluation of diffusion equation for simulating moisture movement within an individual grain kernel. Drying Technology, 6, 21-42, 1988.

Panagiotou, N.M.; Krokida, M. K.; Maroulis, Z. B.; Saravacos, G. D. Moisture diffusivity: Literature data compilation for foodstuffs. International J.Food Properties, 7(2), 273-299, 2004.

Pandit, R.; Prasad, S. Finite element analysis of microwave heating of potato-transient temperature profiles. Journal of Food Engineering, 60, 193-202, 2003.

Phaphuangwittayakul, W.; Limpiti, S.; Alikhani, Z.A. A batch dryer for unpeeled longan drying. Agricultural Mechanization in Asia, Africa and Latin America, 35(1), 41-44, 2004.

Parker, B.F.; Mujumdar, A.S. Solar drying in agriculture. Drying Technology, 9, 1125-1126, 1991.

Phupaichitkun, S.; Mahayothee, B.; Heawsungcharern, M.; Janjai, S.; Müller, J. Single-layer drying behavior of longan (Dimocarpus longan Lour.). In Proceedings of the Conference on International Agricultural Research for Development, Hohenheim University, Stuttgart, Germany, October 11-13, 2005.

Phupaichitkun, S.; Mahayothee, B.; Waldenmaier, T.; Muller, J. Generalized single-layer model for drying kinetics of unpeeled-longan. International Journal of Agricultural and Biological Engineering , 1(2), 64-71, 2008.

Rahman, M.S. Dried food properties: Challenges ahead. Drying Technology, 23, 695-715, 2005.

Ranjan, R.; Irudayaraj, J.; Reddy, J. N.; Mujumdar, A. S. Finite element simulation and validation of stepwise drying of bananas. Numerical Heat Transfer, Part A: Applications , 45(10), 997-1012, 2004.

Raouzeos, G.S.; Saravacos, G.D. Solar drying of raising. Drying Technology, 4, 633-649, 1986.

Ratti, C.; Mujumdar, A.S. Simulation of packed bed drying of foodstuffs with airflow reversal. Journal of Food Engineering, 26(3), 259-271, 1995.

Ratti, C.; Mujumdar, A.S. Solar drying of foods: modeling and numerical simulation. Solar Energy, 60, 151-157, 1997.

Ratti, C.; Crapiste, G.H. Modeling of batch dryers for shrinkable biological materials. Food Bioprocess Technology, 2, 248-256, 2009.

Romano, V.R.; Marra, F.; Tammara, U. Modeling of microwave heating of food stuff: study on the influence of sample dimensions with a FEM approach. Journal of Food Engineering, 71, 233-241, 2005.

Rossello, C.; Bema, A.; Mulet, A. Solar drying of fruits in a Mediterranean climate. Drying Technology, 8, 305-321, 1990.

Ruiz-Lopez, I.I.; Martinez-Sanchez, C.E.; Cobos-Vivaldo, R.; Herman-Lara, E. Mathematical modeling and simulation of batch drying of food in fixed beds with airflow reversal. Journal of Food Engineering, 89, 310-318, 2008.

Sarker, N.W.; Kunze, O.R.; Strouboulis, T. Transient moisture gradients in rough rice mapped with finite element model and related to fissures after heated air drying. Transactions of the ASAE, 39(2), 625-631, 1996.

Schenck, H.; Hawks, R.J. Theories of Engineering Experimentation. McGraw Hill, New York, 1979.

Schirmer, P.; Janjai, S.; Esper, A.; Smitabhindu, R.; Mühlbauer, W. Experimental investigation of the performance of the solar tunnel dryer for drying bananas. Renewable Energy, 7, 119-129, 1996.

Segerlind, I.J. Applied Finite Element Analysis; second edition, John Wiley and Sons, Inc. New York, 1984.

Sharma, G.P.; Prasad, S. Effective moisture diffusivity of garlic cloves undergoing microwave-convective drying. J. Food Eng., 65, 609-617, 2004.

Sharma, V.K.; Colangelo, A.; Spagna, G. Experimental investigation of different solar driers suitable for fruits and vegetable drying. Renewable Energy, 6, 413-424, 1995.

Simal, S; Garau, M.C.; Femenia, A.; Rosselló, C. A diffusional model a moisture-dependent diffusivity coefficient. Drying Technology, 24, 1365-1372, 2006.

Simate, I.N. Simulation of the mixed-mode natural-convection solar drying of maize. Drying Technology, 19, 1137-1155, 2001.

Simate, I.N. Optimization of mixed mode and indirect mode natural convection solar dryers. Renewable Energy, 28, 435-453, 2003.

Sitompul, J.P.; Istadi.; Sumardiono, S. Modeling and simulation of momentum, heat and mass transfer in a deep-bed grain dryer. Drying Technology, 21(2), 217-229, 2003.

Smitabhindu R.; Janjai S.; Chankong V. Optimization of a solar-assisted drying system for drying bananas. Renewable Energy, 33, 1523-1531, 2008.

Sokhasanj, S.; Lang, W.; Gu, D. Advances in mathematical modeling of heat and mass transfer during throughtflow-air drying of cereal grain. Food Science and Technology Research, 3(3), 226-234, 1997.

Somjai, T.; Achariyaviriya, S.; Achariyaviriya, A.; Namsanguan, K. Strategy for longan drying in two-stage superheated steam and hot air. Journal of Food Engineering, 95, 313-321, 2009.

Srivastava, V.K.; John, J. Deep bed grain drying modeling. Energy Conversion and Management, 43, 1689-1708, 2002.

Sun, D.W.; Woods, J.L. Simulation of heat and mass transfer process during drying in deep grain beds. Drying Technology, 15(10), 2479-2508, 1997.

Steffe, J. F.; Singh, R.P. Diffusivity of starchy endosperm and bran of fresh and rewetted rice. J. food Sci., 45(2) , 356-361, 1980.

Steffe, J. F.; Singh, R.P. Liquid diffusivity of rough rice components. Trans. ASAE, 23(3), 767-774, 782, 1980.

Steffe, J. F.; Singh, R.P. Diffusion coefficients for predicting rice drying behaviour. J. Agric. Enging. Res., 27(6), 489 – 493, 1980.

Surfer. Version 8. Golden software, Inc, USA, 1990.

Talla, A.; Puiggali, J.R.; Jomaa, W.; Jannot, Y. Shrinkage and density evolution during drying of tropical fruits: application to banana. Journal of Food Engineering, 64, 103-109, 2004.

Tang, Z.; Cenkowski, S.; Muir, W.E. Modeling the superheated-steam drying of a fixed bed of brewers' spent grain. Biosystems Engineering, 87(1), 67-77, 2004.

Tippayawong, N.; Tantakitti, C.; Thavornun, S. Energy efficiency improvement in longan dryimg practice. Energy, 33, 1137-1143, 2008.

Tippayawong, N.; Tantakitti, C.; Thavornun, S.; Peerawannitkul, V. Energy conservation in drying of peeled longan by forced convention and hot air recirculation. Biosystems Engineering, 104, 199-204, 2009.

Thompson, T.L.; Peart, R.M.; Foster, G.H. Mathematical simulation of corn drying - A new model. Transactions of the ASAE, 11(4), 582-586, 1967.

Togrul, I. T.; Pehlivan, D. Mathematical modeling of solar drying of apricots in thin layer. Journal of Food Engineering, 55, 209-216, 2002.

Togrul, I. T.; Pehlivan, D. Modeling of drying kinetics of single apricot. Journal of Food Engineering, 58, 23-32, 2003.

Van Arsdel, W.B. Simulation of heat and mass transfer in a non-isothermal system: through flow in the low moisture range. Am. Inst. Chem. Engnrs. Chem. Engng. Progress Symposium Series No. 16, Mass Transfer, 47-58, 1955.

Varish, J.; Dijkanarukkul, P.; Achariyaviriya, A.; Achariyaviriya, S. Combined microwave-hot air drying of peeled longan. Journal of Food Engineering, 81, 459-468, 2007.

Varith, J.; Dijkanarukkul, P.; Achariyaviriya, A.; Achariyaviriya, S. Combined microwave-hot air drying of peeled longan. Food Engineering, 81, 459-468, 2007.

Vlachos, N.A.; Karapantsios, T.D.; Balouktsis, A.I.; Chassapis, D. Design and testing of a new solar tray dryer. Drying Technology , 1243-1271, 2002.

Wang, C.Y.; Singh, R.P. A single layer drying equation for rough rice. ASAE, paper no. 3001, 1978.

Weitz, D.A.; Luque, E.A.; Piacentini, R.D. Solar drying simulation of prunes arranged in thin layers. Drying Technology, 8, 287-303, 1990.

Whith, G.M.; Bridges, T.C.; Loewer, O.J.; Ross, I.J. Seed coat damage in thin layer drying of soybeans as affected by drying conditions. ASAE, paper no.3052, 1978.

Xanthopoulos, G.; Oikonomou, N.; Lambrinos, G. Applicability of a single-layer drying model to predict the drying rate of whole figs. Journal of Food Engineering, 81, 553-559, 2007.

Yagcioglu, A.; Degirmencioglu, A.; Cagatay, F. Drying characteristic of laurel leaves under different conditions. In: A. Bascetincelik (ED.), Proceedings of the 7th International congress on agricultural mechanization and energy (pp. 565-569), Adana, Turkey: Faculty of Agriculture, Cukurova University, 1999.

Yaldiz, O.; Ertekin, C. (a). Thin-layer solar drying of some different vegetables. Drying Technology, 19, 583-596, 2001.

Yaldiz, O.; Ertekin, C. (b). Mathematical modeling of thin layer solar drying of Sultana grapes. Energy, 26, 457-465, 2001.

Yaldyz, O.; Ertekyn, C. Thin layer solar drying of some vegetables. Drying Technology, 19, 583-597, 2001.

Zaman, M.A.; Bala, B.K. Thin layer solar drying of rough rice. Solar Energy, 42, 167-171, 1989.

Zhang, M.; De Baerdemaeker, J.; Schrevens, E. Effects of different varieties and shelf storage conditions of chicory on deteriorative color changes using digital image processing and analysis. Food Research International, 36(7) 669–676, 2003.

Zhang, Q.; Litchfield, J.B. An optimization of intermittent corn drying in a laboratory scale thin layer dryer. Drying Technology, 9, 383-395, 1991.

Zare, D.; Minaei, S.; Mohamad Zadeh, M.; Khoshtaghaza, M.H. Computer simulation of rough rice drying in a batch dryer. Energy Conversion and Management, 47, 3241-3254, 2006.

Zhou, L.; Puri, V.M.; Anatheswaran, R.C.; Yeh, G. Finite element modeling of heat and mass transfer in food materials during microwave heating-model development and validation. Journal of Food Engineering, 25, 509-529, 1995.

Appendixes

Appendix 1

Parts of this thesis have been published in international journals and conference proceedings as follows:

1. Janjai, S.; Lamlert, N.; Mahayothee, B.; Thamrongmas, C.; Bala, B.K.; Precooe, M.; Müller, J. (2011). Thin Layer Drying of Peeled Longan *(Dimocarpus longan Lour.)*. Journal of Food Science and Technology Research, 17, 4. (impact factor = 0.401)

2. Janjai, S.; Bala, B.K.; Lamlert, N.; Mahayothee, B.; Haewsungcharern, M.; Nagel, M.; Müller, J. (2007). Moisture Diffusivities Determination of Different Parts of Longan Fruit. Journal of Food Properties 10, 471-478. (impact factor = 0.82)

3. Janjai, S.; Lamlert, N.; Intawee, P.; Mahayothee, B.; Haewsungcharern, M.; Bala, B.K.; Nagle, M.; Müller, J. (2008). Finite Element Simulation of Drying of Longan. Drying Technology 26, 666-674. (impact factor = 1.048)

4. Janjai, S.; Lamlert, N.; Intawee, P.; Mahayothee, B.; Boonrod, Y.; Haewsungcharern, M.; Bala, B.K.; Nagle, M.; Müller, J. (2009). Solar Drying of Peeled Longan Using a Side Loading Type Solar Tunnel Dryer: Experimental and Simulated Performance. Drying Technology 27, 595-605. (impact factor = 1.048)

5. Janjai, S.; Lamlert , N.; Mahayothee, B.; Sruamsiri, P.; Thamrongmas, C.; Precoppe, M.; Nagle, M.; Bala, B.K.; Müller, J. (2011). Experimental and Simulated Performances of a Batch Type Longan Dryer with Air Flow Reversal Using Biomass Burner as a Heat Source. Drying Technology. (in press, impact factor = 1.048)

6. Lamlert, N.; Janjai, S.; Intawee, P.; Mahayothee, B.; Bala, B.K.; Nagle, M.; Müller, J. Experimental and Simulated Performances of a Roof-integrated Solar Drying System for Deep Bed Drying of Longan**.** Proceedings of the 3rd International conference "Sustainable Energy and Environment (SEE2009)". World Renewable Energy Congress 2009-Asia, 19-22 May, 2009, Bangkok, Thailand.

Appendix 2

Solar Drying of Longan Fruit*

Drying of longan fruit with a roof-integrated solar drying system was also investigated as follows:

A roof-integrated solar drying system designed and constructed in the Solar Energy Research Laboratory, Silpakorn University was used to study the experimental and simulated performances of roof–integrated solar dryer for drying of longan. It is located at Suan Phoeng Educational Park in Ratchaburi Province (13^{o} $32^{/}$ $50^{//}$ N ,99^{o} $48^{/}$ $44^{//}$ E) in Thailand. The dryer consists of a roof-integrated solar collector and a drying bin with an electric motor operated axial fan to provide the required air flow and it is shown in Fig. A1. The roof-integrated collector consists of two arrays of air collectors placed on the roof structure of a building: one facing the south and the other facing the north with a total area of 144 m^2. The arrays of the collectors also serve as the roof of the building. The roof-integrated collector is an insulated black-pained roof serving as an absorber, which is covered with a polycarbonate plate. The drying bin is essentially a deep bed dryer. The dimension of the bin is 1.3 m × 2.4 m × 0.8 m and it is located inside the building. The bin is connected to the middle of collector through a T-type air duct. Solar radiation was measured by pyranometers (Kipp&Zonen, CM11) and temperature was measured by using K-type thermocouples.

Longan fruit was dried to demonstrate the potentiality of the drying system for drying this fruit. Two experiments were carried out in November, 2008. For each drying test, one hundred kilograms of longan fruit was loaded to the drying bin. The experiments were started at 8.00 am and continued until 5.00 pm. During the night the product was kept in the drying bin. The process was repeated until the desired moisture content (about 25% wb) was reached. About 100 g of product sample was taken from the dryer and weighted at 3-h intervals. The moisture content of the product was determined using the oven method.

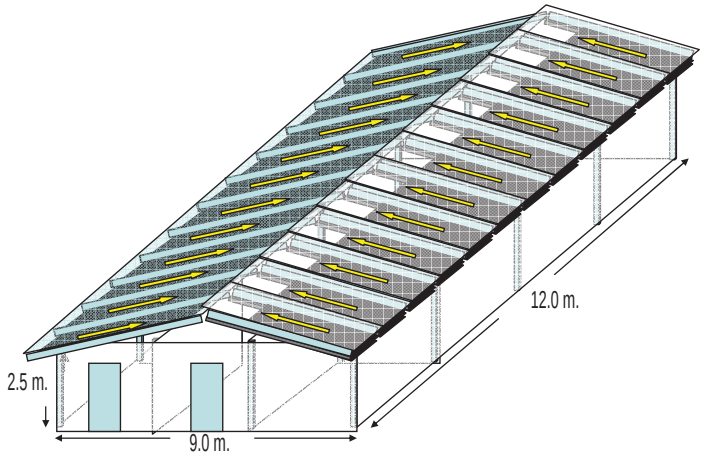

Fig. A1 Roof-integrated solar drying system

* The paper published in the proceeding of the 3rd International conference “Sustainable Energy and Environment (SEE2009)”. World Renewable Energy Congress 2009-Asia.

Heat transfer in the collector is schematically shown in Fig. A2 and energy balances for each component of the collector can be expressed as:

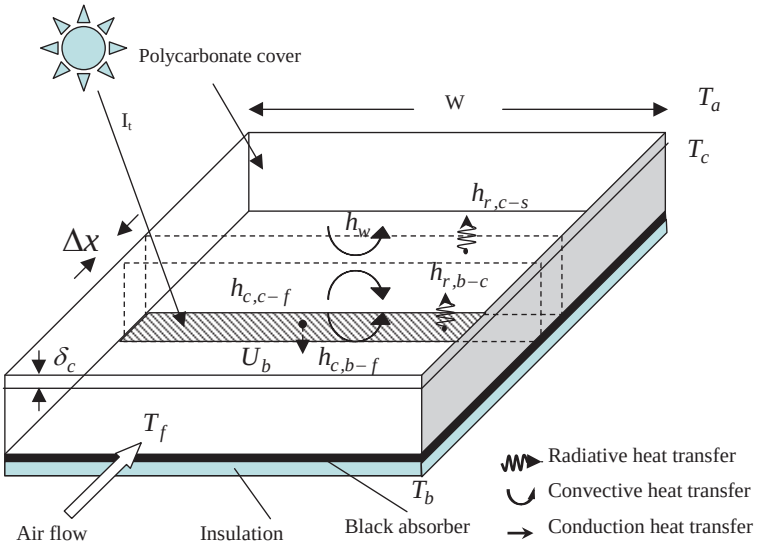

Fig. A2 Heat transfer in the collector

- Polycarbonate cover

$$\rho_c \delta_c C_c \frac{dT_c}{dt} = h_{r,b-c}(T_b - T_c) + h_{c,c-f}(T_f - T_c) + h_w(T_a - T_c) + h_{r,c-s}(T_s - T_c) + \alpha_c I_t \quad (1)$$

- Air stream

$$DG\ C_f \frac{dT_f}{dx} = h_{c,c-f}(T_c - T_f) + h_{c,b-f}(T_b - T_f) \quad (2)$$

- Absorber

$$\rho_b \delta_b c_b \frac{dT_b}{dt} = h_{c,b-f}(T_f - T_b) + h_{r,b-c}(T_c - T_b) + U_b(T_a - T_b) + (\tau\alpha) I_t \quad (3)$$

Energy and mass balance equations in the drying bin can be written as:

- Energy balance

$$m_a (C_a + C_v H) \frac{\partial T_f}{\partial Y} = \rho_p C_v (T_f - T_p) \frac{\partial M}{\partial t} - \rho_p (C_p + C_f M) \frac{\partial T_p}{\partial t} + \rho_p L_p \frac{\partial M}{\partial t} \quad (4)$$

- Heat transfer rate

$$\rho_p (C_p + C_f M) \frac{\partial T_p}{\partial t} = h_v (T_f - T_p) + \rho_p L_p \frac{\partial M}{\partial t} \quad (5)$$

- Mass balance

$$m_a \frac{\partial H}{\partial Y} = -\rho_p \frac{\partial M}{\partial t} \quad (6)$$

- Drying rate equation

$$\frac{M - M_e}{M_0 - M_e} = \exp(-At^B) \quad (7)$$

$$A = \frac{-179.907 + 0.0569\left(\frac{rh}{v}\right) + 7182\exp\left(\frac{-455.2}{T}\right)}{R^2_{norm}}$$

B = 1.0829

Equilibrium moisture content (M_e) is calculated from:

$$a_w = \frac{1}{1 + \left[\frac{b_0 + b_1 T}{M_e}\right]} b_2 \quad (8)$$

where b_0 = 79.9826; b_1= -0.8277; and b_2 = 2.1867.

Equations from (1) to (8) are solved numerically using finite difference technique

Field tests of the dryer for drying of longan were carried out in the months of November, 2008. The variations of solar radiation are shown in Fig. A3. The solar radiations follow similar cyclical patterns for all the days, but there are some fluctuations due to cloud in the sky.

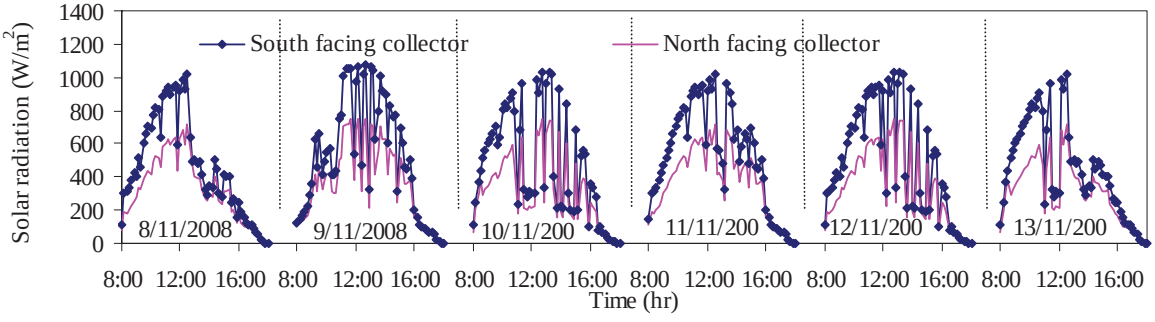

Fig. A3 Solar radiation on the south and north facing solar collector

Figure A4 and Figure A5 show the ambient temperature and the collector outlet temperatures at the middle of the roof for solar radiation incident on the south-facing collectors and north-facing collectors respectively. Since more incident solar radiation was on the south-facing roof as compared to the north-facing roof, the temperature at the outlet of the south-facing roof was higher.

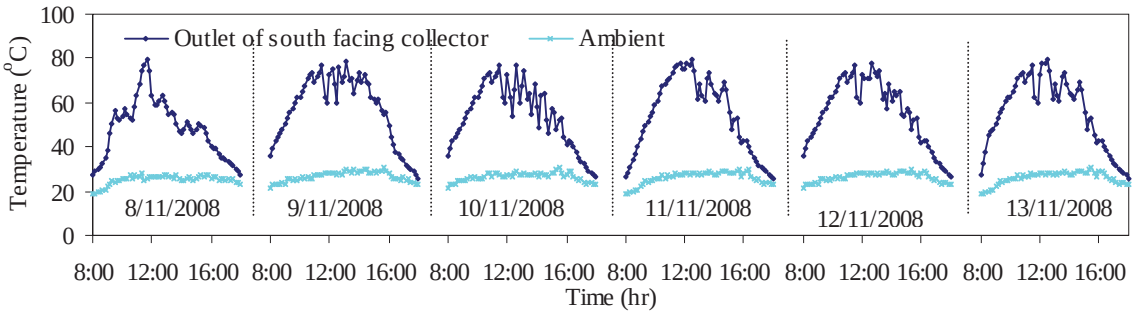

Fig. A4 Variations of the ambient temperature and temperature of the outlet air from the south-facing collector for the drying test of longan

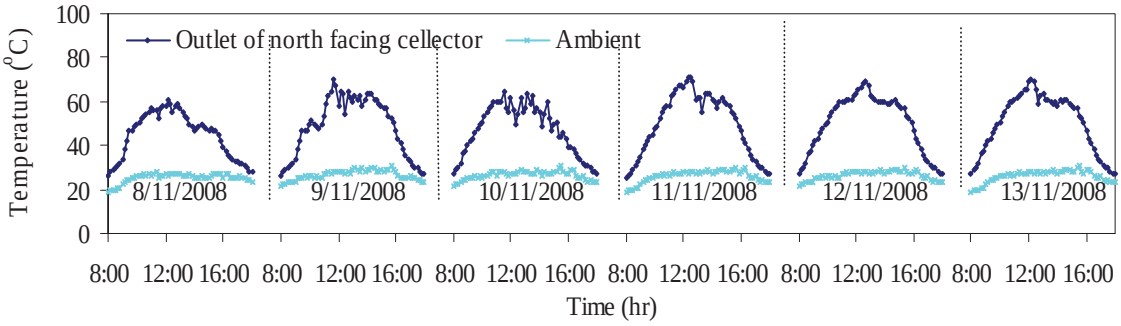

Fig. A5 Variations of the ambient temperature and temperature of the outlet air from the north-facing collector for the drying test of longan

Figure A6 shows the variations of the temperature above the ambient temperature with solar radiation for the drying periods. The average temperature rise is high and it is 17.6°C (sd = 9.2°C) and the high deviations might be attributed to temperature fluctuations due to the clouds.

For clear sky weather conditions, the moisture content of the longan in the drying bin was reduced from an initial value of 70% (wb) to the final value of 25% (wb) within 6 days as shown in Fig. A7. The colour of the dried longan was comparable to that of a high quality dried chili in markets when the colour was tested.

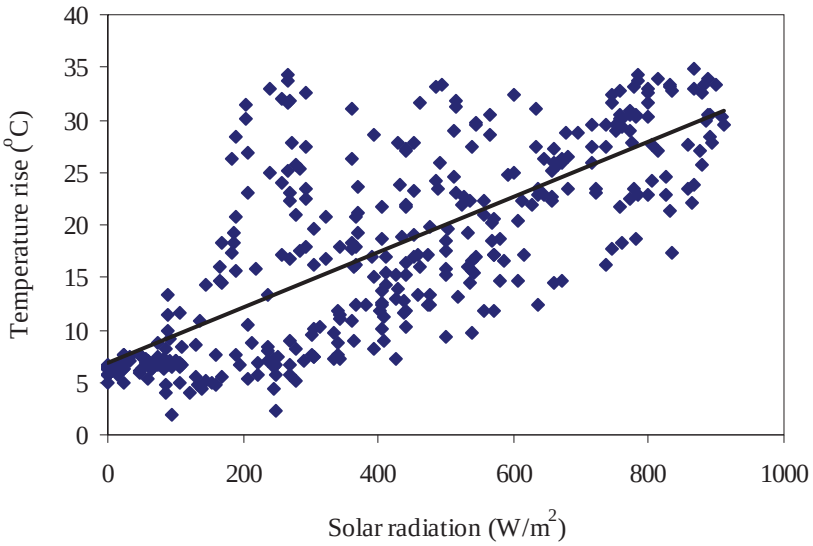

Fig. A6 Average temperature rise above the ambient inside at the outlet of the collector

Figure A7 shows a typical comparison of the predicted and observed moisture contents of longan inside the dryer and the model predicts well the moisture content changes during drying. The model predictions were evaluated on the basis of Root Mean Square Error (RMSE) and RMSE of the prediction of the moisture contents was 8.0%.

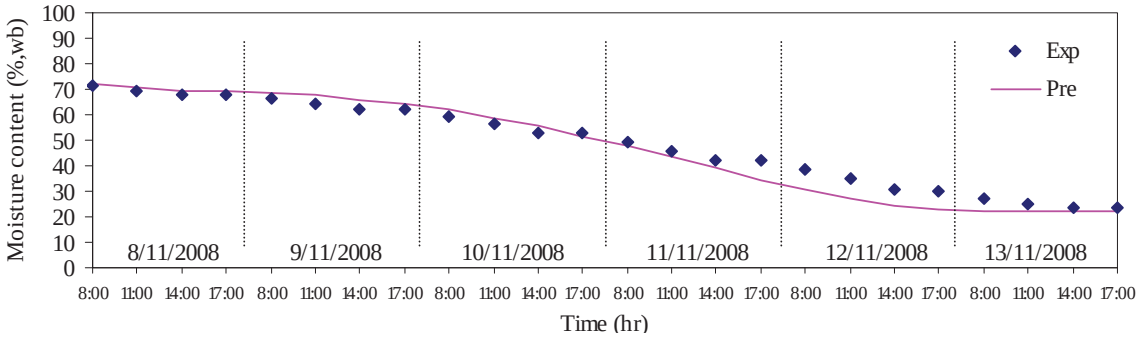

Fig. A7 Comparison of experimental and simulated moisture contents

Solar drying of longan was conducted in a roof-integrated solar dryer. Solar radiation followed similar cyclical patterns for all the days during drying. The average temperature rise inside the dryer was about 17.6°C above the ambient temperature. Moisture content of the longan was reduced from an initial value of 70% (wb) to the final value of 25% (wb) within 6 days. The agreement between the experimental and simulated moisture content of longan during drying was good. As the longan harvesting season (July-September) corresponds to the rainy season with the majority of cloudy days, and each drying batch of whole longan fruit take about 6 days, it is difficult to use this type of solar dryer to dry longan fruit without an additional heater.

Appendix 3

Nomenclature

A parameter of thin layer equation (-)

A_c collector area (m^2)

[A] intermediate parameter matrix (-)

a^*, a^*_{ref} parameter in the colour measurements (-)

a parameter in thin layer drying models (-)

a_1 parameter in the model of Wang and Singh (h^{-1})

a_w water activity (-)

B parameter of thin layer equation (-)

b parameter in thin layer drying models (-)

b^*, b^*_{ref} parameter in the colour measurements (-)

b_0, b_1, b_2 parameter in equilibrium moisture content models (-)

C* colour parameter for chroma (-)

C_a specific heat of air (J/kg-K)

C_{annual} annual cost of the system (USD/year)

C_b specific heat of absorber material (J/kg –K)

C_c specific heat of cover material (J/kg –K)

$C_{electric}$ electricity consumption cost (USD/year)

C_f specific heat of air (J/kg –K)

C_1 labour cost for the construction (USD)

$C_{labour,op}$ labour cost for operating the dryer (USD/year)

C_m material cost of the dryer (USD)

$C_{mant,i}$ maintenance cost (USD/year)

$C_{op,i}$ operating cost (USD/year)

C_p specific heat of peeled longan (J/kg –K)

C_v specific heat of water vapour (J/kg –K)

C_T the total capital cost for the solar dryer (USD)

C_v specific heat of water vapour (J/kg-K)

C_w specific heat of water (J/kg –K)

C_{wood} wood consumption cost (USD/year)

[C] global capacitance matrix (-)

[c] element capacitance matrix (-)

c	parameter in thin layer drying models (-)
D	diffusivity of longan (m^2/s)
D_h	hydraulic diameter of the collector (m)
D_{eff}	effective diffusivity (m^2/s)
D_{flesh}	diffusivity of flesh (m^2/s)
d	diameter of longan fruit (m)
D_{air}	diffusivity of air (m^2/s)
{F}	global load force vector (-)
$\{F_*\}$	intermediate parameter vector (-)
{f}	element load force vector (-)
G	mass flow rate of air ($kg/s\text{-}m^2$)
g	parameter in thin layer drying models (h^{-1})
H	humidity ratio (kg/kg)
h	colour parameter for hue angle (degree)
h_{fg}	latent heat of vaporization of moisture from peeled longan (J/kg)
$h_{r,b\text{-}c}$	radiative heat transfer coefficient between the cover and the absorber ($W/m^2\text{-}K$)
$h_{c,b\text{-}f}$	convective heat transfer coefficient between the absorber and the air ($W/m^2\text{-}K$)
$h_{c,c\text{-}f}$	convective heat transfer coefficient between the cover and the air ($W/m^2\text{-}K$)
$h_{c,p\text{-}f}$	convective heat transfer coefficient between the product and the air ($W/m^2\text{-}K$)
h_m	mass transfer coefficient (m/s)
$h_{r,c\text{-}s}$	radiative heat transfer coefficient between the cover and the sky ($W/m^2\text{-}K$)
$h_{r,p\text{-}c}$	radiative heat transfer coefficient between the cover and the product ($W/m^2\text{-}K$)
h_v	volumetric heat transfer coefficient ($W/m^3\text{-}K$)
h_w	convective heat transfer coefficient between the cover and the ambient due to wind ($W/m^2\text{-}K$)
I_t	incident solar radiation (W/m^2)
[K]	global stiffness matrix (-)
[k]	element stiffness matrix (-)
k	drying rate constant (h^{-1})
k_1	drying rate constant in Page model (h^{-n})
k_a	thermal conductivity of air (W/m-K)
k_b	thermal conductivity of back insulator (W/m-K)
i_{in}	interest rate (%)
i_f	inflation rate (%)
L^*, L^*_{ref}	parameter in the colour measurements (-)
L_p	latent heat of evaporation of product (J/kg)

L_b	thickness of back insulator (m)
M	moisture content of longan fruit (%, db)
M_o	initial moisture content of the components of longan (%, db)
M_{dry}	annual production of dry product (kg)
M_e	equilibrium moisture contents of longan (%, db)
M_f	amount of fresh product per year (kg)
M_i	initial moisture content of longan on a dry basis (%, db)
M_{obs}	observed or experimental moisture content (%, db)
M_{pre}	predicted moisture content (%, db)
MR	moisture content ratio (-)
M_s	surface moisture content on a dry basis (%, db)
m_a	mass flow rate of air (kg/m^2-s)
$[N]$	matrix of interpolating function (-)
Nu	Nusselt number (-)
n	magnitude of the outward normal vector to the surface (-)
n	integer number of the infinite series, n=1, 2, 3,……..
n	empirical constant in Page and modified Page model (-)
[P]	intermediate parameter matrix (-)
P_d	price of the dry product (USD/kg)
P_f	price of the fresh product (USD/kg)
p	parameter in thin layer drying models (h^{-1})
R^2	coefficient of determination (-)
R	coefficient of determination (%)
R_0	universal gas constant (J/mol-K)
Re	Reynolds number (-)
RMSE	root mean square error (%)
r	radius of the cylindrical seed stalk (m)
rh	relative humidity (%)
r_l^2	norm radius of longan fruit (m)
r_o	radius of seed (m)
S	cross sectional area (m^2)
Sc	Schmidt number (-)
T	temperature (ºC)
T_{ab}	absolute temperature (K)
T_a	ambient temperature (K)
T_b	temperature of the absorber (K)
T_c	temperature of the collector cover (K)
T_{c1}	temperature of the cover of the drying unit (K)

T_f	temperature of the air steam in the collector (K)
T_{f1}	temperature of the moist air steam in the drying unit (K)
T_p	product temperature (K)
T_s	sky temperature (K)
t	time (h)
U_b	heat loss coefficient of the absorber through the back insulator (W/m^2-K)
u	air velocity (m/s)
V_0	initial volume (m^3)
V	volume at moisture content M (m^3)
V_a	wind velocity (m/s)
v	velocity of air (m/s)
W	width of the solar collector (m)
x	position (m)
x_i	actual value of the variable (-)
x_{mean}	mean value of the measurements (-)
Y	depth of the product bed (m)
y	spatial coordinate in y direction (-)
$y_{exp,i}$	experimental values (-)
$y_{pre,i}$	predicted values (-)
Z	drying cost (USD/kg)
z	half thickness of the slab (shell, flesh and seed coat) (m)
ΔE	total colour change (-)
Δs	shrinkage of longan flesh (m)
Δt	time step (s)
Δx	space interval (m)
Δx_a	recent thickness of air gap between flesh and shell (m)
Δx_{ar}	thickness of air gap between flesh and shell after the shrinkage of the (-)
Δx_f	recent thickness of flesh (m)
Δx_{fr}	thickness of flesh after the shrinkage (m)
μ	viscosity of air (kg/m/s)
β	shrinkage coefficient (-)
Ω	fruit domain (-)
∇	operator $\frac{\partial}{\partial x}+\frac{\partial}{\partial y}+\frac{\partial}{\partial z}$
α_b	absorbtance of the absorber (-)

α_c	absorbtance of the cover material (-)
α_n	roots of the Bessel function of zero order, n= 1, 2, 3,…….
α_p	absorbtance of peeled longan (-)
δ_b	thickness of the absorber (m)
δ_c	thickness of the cover (m)
δx_i	uncertainty in the measurement (-)
ρ_b	density of the absorber material (kg/m^3)
ρ_{air}	density of air (kg/m^3)
ρ_C	density of the cover material (kg/m^3)
$\rho_{s,\,p}$	density of the peeled longan (kg/m^2)
σ	Stefan Boltzmann's constant (W/m^2.K^4)
τ_c	transmittance of the cover material (-)
$(\tau\alpha)$	transmittance-absorptance product of the system composing of the cover and absorber (-)
ε_c	emissivity of the cover material (-)
ε_b	emissivity of the absorber material (-)
ν	viscosity of air (m^2/s)

Autobiography

Name : Niroot Lamlert
Sex : Male
Date of birth : 4 August 1981
Address : 18 M. 1 T. Angthong A. Muang, Ratchaburi, 70000

Education

2003	Bachelor of Science (Physics) Silpakorn University, Nakhon Pathom, Thailand Topic of individual study: Control Car by Basic Stamp BS-SX
2006	Master of Science (Physics) Silpakorn University, Graduate School Thesis: Performance Improvement and Drying Model Development of a Greenhouse Solar Dryer with Polycarbonate Cover
2007	Doctor of Philosophy (Physics) Silpakorn University, Graduate School Thesis: Drying of Longan: Its Drying Kinetics and Performance of Longan Dryers